Energy Conversion and Management: X 20 (2023) 100442

Contents lists available at ScienceDirect

Energy Conversion and Management: X

journal homepage: www.sciencedirect.com/journal/energy-conversion-and-management-x

H_2-powered aviation – Design and economics of green LH_2 supply for airports

J. Hoelzen, L. Koenemann, L. Kistner, F. Schenke, A. Bensmann *, R. Hanke-Rauschenbach

Leibniz Universität Hannover, Institute of Electric Power Systems, 30167 Hanover, Germany

ARTICLE INFO

Keywords:
Hydrogen aviation
Liquid hydrogen
Renewable energy
Energy system optimization
Hydrogen fuel supply
Hydrogen energy systems
Hydrogen airports

ABSTRACT

The economic competitiveness of hydrogen-powered aviation highly depends on the supply costs of green liquid hydrogen to enable true-zero CO_2 flying. This study uses non-linear energy system optimization to analyze three main liquid hydrogen (LH_2) supply pathways for five locations.

Final liquid hydrogen costs at the dispenser could reach 2.04 USD/kgLH_2 in a 2050 base case scenario for locations with strong renewable energy source conditions. This could lead to cost-competitive flying with hydrogen.

Reflecting techno-economic uncertainties in two additional scenarios, the liquid hydrogen cost span at all five airport locations ranges between 1.37 and 3.48 USD/kgLH_2, if hydrogen import options from larger hydrogen markets are also available. Import setups are of special importance for airports with a weaker renewable energy source situation, e.g., selected Central European airports. There, on-site supply might not only be too expensive, but space requirements for renewable energy sources could be too large for feasible implementation in densely populated regions.

Furthermore, main costs for liquid hydrogen are caused by renewable energy sources, electrolysis systems, and liquefaction plants. Seven detailed design rules are derived for optimized energy systems for these and the storage components. This and the cost results should help infrastructure planners and general industry and policy players prioritize research and development needs.

1. Introduction

Aviation is a hard-to-abate sector without a silver bullet for reducing the sector's climate impact and reaching the industry's net-zero targets [1–7]. Even though the total climate impact of the aviation sector is only around 5% today, current air traffic growth scenarios imply an enormous increase in aviation's climate impact in comparison to a future decarbonized world in most other industries without radical measures [8–11].

Currently, two main options are discussed to tackle this challenge. First, sustainable aviation fuels (SAFs) like biofuels or e-fuels can be used as drop-in fuels for existing aircraft. However, their usage leads to a net and not true zero CO_2 emission reduction [5,12]. Second, new aircraft propulsion and fuel systems using green hydrogen (H_2) are promising options to achieve true zero CO_2 emissions in aviation, but also to reduce other climate impacts from NO_x emissions or from contrail and cirrus cloud creation [1,13–24]. Such systems might be hydrogen-electric using fuel cells and electric motors or direct hydrogen combustion jet engines.

Since most of air travel's emissions stem from commercial aviation and aircraft with more than 20 passengers, the scope of this study is on larger aircraft. For technological feasibility, these commercial H_2-powered aircraft would need to be fueled with and store (onboard) liquefied, cryogenic hydrogen (LH_2) [25–28]. It has a significantly higher volumetric energy density compared to compressed gaseous hydrogen (GH_2) and hence, leads to smaller storages and enables more efficient aircraft designs.

Consequently, deploying a LH_2 supply infrastructure is key for realizing H_2-powered aviation – as soon as possible to enable a broader introduction of such aircraft in 10–20 years and to reduce the climate impact of the aviation sector [29]. Since LH_2 can be generated via different production pathways, only green H_2 from water electrolysis using renewable energy plants is considered in this study. This ensures a real total reduction potential of the climate impact (from "well-to-wheel") using H_2 propulsion for aircraft [1,30–32].

A review article by Hoelzen et al. [33] already emphasized that more than 50 years of research focused on H_2 aircraft propulsion and partially on the required novel H_2 fuel infrastructure. However, crucial operating

* Corresponding author.
E-mail addresses: hoelzen@ifes.uni-hannover.de (J. Hoelzen), astrid.bensmann@ifes.uni-hannover.de (A. Bensmann).

https://doi.org/10.1016/j.ecmx.2023.100442
Received 5 June 2023; Received in revised form 16 August 2023; Accepted 17 August 2023
Available online 23 August 2023

Nomenclature

a	Annuity payment factor
b	Binary optimization variable
C	Cost in USD_{2020}
c	Specific cost in USD_{2020}
E	Electric energy in Wh/kWh/MWh
e	Specific energy consumption in Wh/kWh/MWh
f	Factor (cost or availability)
F	Fill level of storage
i	Interest rate in %
k	Pipe roughness coefficient
k_{BO}	Self-discharging / boil-off loss factor for LH_2 storage
K	Compressibility
κ	Heat capacity ratio
LR	Learning rate
m	Mass in kg
$\dot{m}$	Mass flow in kg/s
n	Amount (integer)
η	Efficiency
P	Electric power in W/kW/MW
p	Pressure
ρ	Density
r	Cost reduction factor
R	Universal gas constant
S	Market size
T_{DP}	Depreciation period in years
T	Temperature in K
t	Time in h
v	Speed in km/h
$\dot{v}$	Flow speed in m/s
w	Work
x	Design capacity
Z	State of a storage component
Z_{H2}	Compressibility factor for hydrogen
λ	Friction factor

Indices

avail	Available
HEX	Heat exchanger
i	Supply component i
ind	Indirect CAPEX
inst	Installation CAPEX
OM	Operation and maintenance
PL	Part-load
refri	Refrigerant
t	Time period/scenario
TAC	Total annual costs

Abbreviations

CAPEX	Capital expenditures
ELY	Electrolysis system
ES	Electric energy storage system
GH_2	Gaseous hydrogen
GH_2Sto	GH_2 storage
GH_2comp	GH_2 compressor
H_2	Hydrogen
HYB	Tag for great hybrid RES location
LCOE	Levelized costs of electricity
LFP	Liquefaction plant
LH_2	Liquid hydrogen
LH_2Sto	LH_2 storage
OPEX	Operating expenditures
PV	Photovoltaics; tag for PV location
RES	Renewable energy source
SEC	Specific energy consumption
tpd	Tons per day
WEAK	Tag for weaker hybrid RES location
WOFF	Tag for wind off-shore location
WON	Tag for wind on-shore location

cost metrics for airlines indicate that the highest uncertainty for the economic future of H_2-powered aviation comes from the future LH_2 supply costs and not the aircraft-related developments.

Relevant previous work on H_2 infrastructure assessments can be distinguished by two main aspects: the focus of application and the applied methodology.

Several high-level economic assessments on LH_2 infrastructure for aviation target the right application. These studies provide good overviews of the topic but focus either only on the refueling system at the airport or use simpler techno-economic calculations [1,34–37].

Contrary to that, detailed studies offer relevant techno-economic depth on single components, such as the design of H_2 liquefaction plants, but not the overall supply chain. Examples and sources can be found in Appendix A.2 where component-specific aspects are described.

Other studies apply more holistic methodological approaches but do not focus on LH_2 supply or aircraft use cases, e.g., [38–43]. These investigate the integration of H_2 energy systems with renewable energy supply (RES). While most articles focus on the general supply chain design, some also analyze geographical contexts using simplified techno-economic models [44,45]. Another broad research field in this category is focusing on distributed hydrogen refueling systems for road vehicles or industrial applications [46–51]. In most of the studies, linear modeling approaches are chosen for energy system optimization to ensure reasonable computability [52]. This often leads to the use of simplified component models and constant parameters. Hence, such analyses cannot fully reflect all techno-economic effects and component design rules.

Only a recent study from Sens et al. [53] analyzes supply chains for a LH_2 end application, heavy-duty vehicles, applying a comprehensive techno-economic study design. Nevertheless, they also use a linear modeling approach neglecting dynamic effects and change of efficiencies when operating RES and H_2 component systems. Furthermore, their study does not focus on aviation and significantly larger concentrated demands at one specific location (airport) which can lead to relevant economies of scale effects [37].

In the present paper, a detailed optimization study is carried out to understand the techno-economics of aviation-dedicated LH_2 supply chains along three research questions:

- What are the main techno-economic factors enabling competitive green LH_2 fuel supply at or near airports and hence, the economic competitiveness of H_2-powered aviation?
- Are there general design rules for such LH_2 on-site production systems to enable the lowest costs?
- How do the derived economics and design rules change if also off-site, import supply chains are considered?

A further novelty of this study is that non-linear characteristics of relevant components are modeled for optimization. This is important because the two main conversion systems, the electrolysis system, and liquefaction plant, have variable efficiencies depending on their operational set point. Investigating these aspects might help future studies to derive more realistic techno-economic assumptions when less complex component descriptions have to be used for computability reasons.

Therefore, this paper is structured as follows. In Section 2, the methodology and the optimization problem are explained. Then, in Section 3, the resulting techno-economics of LH_2 on-site supply chains including design rules and parameter variations in the form of a scenario analysis are shown. In Section 4, the costs of LH_2/GH_2 off-site supply chains are determined based on the selected techno-economic scenarios. Finally, conclusions as well as limitations and future fields of research are derived in Section 5.

For better readability, detailed component models and more detailed overviews of all optimization results are presented in the Appendix and a Supplementary Material file, respectively.

2. Methodology

For a better understanding of the study results, the study design, the optimization methodology, and the scenario definitions are presented in this section.

2.1. General design of study

As a start, the study objectives, the LH_2 supply chain setups that are relevant to the aviation use case, and brief component overviews are introduced.

Objectives

The general aim of the present study is to determine the most economically competitive, green LH_2 supply pathways for airports based on varying LH_2 demand sizes. Therefore, a dedicated deployment of RES and LH_2 supply pathways to an airport is investigated.

It could be argued that larger LH_2 uptake from aviation is not expected before the years 2035 to 2040 [1] and hence, H_2 could then be bought from existing H_2 markets. However, it is assumed that there will be different accessibility to existing H_2 markets for airports in the future depending on the geography and the size of the airport. This justifies the analysis of dedicated LH_2 infrastructure installations. Consequently, this study's approach is relevant for larger airports, where the uptake of H_2 might dominate other close-by H_2 demand applications [37]. There, a dedicated on-site or off-site infrastructure might lead to the lowest supply costs. It is also worth investigating dedicated infrastructure setups for smaller airports without any access to an existing H_2 market. On the other side, if smaller airports have access to an H_2 market i.e. through a GH_2 pipeline or a close-by central production hub, dedicated infrastructure deployments might rather not be too relevant.

Nevertheless, all resulting costs of dedicated LH_2 supply chains for aviation should always be compared to general H_2 market costs to decide on the best supply options.

LH_2 supply system: components and pathways

In general, three component classes are relevant for LH_2 energy systems: conversion, storage, and transport components. Thus, three main supply setups are likely combining the component classes for an airport LH_2 supply chain [33,37,54,55]. In Fig. 1, an LH_2 on-site, LH_2

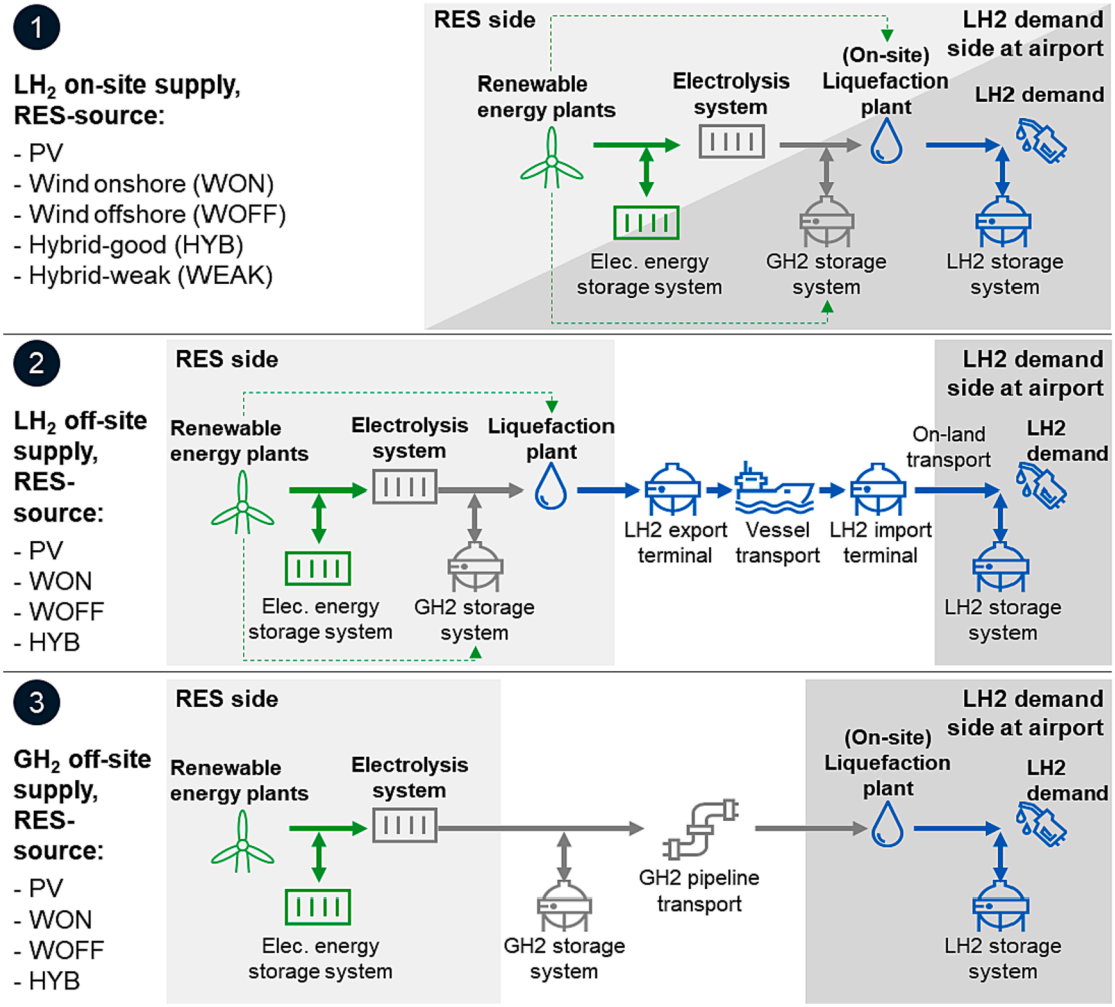

Fig. 1. Considered LH_2 supply pathways to refuel LH_2-powered aircraft in this study; naming of supply setups based on different renewable energy sources (RES): PV – photovoltaics, WON – wind onshore, WOFF – wind offshore, HYB – good hybrid, WEAK – weak hybrid location (see Section 2.3).

off-site, and a GH_2 off-site supply are shown.

In a LH_2 on-site supply scenario (case 1 in Fig. 1) the RES, H_2 production and H_2 liquefaction are at or close to the airport and no longer-distance transport of H_2 is required.

In that setting, the following conversion components are required: green electricity is generated from RES which can be photovoltaics (PV), wind onshore (WON), or wind offshore (WOFF) plants. These power water electrolysis systems (ELY) convert water into GH_2 and oxygen. Such a system might also include a compressor to increase the pressure of the GH_2 output – depending on the electrolysis technology chosen and the system requirements behind the ELY. Then, the GH_2 is cooled down to reach its liquid phase, LH_2, at ~20 K in an H_2 liquefaction plant (LFP).

Alongside these conversion steps, storage systems can buffer and balance fluctuations in production versus demand. Electric energy storage systems (ES) can be combined with the RES, while GH_2 storage systems are placed behind the ELY. For the latter, either underground caverns or aboveground pressurized storages are considered. For both of these options, compressors are installed on the intake side. Given the H_2 output pressure of the ELY the GH_2 compressor increases the H_2 feed to the required nominal pressure of the storage (e.g., 180 bar for a cavern). The use of a constant pressure valve is assumed for unloading the GH_2 storages, so no further compressor power is needed. Lastly, an aboveground LH_2 storage system buffers the liquefied H_2, before it enters the LH_2 refueling system at the airport. In this study, the LH_2 storage includes cryogenic H_2 pumps to fill and empty the storage most efficiently with the least H_2 losses [34,37]. Another option with high losses would be unloading making use of pressure differentials.

In this study, LH_2 refueling systems will not be considered in detail, since the main techno-economics and design choices were already discussed in an own analysis [37].

Compared to the on-site supply, the RES, ELY, and LFP are now at an exporting location in an LH_2 off-site scenario (case 2 in Fig. 1). LH_2 is then transported via large oversea vessels and an on-land transport mode (can also be >100 km) to the airport. Export and import terminals are installed which consist mainly of LH_2 storages and cryopumps for loading and unloading of the LH_2 vessel. For on-land transportation, only LH_2 truck transport systems are considered in this study. However, this could also be done using inland vessels or train systems, e.g., to avoid road congestion. Such transport modes often come with higher costs for very short distances and only similar or lower costs for longer distances above 300 km [56].

In a GH_2 off-site scenario (case 3 in Fig. 1), gaseous H_2 is generated at an export region but then transported via GH_2 pipeline systems to the receiving airport. In that case, the LFP is also placed at the airport which leads to a "disconnect" between the H_2 generation and the LH_2 energy system. The GH_2 pipelines can either be built "greenfield", so installing new pipeline routes, or retrofitting existing natural gas pipelines that are currently or will not be operated anymore in the near- to mid-term future. Furthermore, GH_2 compressor and valve stations are required in a regular distance which depends on several parameters presented in Appendix A.2.4 and discussed in Section 4.2 [46,57,58]. In the retrofitting case, existing stations are replaced and H_2-compatible coatings are applied to the pipes. This is an option currently planned in Europe, called the European Hydrogen Backbone (EHB) [57]. Pipelines are assumed to only transport GH_2 and do not function as flexible storage in the energy system (static load operation). If H_2 is consumed at the importing location, the same amount has to be loaded into the pipeline at the origin / export location. Compared to current operating principles of larger natural gas pipelines this is a valid approach as shown in [57–59].

2.2. Methodology and model equations

The optimization problem is defined by the objective function, optimization variables, main constraints, and operating principles.

Optimization objective function

The overall objective is to minimize total costs for LH_2 supply at airports. Therefore, the total annual costs C_{TAC} per component i are calculated as shown in Eq. 1. The total annual costs are determined for a specific time period (scenario) :

$$\min \sum_i C_{TAC,i,t} = C_{TAC,CAPEX,i,t} + C_{TAC,OPEX,i,t} \quad \text{USD} \tag{1}$$

The total annual costs are composed of capital expenditures (CAPEX) $C_{TAC,CAPEX,i,t}$, and operating expenditures (OPEX) $C_{TAC,OPEX,i,t}$. The CAPEX depends on the sizing x_i of each component (Eq. 2). Applying the annuity payment factor method (Eq. 2 & 5), the CAPEX is determined as follows:

$$C_{TAC,CAPEX,i,t}(x_i) = C_{CAPEX,total,i,t}(x_i) \cdot a_{i,t} \quad \text{USD} \tag{2}$$

$$C_{CAPEX,total,i,t}(x_i) = C_{CAPEX,direct,i,t}(x_i) \cdot f_{inst,i} \cdot f_{ind,i} \cdot \frac{1}{f_{avail,i}} \quad \text{USD} \tag{3}$$

$$C_{CAPEX,direct,i,t}(x_i) = r_{i,t} \cdot C_{CAPEX,direct,i,2020}(x_i) \quad \text{USD} \tag{4}$$

$$a_{i,t} = \frac{(1+i_{i,t})^{T_{DP,i,t}} \cdot i_{i,t}}{(1+i_{i,t})^{T_{DP,i,t}} - 1} \tag{5}$$

In Eq. 3, the total component CAPEX are calculated by multiplying the scenario-independent factors for installation costs $f_{inst,i}$, indirect project costs $f_{ind,i}$, and the availability of each component $f_{avail,i}$ with the direct CAPEX ($C_{CAPEX,direct,i,t}$) of the components. Latter is derived based on direct CAPEX reference curves in 2020 ($C_{CAPEX,direct,i,2020}$) and a cost reduction factor $r_{i,t}$, see Eq. 4. The direct CAPEX functions are provided in Appendix A.1. The cost reduction factors are used to translate costs into the specific time period (scenario) while reflecting learning effects (see Appendix A.1.1). Lastly, the CAPEX calculation uses the annuity factor which is calculated with the interest rate $i_{i,t}$ and the depreciation period $T_{DP,i,t}$ (Eq. 5).

In Eq. 3, the total component CAPEX are calculated by multiplying the scenario-independent factors for installation costs $f_{inst,i}$, indirect project costs $f_{ind,i}$, and the availability of each component $f_{avail,i}$ with the direct CAPEX ($C_{CAPEX,direct,i,t}$) of the components. Latter is derived based on direct CAPEX reference curves in 2020 ($C_{CAPEX,direct,i,2020}$) and a cost reduction factor $r_{i,t}$, see Eq. 4. The direct CAPEX functions are provided in Appendix A.1. The cost reduction factors are used to translate costs into the specific time period (scenario) while reflecting learning effects (see Appendix A.1.1). Lastly, the CAPEX calculation uses the annuity factor which is calculated with the interest rate $i_{i,t}$ and the depreciation period $T_{DP,i,t}$ (Eq. 5).

Total annual costs from OPEX (Eq. 6) are derived based on fixed operations and maintenance (OM) cost factors $c_{OM,i,t}$ for most components. Only the ELY and transport modes have other OM costs $C_{OM,other,i,t}$ which are described in the Appendix A.2.2 and A.2.4.

$$C_{TAC,OPEX,i,t} = C_{CAPEX,total,i,t}(x_i) \cdot c_{OM,i,t} + C_{OM,other,i,t} + C_{H2O,i,t} + C_{refri,i,t} + C_{fuel,i,t} \quad \text{USD} \tag{6}$$

Furthermore, costs for water supply $C_{H2O,i,t}$, loss of refrigerant fluids $C_{refri,i,t}$ and fuel $C_{fuel,i,t}$ are relevant for the ELY, the LFP and transport modes, respectively.

Since the total energy system optimization already reflects the operational costs of drawing electricity by installing RES, electricity costs are accounted for separately and not for each component in this study. The same approach is used for accounting costs for H_2 losses, which are compensated by sizing all required system components bigger.

Optimization variables and main constraints

In the following, technical aspects are highlighted of how these LH_2 supply pathways are optimized – starting with the optimization

variables.

The optimization variables are shown in Table 1. The sizing of compressors and cryopumps are not treated as separate optimization variables and are always designed accordingly to the storage size and required charging / discharging mass flows.

In addition to the design sizes, the decision of building a storage component or not is optimized using binary variables (row 8). Lastly, the pressure level of the GH_2 as the output of the ELY is also subject to optimization (row 9).

Main constraints exist for each component system and are discussed in detail in Appendix A.2. In general, constraints are that maximum power or mass flow settings as well as minimum and maximum fill levels of all storage systems must not be exceeded. Additionally, storage fill levels must be equal or larger at the end of the simulation compared to the initial state of charge.

Other modeling constraints result from the balance equations of the different components that are interconnected on an electric power, GH_2 mass flow, and LH_2 mass flow level as shown in Fig. 1. First, the electric power balance is derived in Eq. 7a for the LH_2 on– and off-site supply pathway, for GH_2 off-site cases in Eq. 7b:

$$\text{LH2-on-/off-site} : P_{RES} = P_{ELY} + P_{LFP} + P_{GH2comp} + P_{ES}\,\text{W} \quad (7a)$$

$$\text{GH2-off-site} : P_{RES} = P_{ELY} + P_{GH2comp} + P_{ES}\,\text{W} \quad (7b)$$

In the LH_2 on-site scenario, the RES (P_{RES}) powers all major components that draw electricity like the ELY (incl. compressors) P_{ELY}, the LFP P_{LFP}, the compressors of the GH_2 storage systems $P_{GH2comp}$ and the ES P_{ES}. For all storage components positive power or mass flow values are defined as charging (vs. negative for discharging). Only the cryopumps of the LH_2 storage system are not connected to the RES but to a local electricity grid as described for LH_2 refueling systems in [37]. This is important because it enables discharging the LH_2 storages to fulfill demands when no RES availability is given (no wind, no radiation).

For off-site LH_2 supply, the balance equation does not change, since the LFP is still placed at the exporting energy system site.

If off-site GH_2 supply (Eq. 7b) is analyzed, the LFP is placed at or close to the airport. Consequently, the electricity for the LFP is also sourced by grid electricity at the airport directly.

Second, the balance equation regarding GH_2 mass flows is defined in Eq. 8a-c:

$$\text{LH2-on-/off-site} : \dot{m}_{ELY} = \dot{m}_{GH2Sto} + \dot{m}_{LFP,in}\,\text{kg/s} \quad (8a)$$

$$\text{GH2-off-site} : \dot{m}_{ELY} = \dot{m}_{GH2Sto} + \dot{m}_{pipe,in} \text{and} \dot{m}_{pipe,out} = \dot{m}_{LFP,in}\,\text{kg/s} \quad (8b,c)$$

The GH_2 mass flow output of the ELY $\dot{m}_{ELY}$ feeds either the LFP directly $\dot{m}_{LFP,in}$ or is stored in one of the two storage $\dot{m}_{GH2Sto}$ options (cavern or above-ground) in an LH_2 on- or off-site setup.

For off-site GH_2 supply, the pipeline system is added before the feed enters the LFP, leading to the separation of the balance equation in Eq. 8b. However, when realizing such a GH_2-off-site system, the GH_2 storages could also be placed differently – at the airport side or even along the pipeline route.

Since different GH_2 pressure levels are required for filling the GH_2 storages (180–200 bar), the LFP (30–80 bar), or the pipeline system (intake at 70 bar), the pressure setting of the ELY output mass flow is a variable for optimization. With that not only the sizing of compressors can be optimized, but also the specific energy consumption of the LFP. As shown in Appendix A.2.3, the minimal work required for liquefaction decreases slightly with higher input feed pressures. Further information on the pressure dependencies for the depicted components is presented in Appendix A.2.2–4.

Third, the LH_2 mass flow balances are shown in Eq. 9a-d:

$$\text{LH2-on-/GH2-off-site} : \dot{m}_{LFP,out} = \dot{m}_{LH2Sto} + \dot{m}_{LH2demand}\,\text{kg/s} \quad (9a)$$

$$\text{LH2-off-site} : \dot{m}_{LFP,out} = \dot{m}_{LH2,export} + \dot{m}_{LH2vessel} \text{and}\,\text{kg/s} \quad (9b)$$

$$\text{LH2-off-site} : \dot{m}_{LH2vessel} = \dot{m}_{LH2,import} + \dot{m}_{LH2truck} \text{and} \quad (9c)$$

$$\text{LH2-off-site} : \dot{m}_{LH2truck} = \dot{m}_{LH2Sto} + \dot{m}_{LH2demand} \quad (9d)$$

In the LH_2 on-site and GH_2 off-site setups, the LFP mass flow output $\dot{m}_{LFP,out}$ is directly linked with the LH_2 demand ($\dot{m}_{LH2demand}$) and the LH_2 buffer storages ($\dot{m}_{LH2Sto}$) at the airport. Only in the off-site LH_2 supply case, the LH_2 output of the LFP is decoupled with the airport side and first transported via vessels ($\dot{m}_{LH2vessel}$) and then with on-land transport modes (truck in this study, $\dot{m}_{LH2truck}$). On the export and import side, there are also storage terminals that can be used for buffering ($\dot{m}_{LH2,export}$, $\dot{m}_{LH2,import}$).

It has to be noted, that the chosen level of detail of the technical component model does not consider differing state variables such as temperatures or LH_2 pressures.

Operation of components: energy management system and paradigms

To enable the optimization of the previously described systems, operating principles for each component have to be defined. Fixed operating rules are chosen to ensure the computability of the optimization even with non-linear models.

The main goal of the energy management system is to maximize the utilization of cost-dominating components, which in this study are the ELY and the LFP. In dependence on the RES availability P_{RES} and the LH_2 demand $\dot{m}_{LH2demand}$ at the airport, these two components are steered to make maximum use of available RES while always fulfilling LH_2 demands for aircraft refueling. In addition to that, the given component constraints also apply.

If storage systems are installed, the state of charge / fill level influences the operation of the components, too. The state Z of the storage component i is defined as empty ("0"), full ("2"), and flexible ("1") when the storage can only be charged, discharged, or both, respectively.

In the LH_2 on-site supply pathway, the ELY is set ($P_{ELY,set}$) for maximum usage of RES ($P_{ELY,set,RES}$) or its output is limited, if no further GH_2 can be liquefied or stored ($P_{ELY,set,GH2}$), see Eq. 10–12.

$$\text{ELY set-value (in W)} : P_{ELY,set} = \min\left(P_{ELY,set,RES}, P_{ELY,set,GH2}\right) \quad (10)$$

$$\text{with } P_{ELY,set,RES} = \begin{cases} P_{RES} - P_{LFP} - P_{GH2comp}, Z_{ES} = 0 \\ P_{RES} + P_{ES,max} - P_{LFP} - P_{GH2comp}, Z_{ES} \neq 0 \end{cases} \quad (11)$$

$$\text{with } P_{ELY,set,GH2} = \begin{cases} P_{ELY}\left(\dot{m}_{LFP,in} + \dot{m}_{GH2Sto,max}\right), Z_{GH2Sto} \neq 2 \\ P_{ELY}\left(\dot{m}_{LFP,in}\right), Z_{GH2Sto} = 2 \end{cases} \quad (12)$$

The LFP operation $\dot{m}_{LFP,in,set}$ is set similarly (Eq.13–15). Here, also the GH_2 feed availability from ELY or GH_2 storages ($\dot{m}_{LFP,in,set,GH2}$) or the offtake of LH_2 from aircraft or an LH_2 storage system ($\dot{m}_{LFP,in,set,demand}$) can

Table 1
Optimization variables considered in this study.

	Component or systems	Optimization variable
1	Renewable energy sources (PV, WON, WOFF) – maximum power rating	$P_{PV,max}$, $P_{WON,max}$, $P_{WOFF,max}$
2	Electrolysis system – max. power rating	$P_{ELY,max}$
3	Electric energy storage – max. electric energy stored	$E_{ES,max}$
4	GH_2 storage (Sto): cavern, above-ground (AG) – max. mass stored and initial state of charge	$m_{GH2Sto,cavern,max}$, $m_{GH2Sto,AG,max}$, $F_{GH2Sto,0}$
5	Liquefaction plant – max. capacity per day	$\dot{m}_{LFP,in,\,max}$
6	LH_2 storage (Sto) – max. mass stored and initial state of charge	$m_{LH2Sto,max}$,,$F_{LH2Sto,0}$
7	Transportation design – annual departures of LH_2 vessels	$n_{vessel,departures}$
8	Binary variables for storage systems i	$b_{built,i}(0,1)$
9	Pressure output of GH_2 from ELY and on GH_2 bus	p_{GH2bus}

limit the maximum operation of the LFP:

$$\text{LFP set-value (in kg/s)} : \dot{m}_{\text{LFP,in,set}} = \min\left(\dot{m}_{\text{LFP,in,set,GH2}}, \dot{m}_{\text{LFP,in,set,demand}}\right) \tag{13}$$

$$\text{with} \quad \dot{m}_{\text{LFP,in,set,GH2}} = \begin{cases} \dot{m}_{\text{ELY}}, Z_{\text{GH2Sto}} = 0 \\ \dot{m}_{\text{ELY}} + \dot{m}_{\text{GH2Sto,max}}, Z_{\text{GH2Sto}} < 0 \end{cases} \tag{14}$$

$$\text{with} \quad \dot{m}_{\text{LFP,in,set,demand}} = \begin{cases} \dot{m}_{\text{LFP,in}}\left(\dot{m}_{\text{LH2demand}} + \dot{m}_{\text{LH2Sto,max}}\right), Z_{\text{LH2Sto}} \neq 2 \\ \dot{m}_{\text{LFP,in}}\left(\dot{m}_{\text{LH2demand}}\right), Z_{\text{LH2Sto}} = 2 \end{cases} \tag{15}$$

The available RES should be used completely to reach maximum capacity factors and hence, minimized levelized costs of electricity (LCOE). However, when the settings of the ELY and LFP have to be reduced as described in Eq. 12 and 15, the renewable energy generation will also be capped.

The operating values for the storage systems are determined based on the ELY and LFP settings following the balance Eq. 7a/b, 8a-c, and 9a-

Table 2
Economic parameters for main components – further details shown in Appendix A.1 and A.2. Note: resulting total specific CAPEX are shown incl. installation and indirect project costs, total cost equations are derived in A.1.

Component	Parameter	Unit	2020 reference	2035 base	2050 base	2050 progressive	Sources
PV (1-axis tracking)	Specific total CAPEX	USD/kW	650	600	400	300	[61–66]
	Depreciation period	Years	30	30	30	40	[61–63,66]
	O&M factor	%	2.5%	2.5%	2.5%	2.5%	[61–63]
Wind onshore	Specific total CAPEX	USD/kW	1,300	1,100	900	675	[61,62,67–69]
	Deprec. period	Years	25	25	25	30	[63,67]
	O&M factor	%	3.6%	3.6%	2.8%	2.8%	[63,67]
Wind offshore	Specific total CAPEX	USD/kW	2,900	2,500	2,250	1,687	[61,62,67–69]
	Deprec. period	Years	25	25	25	30	[63,66,67]
	O&M factor	%	3.2%	3.2%	3.3%	3.3%	[61,63,66,67]
Electric energy storage	Specific total CAPEX	USD/kWh	350	200	150	112	[53,62,64,70]
	Deprec. period	Years	15	15	15	15	[53,62]
	O&M factor	%	3.0%	3.0%	3.0%	3.0%	[53,62]
Electrolysis system	Specific total CAPEX	USD/kW	1,500	438	285	214	[71–76]
	Deprec. period	Years	30	30	30	30	[77–83]
	Stack lifetime[a]	Operating hours	<90 k	90 k	120 k	120 k	[72,75,78,79,81,84]
	O&M factor	%	3.0%	3.0%	3.0%	3.0%	[77,79,81,85–87]
GH_2 compressor	Specific total CAPEX[b]	USD/kW	1,636	1,489	1,243	1,243	[88–92]
	Deprec. period	Years	15	15	15	15	[88,93]
	O&M factor	%	2.0%	2.0%	2.0%	2.0%	[47,88,92,94–96]
Liquefaction plant	Specific total CAPEX[b]	Mn USD/tpd	1.33	1.13	0.84	0.63	[73,89,93,97–103]
	Deprec. period	Years	20	20	20	25	[97,104]
	O&M factor	%	4.0%	4.0%	4.0%	4.0%	[75,104,105]
GH_2 cavern storage	Specific total CAPEX[b]	USD/$kgGH_2$ stored	18	18	18	18	[47,79,88,106–111]
	Deprec. period	Years	30	30	30	40	[108–112]
	O&M factor	%	2.0%	2.0%	2.0%	2.0%	[47,113]
GH_2 above-ground storage	Specific total CAPEX[b]	USD/$kgGH_2$ stored	581	529	442	442	[65,82,110,111,91,97, 99,101,103,107–109]
	Deprec. period	Years	20	20	20	30	[53,88,96]
	O&M factor	%	1.5%	1.5%	1.5%	1.5%	[71,95,96,118]
LH_2 storage	Specific total CAPEX[b]	USD/$kgGH_2$ stored	41	35	26	26	[88,106,119]
	Deprec. period	Years	20	20	20	30	[47,96]
	O&M factor	%	2.0%	2.0%	2.0%	2.0%	[47]
LH_2 cryopump	Specific total CAPEX	USD per kg/h	416	354	264	264	[37,93,99]
	Deprec. period	Years	10	10	10	10	[37,93]
	O&M factor	%	3.0%	3.0%	3.0%	3.0%	[37,93,99]
LH_2 truck	Specific total CAPEX	Mn USD per truck system	1.01	0.86	0.64	0.64	[47,53,75,88,89,100]
	Deprec. period	Years	12	12	12	12	[37]
	O&M factor[c]	%	3.0%	3.0%	3.0%	3.0%	[37]
LH_2 vessel	Specific total CAPEX[b]	Mn USD per vessel	n/a	342	274	274	[53,75,80,101,120–122]
	Deprec. period	Years	n/a	25	25	25	[53,101]
	O&M factor[d]	%	n/a	4.0%	4.0%	4.0%	[53,80,123]
GH_2 pipeline	Specific total CAPEX[b]	Mn USD/km	n/a	3.45	2.76	2.76	[53,80,93]
	Deprec. period	Years	n/a	40	40	40	[53,80]
	O&M factor	%	n/a	1.0%	1.0%	1.0%	[80]

a) stack replacement costs are assumed to be 20% of the total CAPEX (incl. installation and indirect costs) [77,80,83,87].
b) at largest design scaling – more detailed specific CAPEX curves for different component design sizes to be found in Appendix A.2.
c) Further variable costs: driver salary of 35 USD/h and fuel costs of 3 USD/kgH_2 [37].
d) Further variable costs: annual other OPEX costs of 11.3 Mn USD and fuel costs of 2.5 USD/kgH_2 [80,124].

d. It has to be noted that for the GH_2 storages, no re-allocation of GH_2 mass flows is considered between the two options (cavern and above-ground).

If the supply pathway is changed to an LH_2-off-site setup, the same operating rules apply for the energy system up to the point where LH_2 would be fed into the refueling system. The only difference is that a specific demand profile is used for the LH_2 export terminal (discussed in Section 2.3).

For GH_2-off-site supply pathways, the ELY and GH_2 storages are operated also in a similar manner as described above. Only the LFP is now steered more independently since it does not depend on the availability of RES at the export region but can draw electricity from a local grid at the airport flexibly. One limiting factor though is the availability of GH_2 from the ELY and GH_2 storages that are directly fed into the LFP via the pipeline system, which is operated statically as described in Section 2.1.

2.3. Scenario definitions

The optimization problem is solved for several scenarios specified by different techno-economic parameters, RES locations, and airport settings.

Techno-economic parameters

Table 2 shows the main techno-economic parameters of the supply components used in this study for three main scenarios.

Since major LH_2 uptake from aviation is rather expected for 2050 and later [1,2,29,37], the main scenario is called the "2050 base case". It reflects great progress in the deployment of general green H_2 infrastructure for main use cases, e.g., chemicals, and industry. With this, the cost reduction potential compared to today is already significant for GH_2 production, but also LH_2 components would be installed for hard-to-abate transport modes and general transport/trade of H_2. To be able to reflect sensitivities of the cost results from a 2050 base case scenario, two other scenarios are considered: a more conservative one, the "2035 base case" and a very progressive one, the "2050 progressive case". Given these three scenarios, a valid range of resulting LH_2 supply costs in 2050 should result.

For better readability, further parameters and cost functions are derived in Appendix A.1 and A.2. Moreover, all derived costs are transferred to USD_{2020} and cost values from literature are corrected for the right currency as well as inflation effects using the Chemical Engineering Plant Cost Index (CEPCI) [60].

Renewable electricity costs for the energy consumptions of LH_2 cryopumps and the LFP in the GH_2 off-site pathway are assumed to be 50 USD/MWh through a Power Purchase Agreement (PPA) [37,47].

Water for the electrolysis might come from the local supply or desalination if only salt water is available. Costs for the latter are taken to have a rather conservative estimate of water costs given the potential scarcity of water in specific geographies [125]. As shown by Caldera and Breyer (2019) [126], desalinated water including transport costs could cost <2.24 USD/m^3 of water nearly everywhere.

Since the annuity payment factor method is used, a fixed interest rate (cost of capital) is chosen. In this study, RES and electric energy storages have a 4% interest rate [61,67,127]. Markets for these technologies are established with lower financing risks. H_2 generation, conversion, and storage components are assumed to have an interest rate of 6% to reflect slightly larger risk or higher return expectations in H_2 business plans [37,93]. It has to be noted that the interest rate highly depends on the country where the project is planned and executed [59,127]. Since this study focuses on more generic analyses of techno-economics, no further sensitivities from differing interest rates are considered. This will be part of future work.

RES locations and settings

The chosen modeling approach is based on a time resolution of 8760 h per year. Therefore, input profiles of RES availability and the LH_2 demand at the airport are derived. In this part, the choice of RES locations and their characteristics are explained.

It is the main goal of the paper to derive general design rules for LH_2 energy systems as well as best versus worst potential supply costs. Consequently, five generic locations are investigated in this study that stand for specific, "archetypical" RES (weather) conditions:

- PV: strong PV (e.g., Saudi-Arabia),
- WON: strong wind onshore (e.g., Scotland [128,129]),
- WOFF: strong wind offshore (e.g., Denmark / Baltic Sea [130,131]),
- HYB: hybrid location with great wind onshore and PV conditions (e.g., Morocco [132]) and a
- WEAK: hybrid location with weaker conditions for wind onshore and PV (e.g., Central Germany, Frankfurt).

The solar yield and wind speed weather data for the reference year 2019 is obtained from the open-science platform "Renewable.ninja" [133,134] – further assumptions are presented in Appendix A.2.1. Additionally, projections of future wind power performances in the form of power curves are used for wind on– and offshore plants. These are also open-source and published by the U.S. National Renewable Energy Laboratory (NREL) and the International Energy Agency (IEA) [135–137].

The resulting capacity factors of the RES are shown in Fig. 2. Very high capacity factors can be achieved for the wind on- and offshore locations (WON and WOFF). Compared to previous work, e.g., in [44], the full load hours are higher here and might be more accurate, since they reflect future wind turbine performance. Many previous energy system studies use existing (older) wind turbine power curves that might not reflect the technological improvement of larger wind turbines. Great capacity factors at wind locations are followed by the hybrid wind onshore location. PV capacity factors are in general lower due to day-night cycles, but similarly good for the great PV and the good hybrid (HYB) location. At the weaker (WEAK) hybrid location, both capacity factors are significantly lower.

In addition to that, it is assumed that the RES might be placed in a radius of <100 km around the airport to make use of the best local RES sites. This is why costs for very short electricity transmission distances are also reflected, explained in Appendix A.2.1.

There is no grid connection modeled for the ELY and the LFP for two reasons. First, this complies with recent regulations presented by the European Commission [138]. For green H_2 supply, it will be required to have purpose-built renewable energy generation (additionality criteria)

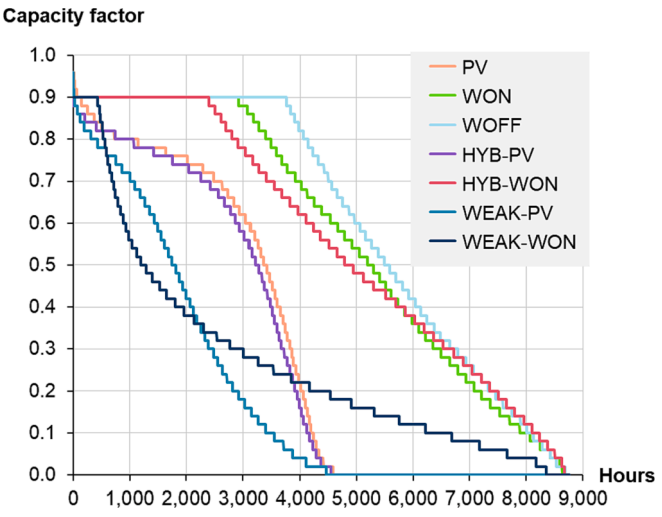

Fig. 2. Capacity factors of RES at chosen locations for the year 2019 (8760 h) incl. array losses for wind parks (see Appendix A.2.1).

that has a temporal and geographical correlation to the H_2 production. Only in a few cases, e.g., when the electricity market already has a share of >90% RES, a grid connection for the ELY would fulfill this regulation. Second, drawing electricity from a grid in times of no wind or solar radiation availability, an LH_2 production system designed for constant (grid) operation might lead to unacceptable loads in such a local grid. Especially at medium and larger airports where LH_2 production would require significant power capacity in that region [37]. In that case, grid supply might be prioritized for all basic energy consumption applications (private, commercial, and main industry sectors) and not for the use of aviation fuel. Nevertheless, the chosen dedicated infrastructure setup without a major grid connection can be seen as a "worst case" cost scenario, since no synergistic integration with local renewable energy systems is included in this analysis.

Airport settings

Lastly, the airport setting with the resulting LH_2 demands from aircraft is briefly characterized. A more detailed derivation of demands, safety and operational aspects of H_2-powered aviation can be found in previous papers [34,37].

Future LH_2 demand projections at airports highly depend on the size of the airport and air travel routes from that airport (short- vs. long-range flights). While these demands could reach levels of greater than 80 k and greater than 300 k tLH_2 per annum (p.a.) at medium and larger airports in a 2050 base case scenario, demands at smaller, national airports could be below 10–20 k tLH_2/a [37].

In addition to the total size of demands, the monthly and daily demands differ by season and daytime, see Fig. 3. Many European airports have a night curfew from 10/11 pm to 5/6 am, but there are also some without such a restriction. Seasonality of air travel demand with peaks in summer and autumn and lows in the winter season are also considered for the profile here.

For the following analysis of LH_2 off-site pathways, the demand curve at an export terminal (loading the LH_2 vessels) is also shown for reference. The vessel is loaded with a constant mass flow over 48 h. The variation of total LH_2 demand in a month is also applied in this off-site setup.

3. Liquid hydrogen on-site supply chains

The techno-economics of LH_2 on-site supply chains are now investigated. The purpose of this analysis is to derive design rules for the on-site energy systems based on different geographic conditions and annual LH_2 demand sizes at airports. Furthermore, the lowest versus highest costs for supply chains should be identified to answer the overarching question of the general economic implications for H_2-powered aviation.

The section is structured into three sections. First, the LH_2 costs are computed and general design rules are explained in detail for one specific LH_2 demand point in the 2050 base case scenario. Second, the techno-economic effects of varying LH_2 demands are highlighted. Third, the sensitivities of the resulting designs and LH_2 costs are tested based on scenarios with different techno-economic parameter assumptions.

3.1. LH_2 energy system design rules for fixed demand setting

This section showcases the optimization results for the on-site supply chains for a fixed annual demand point of 100 k tLH_2/a. The demand point was found to represent a medium to larger sized airport by Hoelzen et al. [37]. Furthermore, most economy–of-scale effects apply to such larger demands and make this point more relevant for deriving general design rules or generic design "recipes" for LH_2 energy systems.

The resulting total LH_2 supply costs at the dispenser (incl. refueling costs) are shown in Fig. 4. Great hybrid RES locations provide the best techno-economic conditions for LH_2 supply chains – costs range from 2.04 USD/kgLH_2 (HYB) to 2.25–2.27 USD/kgLH_2 (WON, PV) and between 3.04 and 3.63 USD/kgLH_2 at WEAK and WOFF, respectively.

At all locations, the RES (electricity) takes the main share of total costs (36–71%). The costs for RES also lead to the main economic difference in supply at the five locations. Looking into the LCOE of renewable energy generation this is emphasized: at PV, WON, HYB, WEAK, and WOFF electricity is generated at levelized costs of 14, 18, 18, 31, and 44 USD/MWh, respectively. While the high RES costs at WEAK locations are caused by low capacity factors, the comparably very high CAPEX of wind offshore turbines leads to the highest LCOE in a 2050 base case scenario at WOFF. Vice versa, the very low CAPEX for PV installations enables the lowest LCOE at PV regions even though their worse capacity factor compared to the wind regions.

Similar trends are observed analyzing the total investment costs of the on-site energy systems. These range from 1.9 Billion (HYB), 2.0 Bn (WON & PV), 2.9 Bn (WEAK), and 3.5 Bn USD (WOFF) with main investments required for RES, followed by the LFP and similar magnitudes for the ELY. CAPEX for the refueling system incl. all (on-site) LH_2 storage systems make up for only a 2–5% share of total investments.

Analysis of optimization results and derivation of design rules based on 100 k tLH_2/a demand point

For a better understanding of the results presented in Fig. 4, the

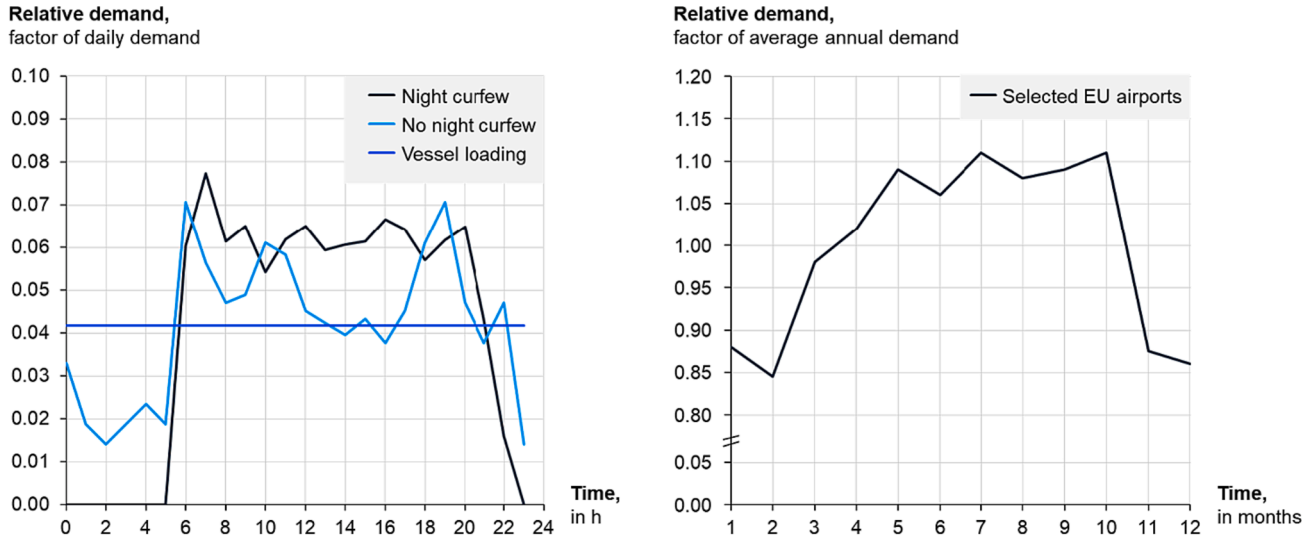

Fig. 3. LH_2 demand profiles – left: daily profile for airports with night curfew, no night curfew, or export regions (vessel loading); right: annual demand variation for an "average" EU airport; plots created based on data from exemplarily chosen airports [139–141] – see a similar approach in [37].

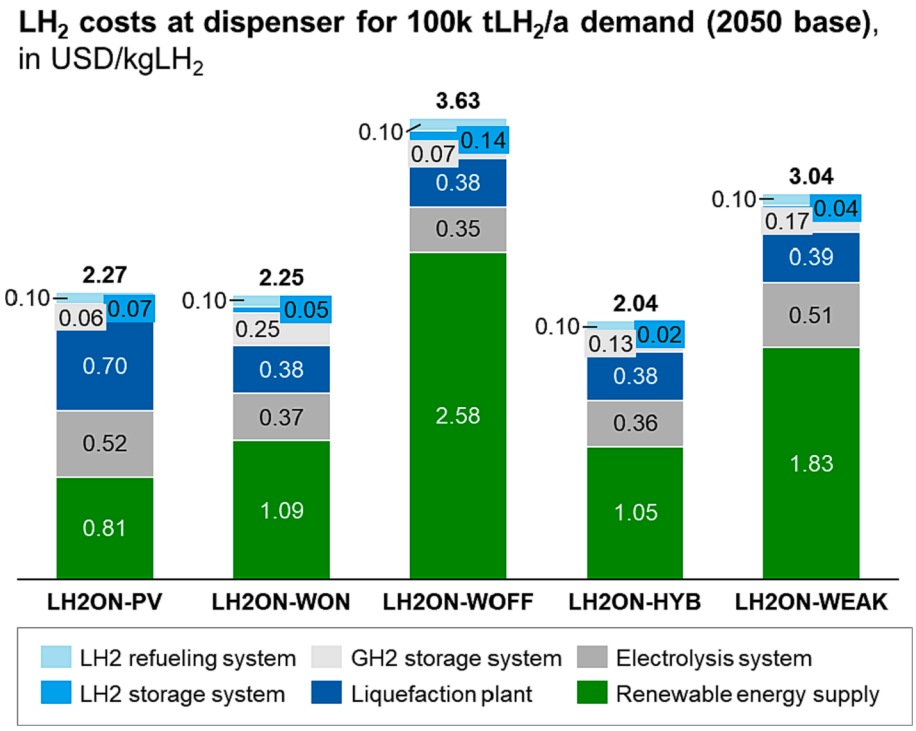

Fig. 4. LH_2 supply costs at the dispenser for on-site setups at five locations: PV, wind onshore (WON), wind offshore (WOFF), great hybrid conditions (HYB), weaker hybrid conditions (WEAK); 2050 base case scenario with 100 k tLH_2/a demand.

optimization data will be analyzed in more detail and seven design rules for LH_2 energy systems (for aviation) are derived.

I. Component selection: Electric energy storage as well as aboveground GH_2 storage capacities are not installed in the 2050 base case scenario (see corresponding columns in Table 3).

Both storage systems have too high CAPEX per energy stored (150 USD/kWh_{el} for ES, 12–15 USD/kWh_{H2} for GH_2 above-ground storage) compared to GH_2 caverns and LH_2 storages (both < 1 USD/kWh_{H2}). Even though the installation of an ES gives flexibility on the electricity balance and hence, would enable higher utilization of the ELY, it leads to very high supply costs.

II. RES: Smallest RES capacity installations are required at great wind on– and offshore and largest for weaker RES locations (see P_{RES} in Fig. 5).

Great PV conditions still lead to more than factor 2 higher capacity requirements vs. the wind setups, because H_2 can only be produced at day times when solar radiation is available. For great hybrid locations, RES installations are 1.5 factor higher than at strong wind regions, making use of both high PV and wind onshore power yields. This factor increases to 3 for WEAK setups due to the low capacity factors, which are also shown as utilization factors in Fig. 6A. In the hybrid setups, no strong preference for PV or wind onshore plant installations is observed (Fig. 5).

Fig. 6a also reveals that renewable energy generation has to be capped in all regions for some time periods, leading to lower realized capacity factors (RES used) than available (RES total). The reason for this is that no ES is installed to buffer the electricity when the ELY operates at maximum power.

Besides the costs and installation requirements, also the land use of the different RES has to be considered. If a land use of 20 MW/km^2 [142] and 100 MW/km^2 [61,143] is assumed for large-scale future wind onshore turbines and 1-axis tracking PV systems, respectively, the land needs become huge – comparable to the area of ~1,500–6,000 soccer fields. In the 100 k tLH_2/a demand setup, 23–83 km^2 of land would need to be available for RES. Such high land uses would justify the existence of wind offshore supply setups with significantly fewer turbines for regions with high land constraints despite higher supply costs.

III. ELY: Ely-system capacities are designed the smallest for locations with the least fluctuating RES profiles throughout the day (see Fig. 5, Table 3)

Table 3
Optimal design for five locations, 2050 base case scenario with 100 k tLH_2/a demand.

LH_2 setup/ location	Component	ELY $P_{ELY,max}$	LFP $\dot{m}_{LFP,in,max}$	Electric energy storage $E_{ES,max}$	Cavern storage $M_{GH2Sto,cavern}$	Aboveground storage $M_{GH2Sto,AG}$	LH_2 storage M_{LH2Sto}	GH_2 pressure behind Ely-system p_{GH2bus}
	Unit	MW	tons per day (tpd)	MWh	tons GH_2	tons GH_2	tons LH_2	bar
LH2ON-PV		1,439	642	–	1,498	–	2,066	30
LH2ON-WON		957	316	–	9,740	–	1,329	61
LH2ON-WOFF		923	331	–	2,084	–	4,701	44
LH2ON-HYB		946	304	–	4,091	–	384	73
LH2ON-WEAK		1,364	314	–	5,672	–	1,018	77

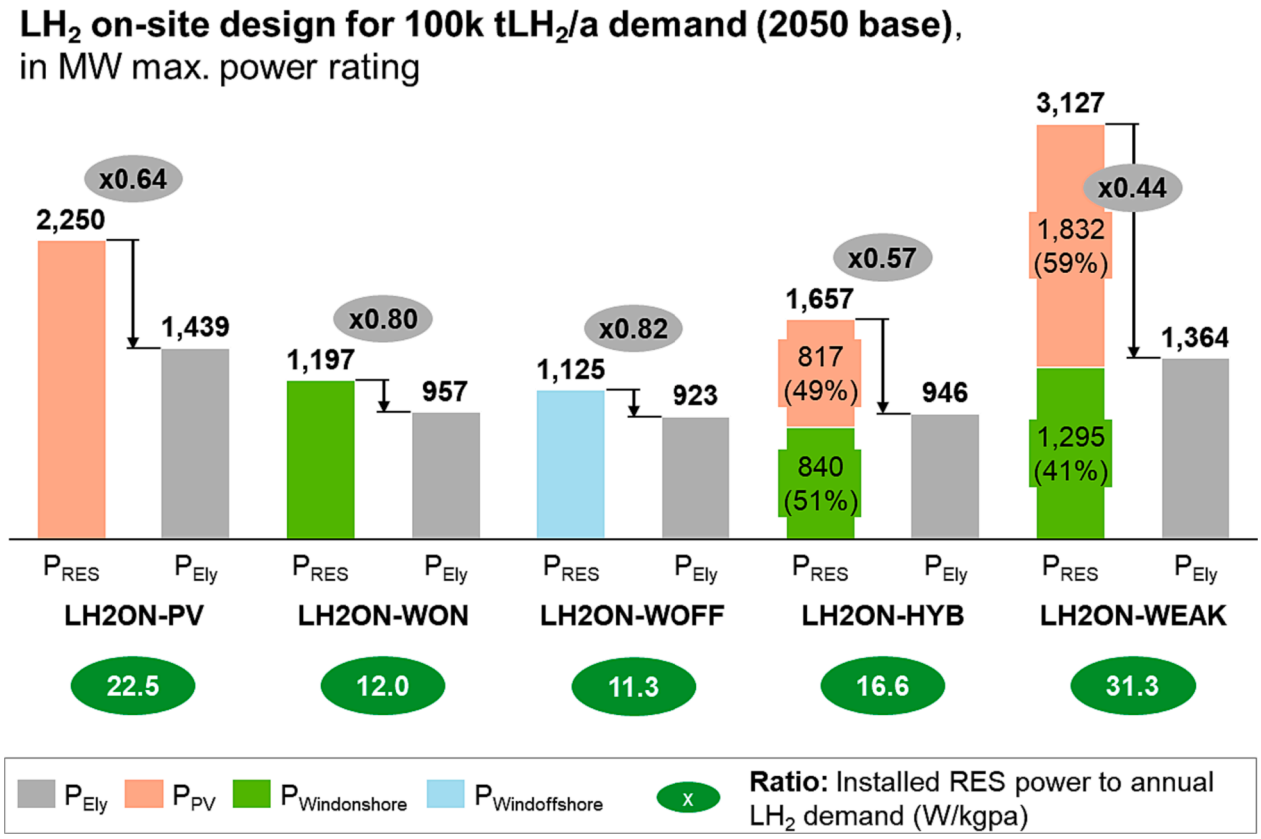

Fig. 5. Design of RES and ELY for five locations, 2050 base case scenario with 100 k tLH_2/a demand.

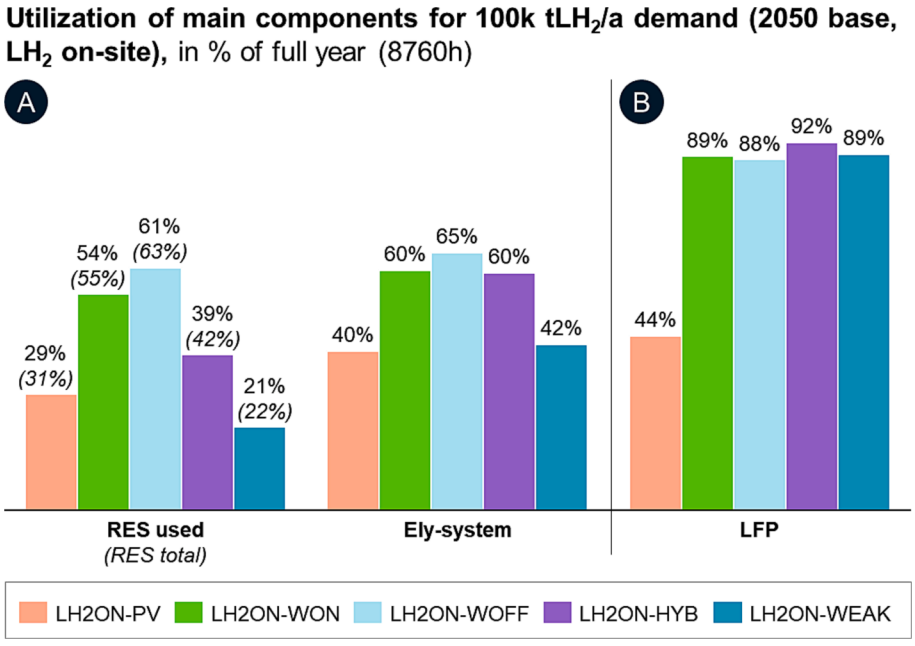

Fig. 6. Annual utilization of main components for five locations, 2050 base case scenario with 100 k tLH_2/a demand – left side, A. RES, ELY; right side, B. LFP.

Since no electric energy storage is installed, the ELY has to be operated flexibly following the availability of RES. Consequently, the smallest ELY capacities are installed at WON, WOFF, and HYB regions, where RES availability is relatively constant throughout the day.

So, the ELY is also designed smaller at the WEAK compared to the PV location due to a more evenly distributed RES availability (no large day and night difference). The resulting utilization of the ELY underlines this design rule, see Fig. 6A and the relative ELY size in relation to average daily LH_2 demands in Fig. 7.

IV. LFP: Its design is optimized for the smallest capacity and hence, maximum utilization due to high costs (mostly CAPEX) and significantly higher specific electricity consumption in part-load operation in all cases (see Table 3).

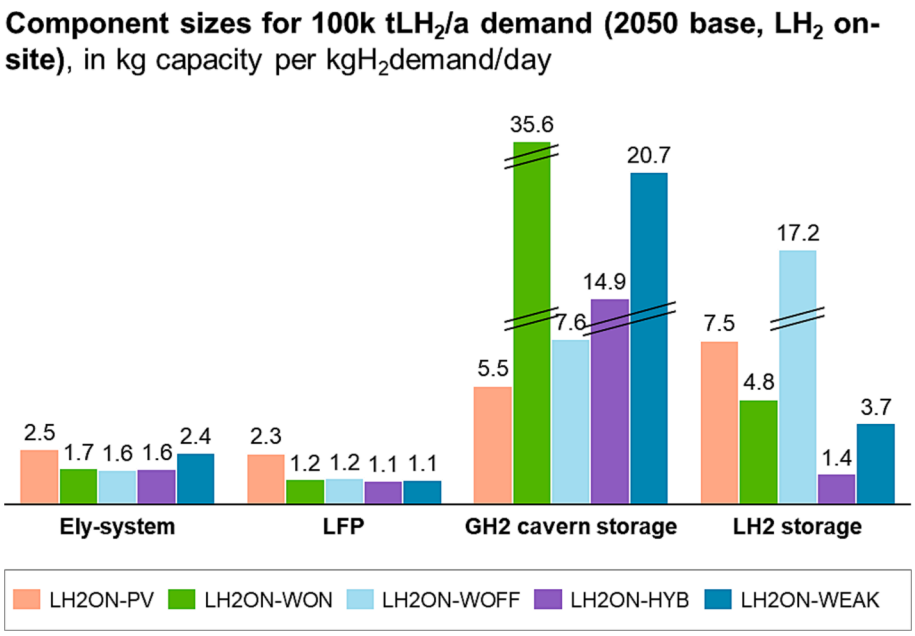

Fig. 7. Relative component design sizes compared to the average daily LH_2 demand (274 tLH_2/d) for five locations, 2050 base case scenario with 100 k tLH_2/a demand – ELY in kgH_2/d output, LFP in kgH_2/d intake and storages in kgH_2stored capacity.

The annual utilization reaches 88–92% (see Fig. 6B) – minor utilization "losses" are caused by time periods with part-load operation. In the case of the ELY (rule III), this is not an issue leading to significantly higher costs, since the ELY's specific energy demand even decreases in part-load operation (see also Fig. 7 for comparison of sizes between LFP and ELY).

Only at the great PV location no electricity is available at night. This is why, plus given that there is no ES installed, the LFP cannot be designed for the highest utilization (44% only). Thus, the LFP is shut off at night (~12 h). The costs for installing ES to enable maximum utilization of the LFP are higher than having a more flexible operation of the LFP and the penalty of higher electricity consumption. It has to be noted that there is no information available on the energy consumption or general feasibility of such an operation of the LFP. Hence, only cost penalties for part-load operations but not for "half day on"/"half day off" operations are considered in this study.

V. Storages: Designs highly depend on RES fluctuations (daily and seasonal). In most cases, building larger GH_2 cavern storages should be preferred versus LH_2 storages (see Table 3 and Fig. 7)

Even though the CAPEX of larger GH_2 cavern and LH_2 storage systems do not differ too much, the main benefit of having a large GH_2 storage is a more constant feeding of the LFP and hence, enabling its maximum utilization (rule IV).

When adding GH_2 and LH_2 storage sizes, total storage capacities are lowest for the PV location where seasonal RES fluctuations are not too distinctive. There, the LH_2 storage is used for the daily mass flow buffering when the sun is not shining, but air traffic is requiring LH_2 as a fuel. Then, the hybrid (HYB, WEAK) locations follow with very small sizing requirements for daily buffering storage in the LH_2 tanks. Wind turbines can supply the energy system also at times without sunlight. However, the seasonal storage in the form of the GH_2 cavern storage has to be sized significantly larger (factor ~ 3 vs. PV) to compensate for larger seasonal fluctuations in RES availability. At WON, both larger seasonal GH_2 and larger daily LH_2 buffer storages are installed to enable the high utilization of the LFP (rule IV).

Only in the WOFF location, a larger LH_2 storage is built than the GH_2 cavern storage. It can be explained by the annual wind power curve which shows not a large seasonal variation of availability over several months in a year, but higher, recurrent fluctuations in each month with very low wind power yields over several days mixed with very high wind power yields on other days. This profile requires a more flexible storage system with high mass flow rates per hour. Since the filling and discharging mass flow rates of the GH_2 cavern storage are more limited due to maximum allowed pressure changes (see details in Appendix A.2.2) than for LH_2 storages, only the latter can be used for this specific requirement in the WOFF setup.

It has to be noted that the resulting GH_2 cavern sizes in this demand setting are already very large. They equal or even exceed cavern deployments that are discussed in Europe with capacities of 2,000–4,000 tGH_2 [144]. Hence, such a large cavern might not always be available due to other H_2 users, even if geological conditions are given. Further discussion on this aspect follows in Section 3.2.

VI. GH_2 pressure: Higher ELY (GH_2) output pressures of >60 bar should be chosen for slightly better economics if larger GH_2 storage systems are installed (see Table 3 – Right column).

This leads to synergies in less compression work when filling GH_2 storages and lower energy consumption for the LFP, because less liquefaction work is required for intake feeds with higher pressure (Appendix A.2.3). At WON, WOFF, HYB, and WEAK, this is the case. In the PV setup, smaller cavern storages and lower utilization of the LFP lead to no additional compression at the output of the ELY (30 bar).

Overall, the cost effects of this choice of GH_2 pressure are limited. Optimizations with fixed pressures show that the resulting costs of designs with not optimized pressures lead to small cost increases of around 0.02–0.04 USD/$kgLH_2$.

VII. Part-load dynamics & H_2 losses: Non-linear (part-load) effects have to be considered when designing LH_2 energy systems (Fig. 8). These lead to a 15–20% higher average energy consumption of LFP than in its design point (~6 kWh/kgH_2). H_2 losses do not significantly influence the optimized design in a 2050 base case on-site supply scenario.

In general, the total energy consumption is similar for all locations

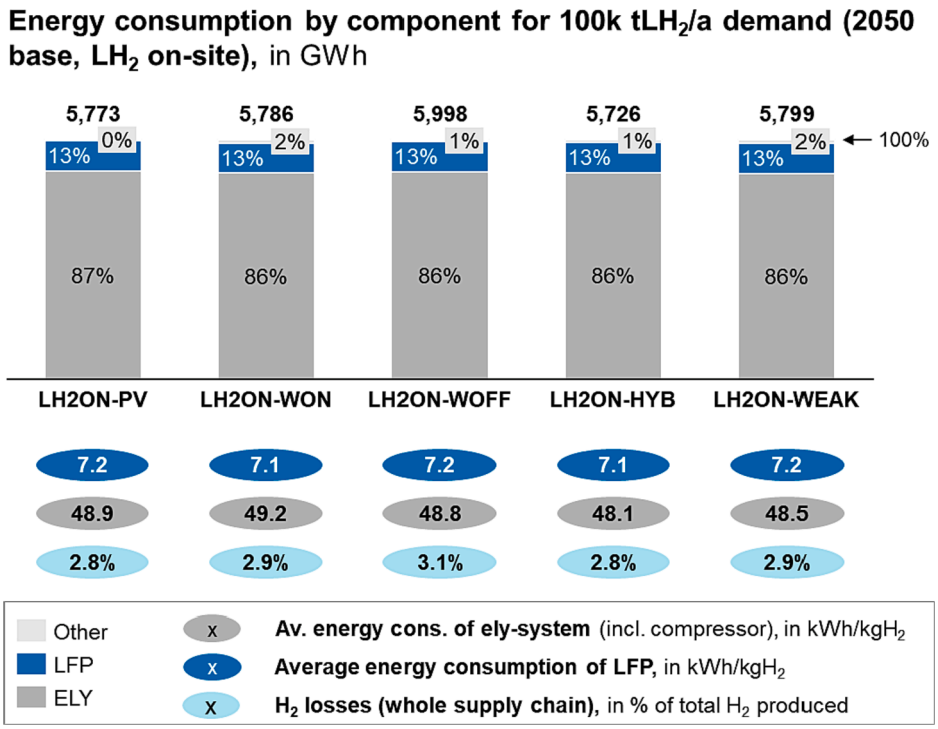

Fig. 8. Total and average energy consumptions as well as total H_2 losses along supply chain for five locations, 2050 base case scenario with 100 k tLH_2/a demand – category "other" describes compressors and cryopumps.

with 5.7–6.0 GWh per year which equals 57–60 kWh of electricity required for the supply of 1 $kgLH_2$. This means that the total energy efficiency on the infrastructure side is 56–58% (based on the LHV of H_2 and for on-site pathways). Also, the relative share of ELY vs. LFP consumption is similar with 86–87% to 13% for all analyzed regions.

However, the average energy consumptions of the ELY and the LFP differ depending on the location. This regional variation is smaller for the LFP with slightly higher consumption for WOFF (see design rule V explanation), for PV and WEAK (see design rule IV). But the average energy consumption of the ELY ranges from 48.1 to 49.2 kWh/kgH_2. The ELY's specific energy consumption decreases in part-load operation, which leads to lower average energy demand for HYB and WEAK setups with more flexible ELY operation (rules III & IV). Only in the WON, WOFF, and PV setups, the ELY is operated more continuously in its design point over the day (shut off at night at the PV location) which leads to a slightly higher average energy demand.

Most H_2 losses along the supply chain stem from the refueling system (~1/3) and the LFP (~1/3) and are very similar for all on-site regions (2.8–3.1% of total supplied LH_2). The remaining losses occur at the compressors and storages – both amounts depending on the designs of the components described in the previous design rules. This is why in the WOFF supply the H_2 mass losses are slightly higher vs. the other regions due to boil-off losses in the LH_2 storage (largest LH_2 storage installed, Fig. 7).

The total LH_2 supply costs shown in Fig. 4 were explained along seven design rules. Main techno-economic factors were derived for on-site supply pathways at a demand of 100 k tLH_2/a that led to economically competitive LH_2 supply costs for H_2-powered aviation. In the next sections, these are further tested and challenged for different demand points and techno-economic scenarios.

Remarks on dependencies of the study design

Small changes in the main study design could affect the discussed results. Therefore, in the following, three main aspects of the scenario definition (in Section 2.3) are briefly reevaluated: (1) the geological availability of GH_2 cavern storage, (2) a differing LH_2 demand profile to an airport without any night flying restrictions (more constant operation, Fig. 3) and (3) different weather data from other years than the reference year 2019. Detailed information on the optimization results can be found in Supplementary Material Fig. S1-3.

First, the unavailability of GH_2 caverns does not have a larger impact on the LH_2 supply costs at PV, WOFF, and HYB regions. However, cost increases are observed for the WEAK setup with a 9% total cost increase – at WON it is more moderate with 5% higher costs.

In all cases, rule I is still valid and no ES or GH_2 aboveground storages are installed but larger LH_2 storages. This leads to minor changes in design rules III and IV since the utilization of the LFP cannot be realized without a constant GH_2 feed anymore (no GH_2 storage). The utilization decreases from ~90% to 70% and less. Only in the PV location, that change in utilization is only moderate, since it was already very low (rule IV). Furthermore, the ELY is sized slightly smaller and better utilized as fluctuations in RES availability are compensated by the larger LFP and the LH_2 buffer storage. In the WEAK region, the oversizing of the LFP leads not only to higher CAPEX and energy costs (part-load operation) for the LFP but also to a 14% cost increase for RES to enable the flexible operation of the LFP.

Second, a study design without a night curfew at the LH_2 demanding airport affects the costs insignificantly at all five locations. The supply costs only change by 0.01–0.03 $USD/kgLH_2$. As described in rule III, the ELY is best sized when demand or RES availability is least fluctuating throughout the day, ELY costs slightly decrease with more constant demand profiles. Only in the PV setup, where no RES is available at night, this leads to minor cost increases.

Third, different weather years have a high cost impact at the stronger wind (WON, WOFF, HYB) locations. There the costs change by −1% to +10% in the WON, +5 to +11% in the WOFF, and +4 to +6% in the HYB setup, if weather data is taken from 2017 or 2018. In regions with only or primarily reliance on PV electricity generation, the costs only differ by 1–2%. The main reason for the cost changes is the differences in RES fluctuations and seasonality which cause both changes in design as well as costs for the RES and storages. However, all design rules hold for all locations and reference weather years.

3.2. Variation of annual LH_2 demands

As a next step the LH_2 demand sizes are varied for the five locations to analyze scaling effects, see Fig. 9A.

Only limited cost reduction effects for larger demand settings are observed versus the 100 k tLH_2/a demand. Further cost reductions of 0.05–0.07 USD/$kgLH_2$ are gained in the WON, WOFF, HYB, and WEAK setups. At the best location, HYB, costs decrease to 1.98 USD/$kgLH_2$. The reason for this trend in these four regions is a further specific cost reduction for the LFP. In this study, it is assumed that the LFP reaches all economies of scale effects at a capacity rating of 500 tLH_2 per day (tpd). Consequently, less cost decreases are achieved for larger demands in the PV location with 0.02 USD/$kgLH_2$, because the LFP is already designed larger than 500 tpd in the 100 k tLH_2/a demand setting. Only a few further improvements in specific CAPEX for storage are reached.

In all these setups, no changes in design rules are observed.

For smaller demand settings than 100 k tLH_2/a, cost effects are significant and lead to nearly doubling of figures for very low annual demands. Lowering the demand from 100 k to 20 k tLH_2/a, supply costs increase by 15%, 14%, 9%, 15% and 11% for PV, WON, WOFF, HYB, and WEAK locations, respectively. From 20 k to 5 k tLH_2/a demands (an average of ~14 tLH_2 demand per day), the cost increase is reaching levels of 25–41% compared to the 100 k tLH_2/a demand setting.

The underlying effects are explained along two main design effects that apply especially below 20 k tLH_2/a settings. Design aspects depicted for the 5 k tLH_2/a settings are shown in the Supplementary Material (Fig. S4-8 and Table S1).

First, since specific CAPEX for GH_2 cavern storages increases significantly more for smaller capacities compared to LH_2 storages (Appendix A.2.2 and A.2.3), only LH_2 storages are installed in these energy systems. So, even in smaller demand settings, a design without electric energy storage or GH_2 above-ground storages is more economical (design rule I). Only for the WEAK location the flexibility of having a cavern buffer storage in the GH_2 balance between ELY and LFP, is still slightly less expensive than oversizing the LFP and other systems.

This is why the utilization of the LFP decreases again from ~90% to ~70% and hence, the oversizing of RES and LFP increases for the regions without a GH_2 storage installation – as already described in the remarks aspect in Section 3.1 (rules II, IV). In addition to that, the ELY output pressure is designed to be the default setting (30 bar), not requiring a compressor in the ELY which is in line with design rule VI.

Second, for all regions, the LFP is designed below a 100 tpd capacity except for PV where this effect applies for demands at and below 10 k tLH_2/a. In this smaller sizing, the CAPEX increase significantly as well as the specific energy consumption from an average of ~7 kWh/kgH_2 to 10–12 kWh/kgH_2 for 2.5–10 k tLH_2/a and even 13–15 kWh/kgH_2 for 1 k tLH_2/a demand. In the latter setting, a very small LFP with <10 tLH_2pd capacity is installed. Consequently, the part-load dynamics of the LFP are even stronger in such settings, as described in design rule VII. See also Appendix A.2.3 for detailed cost and efficiency characteristics of the LFP.

3.3. Scenario analysis of on-site LH_2 setups

As described in Section 2.3, there is a high uncertainty for the techno-economic parameter assumptions for the year 2050. In the present model setup, the number of uncertain techno-economic parameters is too large for a comprehensive sensitivity analysis. This is why, the impact is analyzed based on two additional scenarios – one worse (2035 base) and the other very optimistic (2050 progressive) than the parameter set of the 2050 base case scenario previously discussed, see results in Fig. 9B. It has to be noted that in this work only the techno-economic assumptions for each component are varied. An important other cost aspect in the annuity payment factor method is the interest rate/cost of capital. This parameter often differs by country and the project which has to be financed [59]. The analysis of the LH_2 cost impact from changing the interest rate will be the subject of future work.

The resulting cost bands for each location around the 2050 base case range from 1.56 to 3.22 (-31%/+42%), 1.59–3.00 (-28%/+33%), 2.53–4.25 (-29%/+17%), 1.37–2.77 (-31%/+36%), 2.06–4.16 USD/$kgLH_2$ (-31%/+37%) for demands of 100 k tLH_2/a or more at PV, WON, WOFF, HYB, and WEAK, respectively. This shows that at the best sites (WON, HYB) costs are always below 3 USD/$kgLH_2$ and could even reach levels of 1.40–1.60 USD/$kgLH_2$ in a very optimistic scenario.

The cost bands are significantly larger for very small demands at 5 k tLH_2/a with 2.21–4.47, 2.24–4.20, 3.32–5.44, 1.94–3.80, 2.84–5.47 USD/$kgLH_2$ for the PV, WON, WOFF, HYB and WEAK sites, respectively. At WOFF sites, the high CAPEX assumptions of wind turbines in all scenarios compared to the other setups still cause the highest LH_2 costs. Even with more optimistic wind offshore CAPEX in the 2050 progressive case, LH_2 supply costs at WOFF are more expensive than from PV, WON or HYB locations in the 2050 base case.

The future supply costs at WEAK also represent a large uncertainty for the economics of H_2-powered aviation with cost levels above 4 USD/$kgLH_2$ for larger and more than 5 USD/$kgLH_2$ for very small demands.

In any of the scenarios and sites, design rule I is not changing and no electric energy and GH_2 above-ground storages are installed even if they become less costly. Further design and cost effects are discussed for both scenarios separately.

Scenario: 2035 base case

This scenario depicts more conservative techno-economic assumptions, mostly for the CAPEX projections of all components including the RES plants. This is why the total LH_2 supply costs increase to 2.77–4.25 USD/$kgLH_2$. The main factor behind this is higher costs for electricity supply with LCOEs of 20, 24, 24, 43, and 47 USD/MWh for the PV, WON, HYB, WEAK and WOFF locations, respectively. Relative CAPEX reductions between the 2035 and the 2050 base case scenarios are lowest for wind offshore parks and highest for PV installations. Consequently, total investment needs increase less at WOFF by 13% and more drastically at the other sites by 28–44% compared to the 2050 base case. All information on costs and design of the resulting LH_2 energy systems are presented in Supplementary Material Fig. S9-13 and Table S2.

PV locations show the largest increase in total costs compared to other locations, e.g., 42% for the 100 k tLH_2/a setting. In the base case 2050, already high cost penalties apply at PV sites for oversizing the LFP and ELY. For the 2035 base scenario with higher specific CAPEX for both components, it is leading to the highest supply cost increase, proving that design rules III and IV are still valid. In addition to that, the costs for RES are 44% higher and hence, cause more expensive LH_2 supply (design rule II).

The contrary is applying to the WOFF location with the smallest total cost increase (17%). Since RES costs increase only moderately and the LFP has a high utilization again, the more conservative techno-economic assumptions do not lead to drastically higher LH_2 costs for WOFF regions.

The energy efficiencies of the ELY and LFP do not change compared to the reference case (2050 base). Hence, installed capacities, RES designs, utilizations, and resulting average energy consumptions are very similar to the 2050 base case (design rules III, IV, VII).

Regarding storages, design rule V proves to be still valid. Larger GH_2 storages are installed for the PV setting since both higher RES and LFP costs make it more economical to buffer more GH_2 and hence, enable slightly higher utilization of the LFP (design rule IV). At WOFF now also larger GH_2 cavern storages are installed since the specific CAPEX does not increase, but for the LH_2 storages, they do. However, larger LH_2 buffer storages are still required to compensate for seasonal and daily fluctuations in both strong wind locations.

Scenario: 2050 progressive case

In this scenario, all CAPEX of RES and H_2 components are reduced

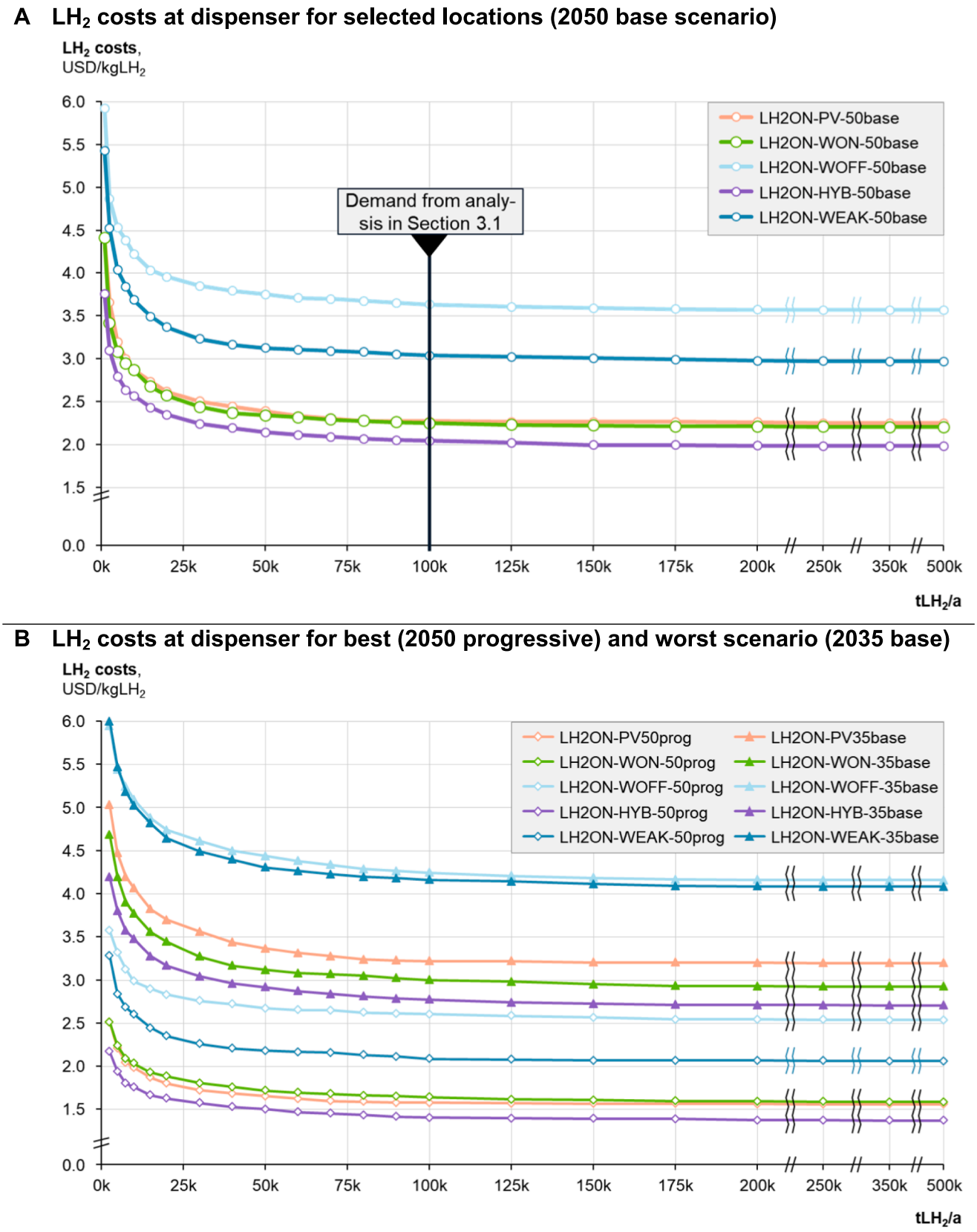

Fig. 9. LH_2 supply costs at the dispenser for on-site setups at five locations for variable annual LH_2 demands at the airport – A. 2050 base case scenario, B. 2035 base and 2050 progressive case scenarios.

due to larger learning effects in a larger H_2 market. Thus, more optimistic efficiencies, operation cost factors, and depreciation periods are assumed for selected components. This leads to a further decrease in total supply costs (Fig. 9B), mostly driven by lower RES costs with LCOEs of 10, 12, 14, 22, and 34 USD/MWh for the PV, HYB, WON, WEAK and WOFF locations, respectively. Total investments decrease by –23 to −30%, see all details in Supplementary Material Figs. S14–S18 and Table S3.

At nearly all sites, the RES and ELY capacity is designed smaller due to an increase of energy efficiency of the ELY by 11% (design rules II and III are still valid). This can also be seen in the new average energy consumption of 43–44 kWh/kgH_2 due to part-load operation (design rule VII).

Since specific CAPEX for LFP is lower, it is generally a bit oversized for more flexible operation compared to the 2050 base case, also leading to decreased storage demands and costs. This is why, storages in total are sized slightly smaller (0–27%) – the effect is largest for WOFF and WON locations with larger seasonal fluctuations in RES availability. Furthermore, LH_2 storage systems are sized larger than in the base case scenario and larger than the GH_2 cavern capacities at WON/WOFF. This strengthens the findings from design rule V for WOFF but also WON. One main reason for the preference of LH_2 storages is that only for them further cost reductions are assumed (longer lifetimes) and not for installations of GH_2 cavern storages in the 2050 progressive scenario.

Intermediate summary

Seven design rules were derived for five locations of which the HYB followed by the PV and WON regions are best suited for lowest cost on-site LH_2 production for H_2-powered aviation. The WOFF location has great RES potential for efficient and not oversized LH_2 energy system designs. However, due to the very high specific CAPEX of offshore wind turbines, its economic LH_2 supply potential might only be given, if space constraints for other RES (e.g., wind onshore) are too high or other supply options are not available.

Contrary to that, the weaker hybrid location does not offer highly efficient and potentially low-cost designs of LH_2 energy systems. Consequently, larger RES capacity installations by a factor of 3 would be required to realize such a WEAK setup which might lead to infeasibility due to limited land availability. As a result, LH_2 off-site (import) options that could leverage more economic LH_2 supply costs at airports within WEAK regions are considered in the next section.

4. Offsite supply chains

In the following, off-site (import) options are investigated for an airport located in the WEAK region, which might enable lower costs than with an on-site LH_2 supply pathway (see previous Section 3).

First, LH_2 import pathways are analyzed (Section 4.1). Then, GH_2 import pathways are derived and compared to the LH_2 import options. In a brief comparison, the effects on the LH_2 energy system design by adding transport options are also explained. As a last step, again a scenario analysis is performed for the supply options for WEAK.

This study focuses on dedicated infrastructure development for LH_2 in aviation. Consequently, a greenfield approach is chosen for the importing supply chain like in the on-site setups. Potentially existing infrastructure like an international GH_2 pipeline system (European Hydrogen Backbone [57]), LH_2, or ammonia vessel transport networks [145–147] is not reflected in the following analysis. As discussed in Section 2, H_2-powered aviation might create new magnitudes of scale for H_2 demands at selected regions around the airport and therefore lead to further cost reduction effects. Furthermore, the transport of hydrogen as ammonia is in most cases costlier than shipping LH_2, if it is the final aggregate of H_2 required at the end consumer (airport) [53]. The conversion process of GH_2 to ammonia and vice versa adds costly and energy-inefficient process steps to LH_2 supply chains.

4.1. LH_2 off-site setups

In this section, the chosen LH_2 off-site setup is described, transport costs are calculated as well as resulting total LH_2 supply costs are discussed.

Setup of LH_2 off-site supply chain

As described in Section 2, LH_2 could be transported via larger oversea vessels on longer distances. In that case, import and export terminals are required as well as on-land truck transport from the importing port to the targeted airport. Thus, it is assumed that the LH_2 production is close to a port where the LH_2 vessel would be loaded in the three exporting regions (PV, WON, HYB).

Since the transport costs depend on the utilization of the export terminal, the LH_2 transport capacity per vessel is optimized as a main aspect of the transport network design (see optimization variable in Table 1 and Appendix A.2.4. Hence, for low demands and short distances there can be setups with only one vessel arriving at the export site per week vs. a continuous arrival of vessels, once the previous vessel has been loaded (48 h). The LH_2 truck on-land transport is calculated based on the optimization of the transport network.

While the energy system setup at the export location does not differ significantly from the on-site production case (see Section 2.1), the need for the LH_2 storage system changes slightly. In on-site setups, it is mostly used as a buffer between the daily liquefaction of H_2 and the direct use of LH_2 at the airport. For the LH_2 export system, the LH_2 storages are required to buffer LH_2 until the next vessel arrives. So, depending on the number of vessels in the transport network, this LH_2 export terminal buffer can be significantly larger.

For a better overview of data, the focus is set on three different trip lengths: short (1,000 km), medium (3,000 km), and long (7,500 km). Exemplary trips could be from Southern Europe to the next northern countries (short distance), from Northern African countries to Central Europe (medium distance), or from the Middle East to Central Europe (longer distance).

In addition, the on-land transport is assumed to be on average 300 km long, because this study looks at generic supply pathways. This length is also used in other studies, e.g., in [74].

LH_2 transport costs

Cost results for the optimized system are shown in Fig. 10 for the three distances using an LH_2 demand mass variation (x-axis). As described above, the costs for the LH_2 export terminal (storage and cryopumps) are considered as part of the main LH_2 energy system and not shown in the LH_2 transport costs.

For an annual demand of 500 k tLH_2, the transport costs over 1,000 and 3,000 km stem from 41% for vessels, 19% for the import terminal (storage and cryopumps), and 40% for the trucks. In the 7,500 km distance, the cost share of LH_2 vessels increases to 58% (import terminal with 13% and truck with 29%). In that demand case, required investments would already range from 1.4 Bn USD (696 Mn USD for vessels, 413 Mn USD for import terminal, and 292 Mn USD for LH_2 trucks) for 1,000 km to 2.1 Bn USD for 7,500 km for the transport network only.

In general, the transport costs decrease significantly with larger LH_2 demands from more than 2.5 $USD/kgLH_2$ for $<$100 k tLH_2/a to around 0.5–0.7 $USD/kgLH_2$ for $>$1,000 k tLH_2/a. Costs for short and medium transport distances differ only by $<$0.01 $USD/kgLH_2$ because in both cases a minimum number of two vessels is required to utilize the transport network (see Appendix A.2.4).

H_2 losses also cause costs in the total energy system but are not represented in Fig. 10. They occur in the form of flash losses while loading the vessel and the LH_2 truck. For all transport distances, boil-off losses on the vessel trip are nearly sufficient to power the vessels' propulsion system. On the truck transport part, nearly no boil-off losses are observed on such shorter distances and fast turnarounds. Hence, the trucks require extra fuel which is accounted for in this study.

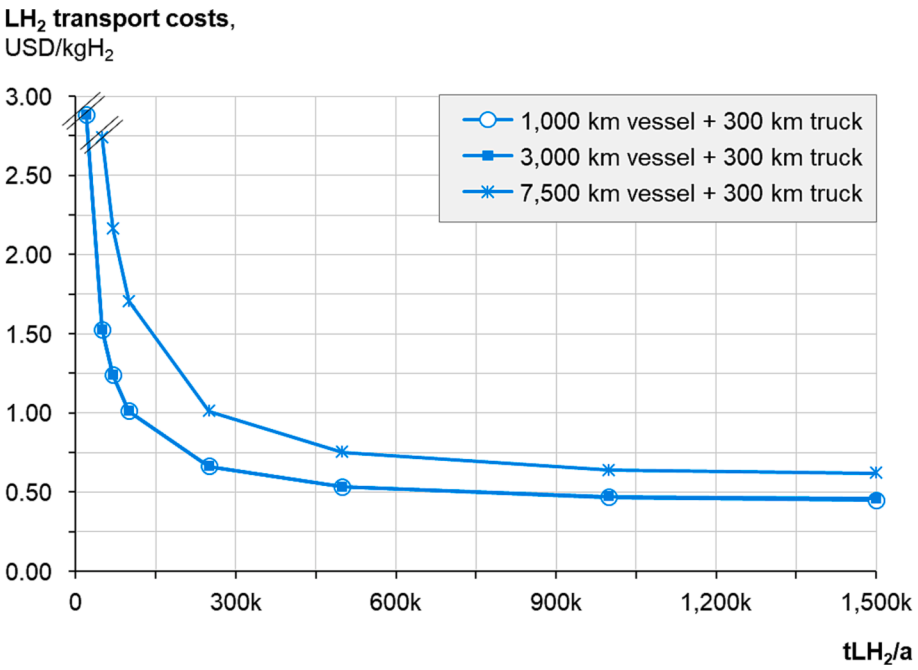

Fig. 10. Transport costs in the 2050 base case scenario for three distances (short: 1,000 km, medium: 3,000 km, long: 7,500 km) with LH_2 oversea vessels and a fixed 300 km truck transport on land from the importing port to the destination airport – costs for importing LH_2 terminal included, export terminal costs excluded and part of "LH_2 energy system".

Total LH_2 import costs

Fig. 11 shows the resulting total LH_2 import costs at the dispenser for an airport at a WEAK location and the 2050 base case scenario. In total, LH_2 costs at the WEAK location can be reduced by up to 0.5.–0.6 USD/$kgLH_2$ with LH_2 off-site supply, if a vessel transport over 1,000 km or 3,000 km from HYB locations at very high annual demands is available.

Generally, LH_2 import from HYB is always more competitive than from WON and PV locations – same as in Section 3 for on-site production. In addition to that finding, the LH_2 import option is less economically competitive compared to on-site supply at WEAK airports for smaller annual demands with increasing transport distances. For the short and medium distances, LH_2 import from an HYB region is the economically best option for demands larger than 150 k tLH_2/a. In the long-distance setup, the break-even demands increase to larger than 400 k tLH_2/a.

More detailed energy system design effects are explained at the end of Section 4.2.

The total cost curves for LH_2 import already show that if very large annual demands are reached, more competitive delivery costs would result vs. the dedicated on-site LH_2 production at the WEAK location (100 k tLH_2/a) with 3.04 USD/$kgLH_2$. To reach such demand levels, an accumulation of demands might be required from several airports or even other H_2-demanding applications in one broader region. It has to be noted that such a deployment highly depends on transport distances

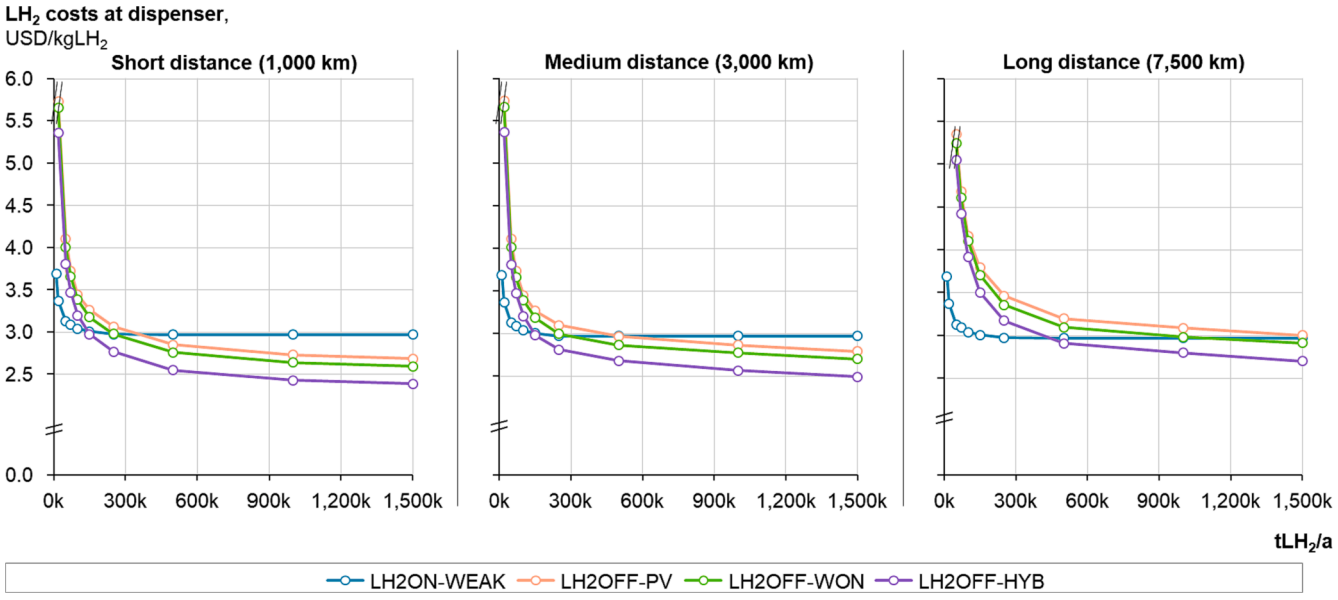

Fig. 11. Costs at the dispenser for receiving airport at WEAK location with LH_2 import (off-site) pathway over three distances compared to costs of on-site LH_2 production, 2050 base case scenario.

between export and import regions and the proximity of the receiving airports to the importing port.

Several studies project H_2 market costs for importing H_2 in several forms (GH_2, NH_3, etc.). However, these do not create a homogenous picture of future H_2 market costs, e.g., in Central Europe, but rather a broad range of future cost projections. Consequently, a comparison of the results of this study with such a range would not lead to a clear picture of whether dedicated LH_2 import scenarios for H_2-powered aviation might be less or more expensive than another H_2 market. Nevertheless, these "greenfield" calculations show the lowest costs of dedicated LH_2 supply (on-site and off-site) infrastructure that has to be underbid by a general H_2 market (plus costs for liquefying GH_2) to be a more economically competitive option.

4.2. GH_2 off-site setups

This section follows the same structure as the previous one. Additionally, a brief overview is given of changes in the energy system design setups for both off-site pathways.

Setup of GH_2 off-site supply chain

The main characteristic of this supply chain setup is the placing of the LFP at the receiving airport and not the exporting H_2 production center. As described in Section 2, a grid connection (renewable electricity power purchase agreement) is used to power the LFP at the airport in this case.

Gaseous H_2 from the export region is then transported through pipeline systems that are either newly built or retrofitted and recommissioned natural gas pipelines (see Section 2.1). For the latter, new coatings, valves, and compressor stations suitable for H_2 usage have to be installed. The need for compressor stations depends on the chosen input and output pressure, the length of the pipeline, its diameter, and the design flow speed of GH_2 – which is an optimization variable. The equations describing the dependencies of these parameters that are required for the optimization of the transport network can be found in Appendix A.2.4.

In this study, only on-land pipeline systems and no routing factors are considered – otherwise, the specific CAPEX factor for newly built pipelines would further increase for undersea pipeline installations. Furthermore, the pipeline is modeled without any storage functionality which is in line with current natural gas operating principles (see Section 2.1).

GH_2 transport costs

The optimized transport costs for the pipelines differ significantly between a new built and a retrofitted system, see Fig. 12. Additionally, a very large cost increase by a factor of 3–4 and 8–11 results from longer pipeline lengths over 3,000 and 7,500 km compared to 1,000 km. A similar effect can be observed for smaller annual H_2 demands – higher specific CAPEX per installed pipeline diameter per kilometer lead to very high transport costs.

Total GH_2 import costs

The resulting total costs for the optimized GH_2 off-site supply are shown in Fig. 13. In total, costs at the WEAK location can be reduced by up to 0.70 USD/kgLH_2 with GH_2 off-site supply when retrofitted pipelines are available over 1,000 km in a 2050 base case scenario from HYB at very high annual demands.

As expected, the GH_2 import costs are lower for retrofitted pipeline setups versus newly built ones, if this option is available. If retrofitted systems for short distances can be used, GH_2 import underbids LH_2 on-site supply costs at WEAK already for demands of 70 k tLH_2/a or larger. With medium distances this is the case for demands of ~400 k tLH_2/a, while for longer distances cost parity with the on-site production is never achieved.

In newly built setups, GH_2 import only becomes an economically more attractive option for very large annual LH_2 demands. For short and medium distances from HYB, PV, or WON export regions, LH_2 supply costs at WEAK could be reduced by up to 0.58 USD/kgLH_2 for very large demands. In long-distance import cases, newly built pipelines also never lead to better LH_2 costs than the on-site supply (see right graphs Fig. 13).

Contrary to the LH_2 off-site scenarios, import costs from WON locations are more expensive than from PV locations in the GH_2 off-site supply. The cause will be explained in the following.

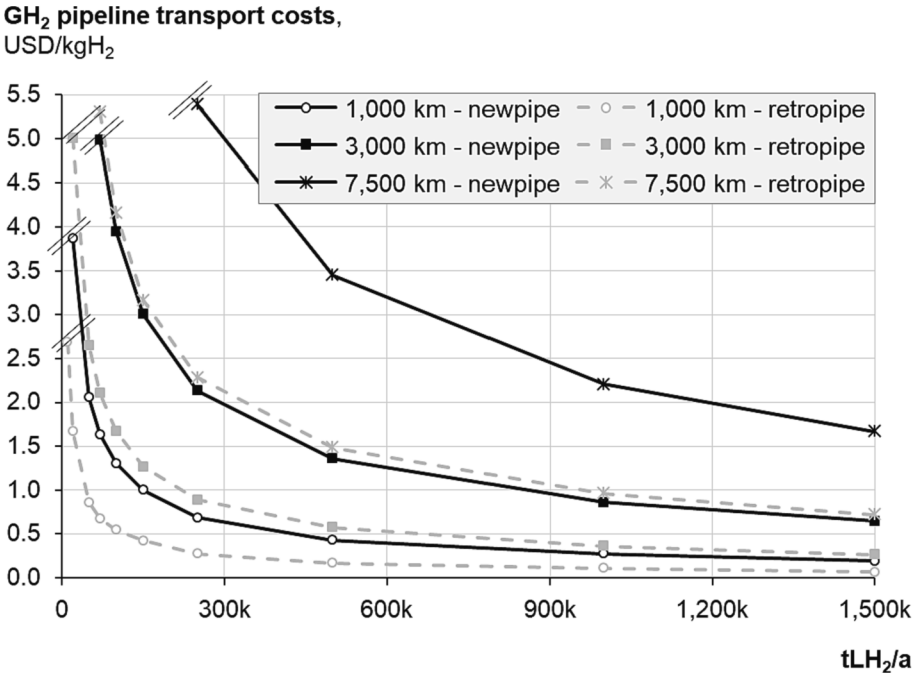

Fig. 12. Transport costs in the 2050 base case scenario for three distances (short: 1,000 km, medium: 3,000 km, long: 7,500 km) with GH_2 pipelines on land (new and retrofitted pipelines) from the importing site to the destination airport – costs for compressor systems included.

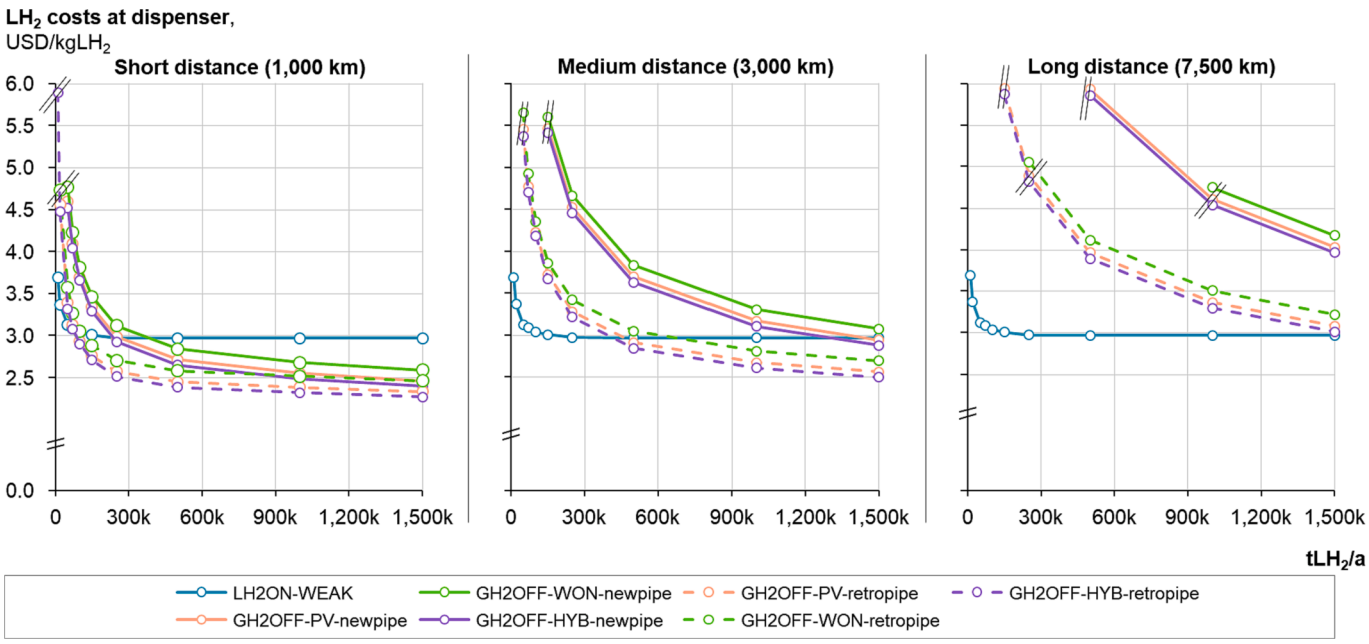

Fig. 13. Costs at the dispenser for receiving airport at WEAK location with GH_2 import (off-site) pathway over three distances compared to costs of on-site LH_2 production; two options with newly built and retrofitted pipelines; 2050 base case scenario.

Remarks on energy system designs for LH_2 and GH_2 off-site pathways

This study does not aim to answer the economics of LH_2 supply at five generic locations only, but also to investigate design aspects and main factors leading to less costly supply. The energy system design effects for off-site supply differ from on-site pathways and are analyzed in the following for the 100 k tLH_2/a reference base case scenario (see Fig. 14).

First, LH_2 import requires larger export buffer storages as part of the LH_2 production site, costs for LH_2 storages increase by 0.07–0.15 USD/$kgLH_2$. As mentioned earlier, only two vessels would be required to establish such a transport network and these would only be loaded once per week at the export region. Hence, the produced LH_2 has to be stored at the export terminal for five days until the next vessel arrives and is loaded (48 h). This even leads to a change in design rule V (storages), because in the HYB location the preference switches to the installation of LH_2 storages only (see also Supplementary Material Figs. S19–S23 and

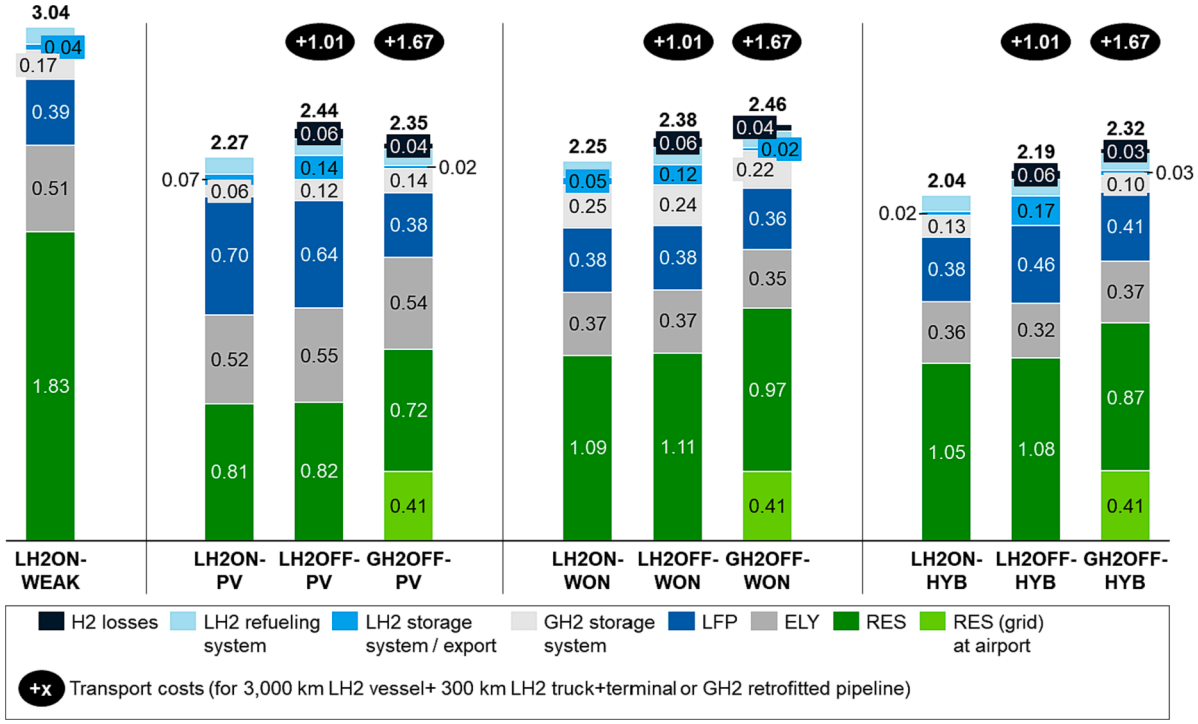

Fig. 14. LH_2 energy system costs (transport & import terminal costs shown in bubbles separately, have to be added), 2050 base case scenario with 100 k tLH_2/a demand – comparing energy system designs: reference LH_2 on-site system at WEAK location (left) and comparison of LH2ON, LH2OFF and GH2OFF systems at PV, WON and HYB location; tag for the 0.1 USD/$kgLH_2$ refueling costs not shown, because the refueling costs are not subject for change for all setups.

Table S4). Since LH_2 storages are required for buffering for export, it becomes slightly less expensive to operate the LFP more flexibly with a lower utilization than installing also a GH_2 cavern storage – whose specific CAPEX increase significantly for smaller installation sizes. Other design rules are not affected in the LH_2 off-site setups.

Second, both import setups have higher total H_2 losses along the supply chain, especially in LH_2 off-site cases over longer distances. These are caused by flash losses while filling LH_2 from the terminal to a vessel and a truck as well as boil-off losses in LH_2 storages and GH_2 losses in pipeline compressor stations. Hence, the LH_2 energy system is sized larger to compensate for these losses. These additional H_2 losses lead to an extra cost increase of 0.06 USD/kgLH_2 (Fig. 14) for LH_2 import and 0.03–0.04 USD/kgLH_2 for GH_2 pipeline import.

Third, GH_2 off-site setups come with higher total electricity costs, since the LFP at the airport is sourced with a green power purchase agreement at fixed costs of 50 USD/MWh. If a deployment of dedicated RES at the airport would be the only solution to power the LFP, total electricity costs would increase even more. Only for the GH_2 off-site supply pathways from PV locations this effect is not as strong. As explained in Section 3.1, the LFP is oversized for on-site PV setups, since no RES is available at night (design rule IV). Hence, the LFP can only be operated during the day which requires nearly doubling of design capacities. In the GH_2 off-site supply, the LFP capacity at the WEAK airport can be sized smallest with constant electricity availability from a local grid. This is why, the LFP utilization increases to 90% also for the PV GH_2 off-site pathway and smaller LH_2 buffer storages are built (design rule V), see also Supplementary Material Figs. S24–S28 and Table S5. Consequently, the GH_2 import from stronger PV regions becomes more competitive than from WON.

4.3. Scenario analysis for import options

In the next step, like in Section 3.3, not only the 2050 base but also the 2035 base and the 2050 progressive case scenarios are considered for supply options to or at the WEAK location. Combining all scenarios and all supply pathway options enables a comprehensive evaluation of the future LH_2 cost ranges at an airport with weaker RES conditions and hence, the techno-economic potential for H_2-powered aviation from an LH_2 fuel perspective.

In Fig. 15A and 15B, the costs of the LH_2 on-site WEAK setups are compared to the best off-site supply for all three scenarios, three transport distances and given that only new pipeline installations (A) or also retrofitted pipeline options (B) are available, respectively. All detailed results can be found in Supplementary Material Figs. S29–S32.

For the sake of clarity, only the best off-site results – the location and supply pathway – are shown for each scenario.

Best off-site supply pathways without availability of retrofitted pipelines

If new pipelines need to be installed, then only an LH_2 import setup is the most economical choice for all demands and all distances. Only for short distances the GH_2 import is the best option for demands of 250 k tLH_2/a or larger in a 2035 base scenario (see the purple line in the top left graph of Fig. 15A that changes from a solid to a dotted line).

The figure can be characterized by three cost bands that create one final cost interval for future LH_2 costs at WEAK airports. Cost band "I" (includes also improved upper-cost band "II") shows the on-site LH_2 cost range at the WEAK airport location when no import options would be available, explained in Section 3.3.

On the upper end of the cost band "I", LH_2 off-site supply could reduce the costs at WEAK by up to 1.04 USD/kgLH_2 for very large demands and short distances in the 2035 base case scenario. For medium and long distances this improvement potential is 0.81 USD/kgLH_2 and 0.59 USD/kgLH_2, respectively. In addition, the HYB location always offers the best export costs in the 2035 base but also the 2050 progressive scenario.

On the other side, with optimistic cost assumptions (2050 progressive), LH_2 off-site supply costs are decreased only slightly (lower cost band "III"). While in a short distance setup the costs can be reduced by 0.35 USD/kgLH_2, cost reductions are lower for long distance import supply with 0.09 USD/kgLH_2.

In total and for demand scenarios of 100 k tLH_2/a, the best resulting supply costs at the airport in a weak RES region would be 2.09 USD/kgLH_2 for all distances as a result of on-site supply deployment and 2050 progressive techno-economic assumptions. Furthermore, the highest cost range in a 2035 base case can be decreased from 4.16 USD/kgLH_2 (on-site) to 4.07 and 4.08 USD/kgLH_2 for short and medium import transport distances and LH_2 import, respectively.

If large demands of 1,500 k tLH_2/a or import for a broader H_2 market are considered, off-site scenarios always lead to the best costs. Then, for short distances, the cost range at WEAK airports decreases to 1.71–3.04 USD/kgLH_2 with LH_2 off-site in the progressive and with GH_2 off-site supply (new pipeline) in the more conservative scenario. For medium and long distances, LH_2 off-site supply always leads to best cost ranges of 1.79–3.27 and 1.97–3.48 USD/kgLH_2, respectively.

Best off-site supply pathways including retrofitted pipelines

If a retrofit pipeline option exists, GH_2 off-site supply chains become more economical than LH_2 off-site setups in all short and partial also in medium-distance scenarios (Fig. 15B).

Even though the costs for the GH_2 off-site energy system increase (Section 4.2, Fig. 14), the total LH_2 supply costs decrease in combination with the significantly lower transport costs for retrofitted pipelines compared to LH_2 vessel imports. Only for longer distances the LH_2 off-site supply chain is still the best option in all scenarios. This result is also in alignment with other studies considering H_2 transport options, e.g., in [74,148,149].

For medium distances, both LH_2 and GH_2 import can play a leading role. In the 2035 base case scenario, import via retrofitted pipelines is more economical for larger demands above 500 k tLH_2/a due to two reasons. First, the specific CAPEX for the retrofitted pipeline deployment decreases significantly for larger installed diameters. With these reduced CAPEX, the pipeline becomes the optimal transport option compared to the LH_2 vessels. Second, the specific costs for LH_2 storage are significantly higher than for GH_2 storage systems in the 2035 base case scenario only. In the LH_2 off-site setups, these storages are required with high capacities for the export and import terminals. On the contrary, only smaller LH_2 storages are installed in the GH_2 off-site scenario at the airport, which is sized comparably small as expressed in costs (see Fig. 14 or Table S5 in the Supplementary Material).

Table S5

For demand scenarios of 100 k tLH_2/a, on-site supply is still the most economical choice in a 2050 progressive case. However, the upper cost range can be further decreased with retrofitted pipeline import options for short distances to 3.59 USD/kgLH_2. For the very large demand setting of 1,500 k tLH_2/a, costs can be reduced with GH_2 import setups to 1.68 USD/kgLH_2 in the best case for short distances.

So, total cost uncertainties can be reduced to a maximum of 2.91 or 3.16 USD/kgLH_2 in a region with a large H_2 market (1,500 k tLH_2/a) where retrofitted pipelines are available in short and medium distances.

Implications for resulting LH_2 supply costs at airports

From the presented results, three overarching aspects are highlighted for the economic future of H_2-powered aviation.

First, LH_2 cost uncertainties can be significantly reduced even at airports with weaker weather conditions for renewable energy generation and hence, H_2 production. Also, LH_2 costs at the dispenser are most likely below 4 USD/kgLH_2 in a more conservative scenario, lower import demands (100 k tLH_2/a), and when dedicated infrastructure deployment is required (no retrofit available). If larger LH_2 import markets can be created (1,500 k tLH_2/a), then the highest cost mark might be even reduced to below 3.05 or 3.30 USD/kgLH_2 due to import options via short and medium distances, respectively.

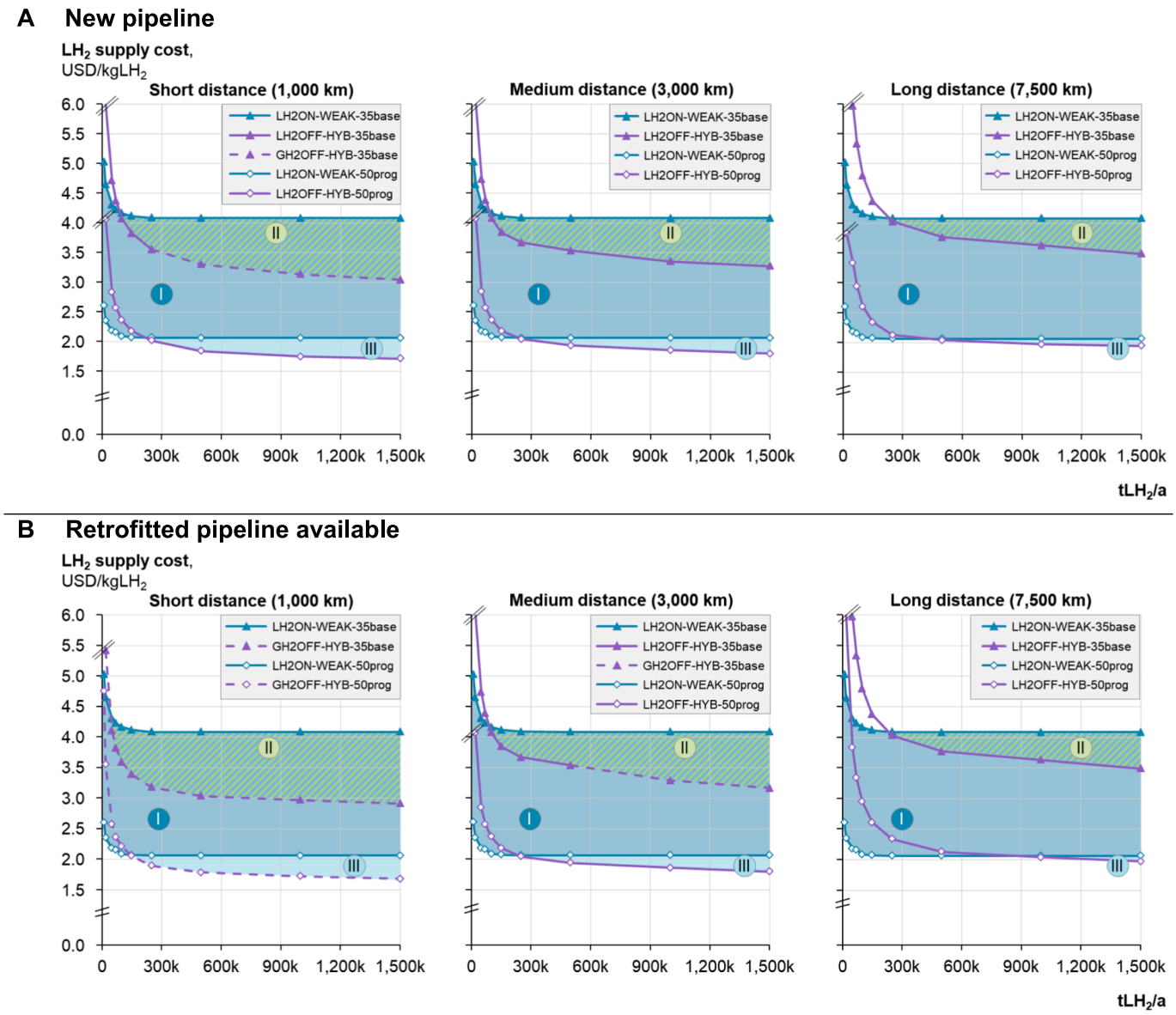

Fig. 15. Total LH_2 supply costs at the dispenser for three transport distances considering only a GH_2 off-site supply pathway with A. new pipeline system installations (top) or B. with retrofitted pipeline systems (bottom); in each graph only the best off-site (LH_2/GH_2) supply cost curve to WEAK for each scenario (2035 base, 2050 base, 2050 progressive) is shown and compared to the LH_2 on-site cost curve at the WEAK location; three cost bands highlighted in each sub-figure ("I" for the cost range of the LH2ON-WEAK setups, "II" for reduced costs in the 2035 base scenario due to import options, "III" for the cost range in which import pathways underbid the 2050 progressive LH2ON-WEAK scenario).

Second, in regions with main air travel markets like Central Europe, "worst case" LH_2 supply costs could even be lower than in other regions where no retrofitting option would be available. In Europe, plans exist to retrofit large parts of existing natural gas pipeline networks for H_2 use ("European Hydrogen Backbone").

Third, also smaller airports (e.g., with a demand of <100 k tLH_2/a) might profit from potentially lower H_2 market prices through large-scale import compared to the costs with a dedicated infrastructure deployment approach discussed earlier. Therefore, aggregation of larger H_2 demands would be required in a broader region driving the previously shown economies of scale for H_2 import scenarios (>500 k tLH_2/a). This might especially be the case for GH_2 markets with pipeline transport via retrofitted systems like the European Hydrogen Backbone. However, if only LH_2 import supply would be available in a region (e.g., for islands or no existing pipelines), LH_2 market assumptions are more critical. Since most other large-scale H_2 applications do not require LH_2 for end use, other forms (aggregates) for H_2 import like ammonia shipping might already be implemented which would then hinder achieving beneficial LH_2 market masses for LH_2 import deployments in such regions.

5. Conclusion

Three LH_2 supply pathways were analyzed at five generic RES locations. The novelty of this study is a detailed techno-economic assessment with non-linear energy system optimization. The targeted application is aviation and H_2-powered aircraft, but the cost results could also be useful for supply economics of other applications with larger (central) uses of LH_2.

Main insights for designing LH_2 energy systems

The major share of costs is caused by the renewable electricity supply, which results from costs for RES plants and their capacity factor

depending on the weather at the generation site. In very good conditions, on-site LH_2 production could be economically competitive with final costs of 2.04 USD/kgLH_2 at a medium-large airport in a 2050 base case scenario. Then, LH_2 costs would still be 21% more expensive than equivalent kerosene costs from 2019 (1.70 USD/kgLH_2) as shown in Hoelzen et al. [33]. However, this cost difference might not be given in 20–30 years, if oil costs and carbon or even novel climate impact taxes for kerosene usage increase. If kerosene costs would stay as low as assumed in [33] (0.60 USD/kg kerosene), a carbon tax of 111 USD/tCO_2 would lead to parity of LH_2 and kerosene costs in the 2050 base case.

Wind offshore sites have great weather conditions that enable very high utilization of all energy system components. Nevertheless, resulting LH_2 supply costs are least competitive compared to the four other regions examined due to the very high CAPEX for the offshore wind park.

Besides RES conditions, CAPEX reductions and efficient designs for the LFP and ELY are key for lower LH_2 supply costs, both having similar total cost shares. As part of the derived design rules, it is found that LFP should always be designed for the highest possible utilization (~90%), while the ELY is operated more flexibly.

The lowest cost shares account for storages and the refueling system. In addition, ES or GH_2 aboveground storages are not installed in any scenario and hence, not influencing optimal energy system designs.

Uncertainties are coming from all techno-economic assumptions, but are mostly driven by the CAPEX of RES causing supply cost ranges at best LH_2 on-site production spots of 1.37–4.19 USD/kgLH_2 in a more conservative vs. a more optimistic scenario. Furthermore, weather year data also influences cost uncertainties by up to 11% of the supply costs. Demand profiles at the airport do not have a larger design and cost impact as well as the availability of GH_2 cavern storages. Only at weaker RES locations, a clear cost impact is found with a 9% increase if no cavern is available.

Nevertheless, import (off-site production) pathways might be a more economical supply solution for airports in the WEAK region. Besides the economics, another justification for import is the onsite availability of space for RES or cavern storage. Since installed RES capacities at WEAK are factor three larger (83 km^2) than at most locations, resulting space requirements would be a significant constraint. However, if import options are available from regions within short or medium transport distances and for high LH_2 demands, supply costs might be reduced to <3.30 (LH_2 import) or 3.20 USD/kgLH_2 (retrofitted pipeline import) at WEAK.

Furthermore, the investigation of import pathways also shows potential cost trends in H_2 markets. In that case, smaller airports with low LH_2 demands could profit from such a market, if accessible. This is also in line with the justification of the chosen study design that does not focus on dedicated LH_2 supply chain deployment for smaller airports that have access to local H_2 markets.

Limitations of study and research agenda

The results of this paper are highly dependent on the techno-economic assumptions. While there are many studies on future cost developments for RES and ELY, limited research is available for the other components. More detailed studies and demonstrations are needed to reduce high uncertainties in the cost projections until 2050. This is especially the case for the LFP and H_2 transport. The assumptions of the LFP's performance rely on three main authoring groups: the IDEALHY project [97], Linde Kryotechnik [150], and SINTEF [151]. Real performance data from an operating large-scale LFP would help future LH_2 energy system studies validate their results. Furthermore, the lifetime effects of operating an LFP in part-load or the energy consumption of shutting it off for 12 h per day (see PV results in this study) should be tested.

Thus, the development of safe and high-performing loading and unloading equipment for LH_2 vessels or trucks is needed. Only when H_2 losses can be minimized, off-site supply chains over longer distances should be realized. On the GH_2 transport side, the operational principle incl. a potential storage function of the pipelines should be further investigated to potentially reduce storage costs.

Another limitation of this study is that the costs are derived from generic RES and airport setups. More detailed studies on specific geographies could be based on this study to determine future costs of operating H_2-powered aircraft more precisely, see for example the HyNEAT project [152]. Given a more geospatial approach to determining LH_2 supply costs, also the impact of existing/future RES and H_2 markets should be reflected. While this study focuses on dedicated, nearly isolated infrastructure deployment to ensure computability, the general or even time-resolved (hourly) influence of buying RES, GH_2, or even LH_2 at markets might then lead to further cost reductions. Otherwise, a case study approach for selected airports might also provide relevant insights into future economics of H_2-powered aviation.

With a focus on airports, three further aspects should be looked into. First, business modeling of LH_2 infrastructure at the airport and financing of such new projects could play an important role. This could affect main techno-economic parameters such as an interest rate in the here chosen annuity payment factor method. Second, H_2 market designs at and around specific airports. In Germany, an auction platform (H2GLOBAL) is currently being designed to drive down H_2 costs, especially for import options which could lead to even lower costs of H_2 at airports [153]. Third and last, safety and operational studies for LH_2 infrastructure deployments at airports are needed. It has to be ensured that the concepts, e.g., of on-site production, are feasible for safe implementation at airports.

Overall, this study not only contributes to a better understanding of techno-economics and the design of LH_2 energy systems for airports but also reduces very high cost uncertainties that were derived in a previous study [33]: average LH_2 supply cost uncertainties were as high as 5.00 and 8.20 USD/kgLH_2 based on literature reviews. Since such values could not be reproduced in this study with the more conservative techno-economic scenarios, they can be evaluated as unrealistic. Hence, economic competitiveness for H_2-powered aviation from an LH_2 supply perspective might be given at most airports in this world, if previously defined assumptions and research and development goals can be achieved. This can be seen as another step towards true-zero carbon emissions for aviation.

Declaration of Competing Interest

The authors declare that they have no known competing financial interests or personal relationships that could have appeared to influence the work reported in this paper.

Data availability

Data will be made available on request.

Acknowledgements

Julian Hoelzen and Richard Hanke-Rauschenbach acknowledge funding from the Deutsche Forschungsgemeinschaft (DFG, German Research Foundation) under Germany's Excellence Strategy – EXC2163/1 – Sustainable and Energy Efficient Aviation (Project-ID 390881007). Finn Schenke and Astrid Bensmann acknowledge financial support by the Federal Ministry of Education and Research of Germany in the framework of HyNEAT under grant no. 03SF0670A. The results presented were achieved by computations carried out on the cluster system at the Leibniz Universität Hannover, Germany.

Appendix

The appendix is divided into two parts. First, further information is given on the methodology to derive CAPEX and future cost projections. Second, detailed techno-economics are derived for each component group described in Section 2.

A.1.1. Direct CAPEX incl. Scaling approach and concept of learning rates

The learning rate concept is a standard approach to project future costs in energy technologies and is frequently done in research, e.g., [154–158]. For a 2050 cost forecast, the direct CAPEX for the reference year 2020 are calculated and then translated into 2050 CAPEX based on specific learning rates. In Eq. 4 (Section 2.2), they are represented by the cost reduction factor $r_{i,t}$ for each component i.

A.1.1.1. Reference 2020 direct CAPEX

Direct CAPEX $C_{\mathrm{CAPEX,direct},i,2020}(x_i)$ are derived in detail for each component in Appendix A.2. As a summary, the 2020 direct CAPEX cost functions are based on the following Eq. A1 and A2:

$$C_{\mathrm{CAPEX,direct},i,2020}(x_i) = c_{i,2020}(x_i)^{*}x_i \tag{A1}$$

with

$$c_{i,2020}(x_i) = f_{\mathrm{a},i}{}^{*}x_i^{-f_{\mathrm{b},i}} \tag{A2}$$

The specific cost factor $c_{i,2020}(x_i)$ for each component depends on the scaling factors $f_{\mathrm{a},i}$ and $f_{\mathrm{b},i}$, both shown in Table A1 for all relevant components. While this scaling approach is used for most H_2 components, it is assumed that the RES plants and the electrolysis will not scale with larger design capacities. Reasoning is that these components are built modularly and hence, only learning rate effects apply.

Table A1
Specific direct CAPEX functions in 2020 for selected components from regressions shown in Appendix A.2.

Component i	**Cost scaling factor** $f_{\mathrm{a},i}$ for $c_{i,2020}$	**Cost scaling factor** $f_{\mathrm{b},i}$ for $c_{i,2020}$	**Cost function defined for** $x_i \leq$	**Fixed cost value** $c_{i,2020}$ for $x_i >$ (see left)
GH_2 compressor	16.3 USD_{2020}/W_{el}	0.163	16 MW_{el} power	1.1 USD_{2020}/W_{el}
GH_2 salt cavern	3,239 USD_{2020}/kg_{GH2}	0.355	4,000 t_{GH2} stored	15 USD_{2020}/kg_{GH2}
GH_2 aboveground storage	776.9 USD_{2020}/kg_{GH2}	0.053	500 t_{GH2} stored	385 USD_{2020}/kg_{GH2}
H_2 liquefaction plant (LFP)	7,389,583 USD_{2020}/tpd_{LH2}	0.276	500 tpd_{LH2}	1,330,000 USD_{2020}/tpd_{LH2}
LH_2 storage	126 USD_{2020}/kg_{LH2}	0.125	400tLH_2 stored	25 USD_{2020}/kg_{LH2}

Furthermore, the CAPEX functions do not apply for very large design sizes, but a fixed cost value is used, see Table A1. Otherwise, the cost functions would lead to further decrease of costs, which might not be realistic and such large plants might never be realized. The GH_2 compressor size is limited to 16 MW_{el} which is a maximum size found in the report of the H2A Delivery Model [99]. Cost effects for salt and rock cavern are kept fixed above 4 Mn $kgGH_2$ as shown by [106]. For GH_2 aboveground storages, no larger facilities were found in literature. Largest size of a planned LFP is around 300 tpd, so a limit of 500 tpd is chosen. Above that design, it is more likely to see a modularization of LFP plants, since cost savings might be limited and modular plants could allow a more flexible operation. For LH_2 storages, the largest installed projects are at the NASA site with around 300 tLH_2 stored [159].

A.1.1.2. Cost reduction factors due to learning rate concept

Projection of CAPEX functions (Eq. 4, Section 2.2) for a scenario or future point in time t are calculated with cost reduction factors, the learning rate $LR_{i,t}$ and the relevant market sizes $S_{i,t}$ (see Table A2):

$$r_{i,t} = \left(\frac{S_{i,t}}{S_{i,2020}}\right)^{b_{i,t}} \tag{A3}$$

with

$$b_{i,t} = \frac{\log(1 - LR_{i,t})}{\log(2)} \tag{A4}$$

Table A2
Overview of this study's assumptions for learning rate effects behind all components and underlying sources; mean values of market sizes are calculated based on the values found in indicated studies.

Component i	**Relevant market size today** $S_{i,2020}$	**Forecasted market size in 2035** $S_{i,2035}$	**Forecasted market size in 2050** $S_{i,2050}$	**Learning rate until 2035** $LR_{i,2035}$	**Learning rate 2035–2050 base** $LR_{i,2050}$	**Resulting cost reduction in 2035 base vs. 2020 costs** ($1\text{-}r_{i,2035}$)	**Resulting cost reduction in 2050 base vs. 2020 costs** ($1\text{-}r_{i,2050}$)
ELY	0.29 GW ELY cap. installed [82]	230 GW [76,82,84,160]	3,800 GW [76,82,84,160]	12%	10%	71%	81%
GH_2 compressor	90 Mn tGH_2 p. a. [82]	150 Mn tGH_2 p. a. [76,82,84,148,160]	500 Mn tGH_2 p. a. [76,82,84,148,160]	12%	10%	9%	24%
GH_2 above-ground storage	*Same market assumptions as for GH_2 compressor*			12%	10%	9%	24%

(*continued on next page*)

Table A2 (*continued*)

Component i	Relevant market size today $S_{i,2020}$	Forecasted market size in 2035 $S_{i,2035}$	Forecasted market size in 2050 $S_{i,2050}$	Learning rate until 2035 $LR_{i,2035}$	Learning rate 2035–2050 base $LR_{i,2050}$	Resulting cost reduction in 2035 base vs. 2020 costs ($1\text{-}r_{i,2035}$)	Resulting cost reduction in 2050 base vs. 2020 costs ($1\text{-}r_{i,2050}$)
LFP	0.2 Mn tLH_2 p. a. [149]	2 Mn tLH_2 p. a.	105 Mn tLH_2 p. a.	5%	10%	15%	54%
LH_2 storage	*Same market assumptions as for LFP*			5%	10%	15%	54%

For the ELY, installed capacities of water electrolysis systems are considered – excluding grey GH_2 production. Learning rates for such systems vary largely [72,74,82,161], here 12% is assumed for the main growth period until 2035 and 10% later on.

GH_2 compressor and GH_2 aboveground storages are already in use today for the current H_2 production capacities and distribution equipment. Consequently, the total H_2 market is taken to calculate cost reduction factors. Since, GH_2 cavern storages are highly individual for each project, no learning rates based on market sizes are used.

For LH_2 components, no specific market reports are found. The market size is derived as follows. In 2015, the global H_2 liquefaction capacity was around 350 tpd capacity [119] with another 250 tpd announced until 2020 [149]. If it is assumed that 600 tpd LFP capacity were operated on 365 days, this results in an annual LH_2 production amount of around 0.2 Mn tLH_2 for 2020. As a next step, H_2 market forecasts are screened for demands that might require LH_2 and not compressed GH_2 in the future. Next to aviation, this could be heavy-duty trucking and the maritime sector. It is assumed that 20% of these applications could be either fueled by LH_2 or the supply to refueling stations would be via the LH_2 route. With an average demand of 10 Mn tH_2 p.a. [82,148,160] the LH_2 share would be 2 Mn tLH_2 in 2035.

In 2050, this study includes further LH_2 demands from H_2-powered aircraft. An average value of 70 Mn tLH_2 p.a. is taken from two studies [1,13] predicting demand values of 20–130 Mn tLH_2 for H_2 in aviation in 2050. Thus, again 20% of the average market size of H_2-powered trucks and maritime applications (about 170 Mn tH_2 p.a.) are added – a total resulting LH_2 market size of around 105 Mn tLH_2.

Since relevant LH_2 markets are not expected to grow significantly before the 2030 s, but rather between 2035 and 2050, the learning rates are estimated to be higher for the second period than for the first. Consequently, a learning rate of 5% is assumed for the time period between 2020 and 2035 and 10% for 2035–2050. Such an approach of different learning rates distinguishing between an early, intermediate and mature market phase is also used in previous studies, e.g., by CSIRO [162].

All resulting cost reduction factors are well in line with other reports like from ANL [89] or the Hydrogen Council [74]. For the 2050 progressive scenario, the CAPEX are further reduced by 25% in all relevant cases compared to the 2050 base case (see Table 2, Section 2.3).

A.1.2. Installation, indirect CAPEX and other economic parameters

Direct CAPEX only consider the equipment costs. However, the supply components need to be installed and the project also includes further costs like for engineering design, project contingencies and owner's costs, e.g., for financing the project. These costs are reflected by the cost factors $f_{inst,i}$ and $f_{ind,i}$ for each component, see Table A3 and Eq. 3 in Section 2.2.

Several literature sources are found on installation and indirect CAPEX cost factors. In most cases, installation CAPEX factors vary between 1.1 and 1.3 [73,83,87,116,163]. In this study, factor 1.2 is taken for all GH_2 and 1.3 for more (thermodynamically) complex LH_2 components. The RES, ES and LFP CAPEX functions already describe total CAPEX.

Indirect CAPEX factor assumptions mostly range from 1.2 to 1.3 for different applications [73,83,87]. Consequently, an average value of 1.25 is chosen for all components.

On the availability factor, only a limited amount of sources is available. In general, it is assumed that storage components have a slightly higher availability than conversion components. Latter often require shorter maintenance intervals. An availability factor of 98% for conversion components is taken in [83] for the ELY, in [99] also for the LFP and in [164] for the RES components. Hence, the availability of storages is assumed to be around 99% which is in accordance with [83].

Table A3
Further economic assumptions for selected supply chain component – parameters not changing over considered time periods.

Component i	Installation CAPEX factor $f_{inst,i}$	Indirect CAPEX factor $f_{ind,i}$ (incl. engineering & design, project contingency etc.)	Availability rate $f_{avail,i}$
Electrolysis system	1.2	1.25	98%
GH_2 compressor	1.2	1.25	98%
GH_2 cavern storage	Already included in CAPEX function	1.25	99%
GH_2 aboveground storage	1.2	1.25	99%
H_2 liquefaction plant (LFP)	Already included in CAPEX function		98%
LH_2 storage & cryopumps	1.3	1.25	99% for storage and 98% for cryopumps

A.2. Component specific assumptions and models

In this part, all relevant techno-economic parameters and models are derived along the three energy balances of electricity, GH_2 and LH_2. All techno-economic parameters that are not explicitly discussed in the following are shown in Section 2.3 Table 2.

A.2.1. Renewable energy supply, transmission and electric energy storage

Renewable electricity is generated via utility/large-scale PV, onshore and offshore wind parks. For all three options, an availability curve for a specific location is generated with data from the open-source platform "Renewable.ninjas" [133,134]. Furthermore, AC electricity transmission is assumed for the short distances between best locations for the RES and the H_2 energy system. Thus, an ES can increase flexibility of operating electricity sourced components.

Photovoltaics (PV). In this study, one-axis azimuth tracking PV systems with 5% system losses are used, since they offer the best cost to output value at the chosen locations. While the azimuth value is fixed at 180 degrees, the tilt value differs for each site. Coordinates for the weather data profiles (solar yield) are shown in Table A4.

Wind on- and offshore. In general, land use of wind turbines is a limiting factor for new installations [165]. Therefore, a trade-off between larger power ratings of the turbines and its performance must be made for wind onshore plants. Hence, a 7 MW turbine is selected as suggested in [67] for the 2050 technology projection (today the average is around 4 MW). This turbine is characterized by a 150 m hub height, 200 m rotor diameter and a resulting specific power around 225 W/m^2 are selected in accordance with [63,67,137].

Table A4
Coordinates for weather data sourcing via open-source tool "Renewable.ninja" [133,134].

Location	Coordinates for solar yield data	Coordinates for wind speed data
PV	28.1759, 36.0174	–
Wind on-shore (WON)	–	57.4890, −2.2560
Wind off-shore (WOFF)	–	55.9211, 7.5256
Great hybrid (HYB)	27.9459, −10.4636	28.3574, −11.2906
Weak hybrid (WEAK)	50.2205, 8.7154	50.2205, 8.7154

For offshore wind parks, the IEA/NREL reference offshore turbine for 2050 is taken [135], which has a power rating of 15 MW with a 150 m hub height, 240 m rotor diameter and a specific power of 330 W/m^2.

The locations for the wind power plants are also shown in Table A4. Scotland is chosen for WON due to its great potential and space availabilities compared to other countries like Denmark and Germany (<5–10 GW). For offshore wind parks there is still great potential at many sites, here, a space in the Northern Sea is selected [130,131].

The LH_2 energy systems considered in this study require the installation of several wind turbines already for very small annual LH_2 demands. Previous studies highlight that forming such wind parks at sites with limited availability of space can cause significant aerodynamic losses for all wind turbines (on average) in that park. Such array losses are highly dependent on several park parameters (number, placing, height or rotor diameters of turbines) and the specific geography that is investigated [166]. In this study, an representative average energy loss for on– and offshore wind parks of 10% is chosen for all sites, a mean value based on [167–175].

Electricity transmission. Since space availability for RES is not always directly at the airport or not both PV and wind sites are directly co-located, electricity transmission over 50 to 100 km is assumed on average.

On short distances, high voltage AC (HVAC) transmission is less expensive than HVDC due to costly converter stations [176–179]. Based on values from [178] and [179] costs for HVAC cables are 0.3 USD/kW/km which is also in line with [180,181]. Furthermore, substations incl. transformers are needed which cost 7.8 USD/kW [178]. This results in total transmission costs of 30 USD/kW for 75 km distances. Since this technology is state-of-the-art, no cost differences are assumed for the different techno-economic scenarios.

For the depreciation period, a lifetime of 40 years is assumed with 100% availability [178,182]. Electricity losses for the 75 km due to the cables and the substations are 2.5% [178,183].

Electric energy storages. There are several electric energy storage technologies available. Here, a Lithium-Ion based grid storage with a 4-hours-durability is chosen. It is modelled via an energy balance. The efficiency is assumed to be 95% for charging and discharging (~90% total efficiency) [53,62].

A.2.2. Gaseous hydrogen equipment

Techno-economics of the ELY, compressors and GH_2 storages are explained in this section.

Electrolysis systems. Several water electrolysis technologies are available, but only two low-temperature ELY are currently discussed for H_2 generation in combination with RES and without making use of any heat sources: polymer electrolyte membrane (PEMEL) and alkaline electrolysis (AEL). Long-term projections of both technologies' performances are quite similar, which is why generic techno-economic assumptions are derived in the following.

In Fig. A2.1, the system efficiency of low-temperature water electrolysis and the relative GH_2 mass output are shown for rated power and part-load operations. The system describes the electrolysis stacks, cooling, purification, drying and control, but not compression of GH_2. The curve characteristics are derived based on a realized Siemens PEMEL (excluding compressors) [184]. The absolute energy consumption for the stack and system energy consumption (around 50 kWh/kgH_2 at rated power) are in line with values found in several sources [76,78,81,83,84,108,185,186]. The chosen consumption also represents the degradation of the stacks leading to 3–5% less performance on average over the whole ELY lifetime [85]. More progressive assumptions (green graph) leading to a system energy consumption of 45 kWh/kg are based on values from [72,82,87].

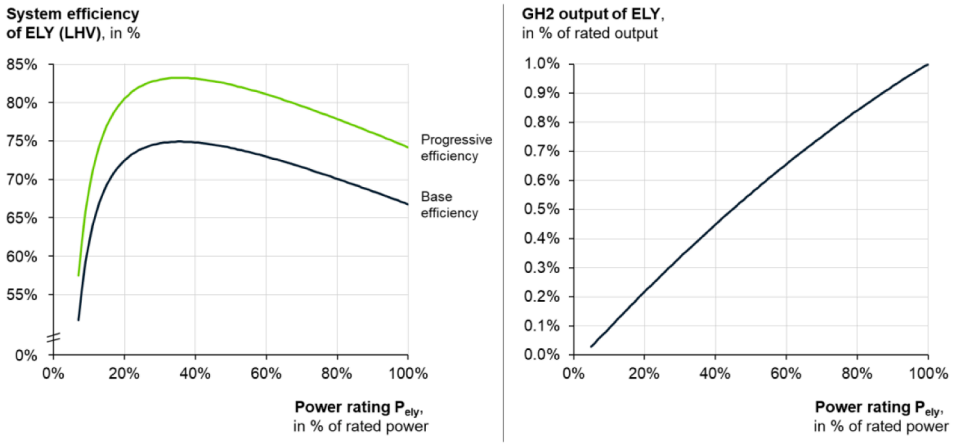

Fig. A2.1. Electric energy efficiency of chosen electrolysis system in dependence of the relative system power rating – left: system efficiency (LHV) with base efficiency of 50 kWh/kgH_2 on a system level for 2035 base, 2050 base case scenarios and progressive efficiency of 45 kWh/kgH_2 for 2050 progressive case scenario; right: relative GH_2 mass flow rate in dependence of power setting.

The default pressure output behind the electrolysis stacks and before a potentially installed ELY-compressor is 30 bar. The freshwater consumption of 13 L per kg H_2 generated is taken from [53,187].

Regarding the economics of the ELY, CAPEX scaling factors are limited, if plant sizes are larger than 5–10 MW [72,76,78,82,188,189]. Hence, fixed direct CAPEX are considered – 1,000 USD/kW_{el} in the reference year (2020). Based on the learning rates, these decrease to 292, 190 and 143 USD/kW_{el} in the 2035 base, 2050 base and 2050 progressive cases, respectively.

The operating cost factor $c_{OM,ELY,t}$ (Eq.6) for the ELY is calculated based on a fixed operations & maintenance (OM) factor $c_{OM,ELY,fixed,t}$ and a lifetime depending OM factor $c_{OM,ELY,stack,t}$, see Eq. A(5). The latter accounts for replacement costs of ELY stacks, when their end of lifetime is reached. Therefore, the cost factor for replacing the stacks $c_{ELY,stack}$ depends on the total CAPEX, the operating hours in the specific year of investigation t_{on} and lifetime of the ELY stacks $t_{ELY,stack,life}$ (Eq. A6):

$$c_{OM,ELY,t} = c_{OM,ELY,fixed,t} + c_{OM,ELY,stack,t} \tag{A5}$$

with

$$c_{OM,ELY,stack,t} = c_{ELY,stack} * \frac{t_{on}}{t_{ELY,stack,life}} \tag{A6}$$

Main parameters are shown in Table 2 (Section 2.3).

Gaseous hydrogen compressors. Compressors are installed as part of the electrolysis system to increase the pressure of the GH_2 mass flow and as part of the GH_2 storages or the GH_2 pipeline for loading them at the right input pressure. For larger mass flows, which are required in this study, reciprocating compressors are often used. The required electric power rating of the compressor $P_{GH2comp}$ is calculated as shown in Eq. A7 and A8:

$$P_{GH2comp} = \frac{1}{\eta} \cdot \frac{\kappa}{\kappa - 1} \cdot \frac{R \cdot Z_{H2} \cdot T_{in}}{n_{H2}} \cdot \left(\left(\frac{p_{out}}{p_{in}} \right)^{\left(1 - \frac{1}{\kappa}\right)} - 1 \right) \cdot \dot{m}_{GH2comp,in} \tag{A7}$$

with

$$\eta = \eta_{isen} \cdot \eta_{ele} \cdot \eta_{motor} \tag{A8}$$

Inputs are the universal gas constant R (8.314 J/(mol*K)) and the temperature of the GH_2 feed T_{in} which is assumed to be equal to an average ambient temperature of 288.15 K. Multi-stage compressors and cooling of these compressors stages should lead to constant temperatures for GH_2 compression. The compressibility factor Z_{H2} (1.0059) is relatively constant in a GH_2 pressure range of 30–200 bar [190]. Further constants are κ (1.4), the molar mass of H_2 n_{H2} (2.01588 g/mol), the isentropic efficiency η_{isen} (85%) [92,99], the electric efficiency η_{ele} (95%) [99] and the motor efficiency η_{motor} (91%) [99].

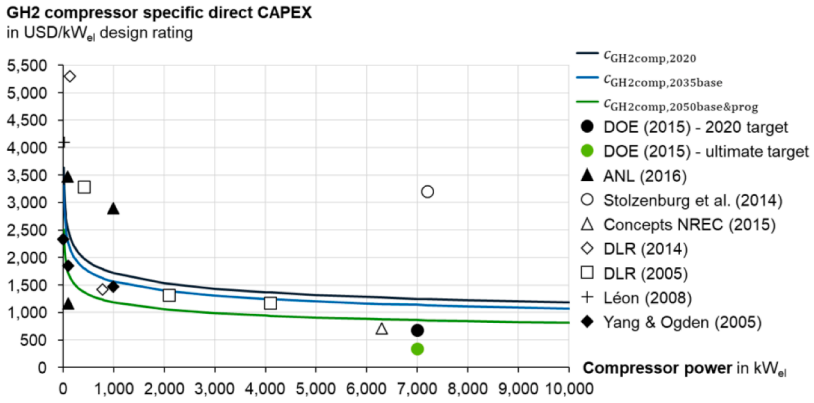

Fig. A2.2. Direct CAPEX functions for GH_2 compressor systems based on DOE [88], Argonne National Laboratory [89], Stolzenburg et al. [79], Concepts NREC report [191], DLR [90,112], Léon [91], Yang & Ogden [92].

The input pressure p_{in} for the incoming GH_2 feed is an optimization variable. The resulting output pressure p_{out} behind the compressor is given by the operating pressure of the storages or the pipeline.

Furthermore, H_2 losses occur at every compressor station with 0.5% per kgGH_2 feed [47,53], which is reduced to 0.4% in the 2050 progressive scenario [88].

Direct CAPEX are derived from sources that focus on lower-pressure compressors (120–200 bar target pressures), shown in Fig. A2.2.

Gaseous hydrogen storage. GH_2 is stored in underground caverns or aboveground pressure tanks that store H_2 at maximum pressures of 180 bar and 200 bar, respectively. For both, only H_2 losses are computed for the compressors when filling the storages ($\dot{m}_{GH2Sto,in}$) – no losses are assumed for storing GH_2 or unloading ($\dot{m}_{GH2Sto,out}$). A constant throttle valve is used for unloading at the minimum allowable storage pressure. This minimum pressure is equal to the pressure on the GH_2 balance which is an optimization variable (Section 2.2). The stored mass m_{GH2Sto} is computed as follows (Eq. A(9)):

$$\frac{d}{dt}m_{GH2Sto} = \dot{m}_{GH2Sto,in} - \dot{m}_{GH2Sto,out} \tag{A9}$$

Furthermore, maximum loading and unloading mass flows constraint the operation of the storages. While this is of minor importance for the aboveground tanks (several hours for full loading/unloading assumed), the mass flow into/out of the underground storage is limited to a maximum pressure change of 10 bar per day inside the cavern [79,108,192]. This equals a change of around 8% of the total mass in the storage per day. Reason for this constraint is the thermo-mechanical stress in the geological formation when loading/unloading, which has to be limited for stable operation and long lifetimes.

CAPEX functions for the storage systems (excl. compressors) are shown in Figs. A2.3–A2.4.

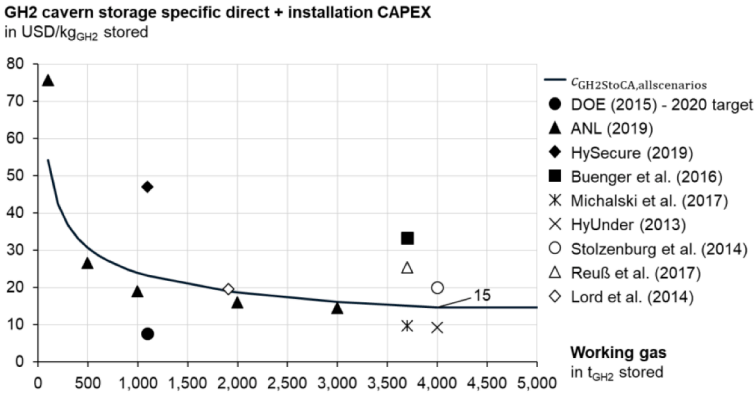

Fig. A2.3. Direct and installation CAPEX functions for GH_2 cavern systems based on DOE [88], Argonne National Laboratory [89], HySecure project [107], Buenger et al. [108], Michalski et al. [109], HyUnder project [110], Stolzenburg et al. [79], Reuß et al. [47] and Lord et al. [111].

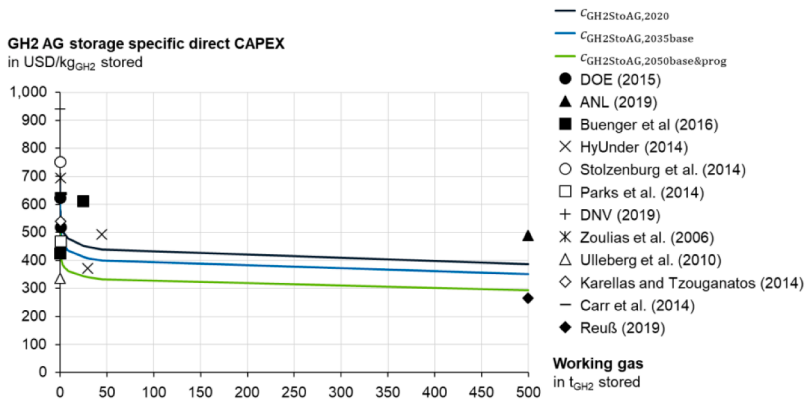

Fig. A2.4. Direct CAPEX functions for GH_2 aboveground systems based on DOE [88], Argonne National Laboratory [89], Buenger et al. [108], HyUnder project [110], Stolzenburg et al. [79], Parks et al. [116], DNV [117], Zoulias et al. [118], Ulleberg et al. [95], Karellas and Tzouganatos [114], Carr et al. [115] and Reuß et al. [47].

A.2.3. Liquid hydrogen equipment

This section describes all stationary LH_2 equipment, the LFP and storage systems.

Liquefaction plants. In the following, the specific energy consumption (SEC), losses and CAPEX are derived for the LFP.

The SEC depends on the ideal, minimal theoretical, liquefaction work $w_{LFP,ideal}$ which changes with different conditions of the GH_2 feed and the targeted end state of LH_2 after the liquefaction [193]. When the GH_2 feed is between 1 and 100 bar at a temperature of 288.15 K (as in [194]) with standard saturation of ortho- to *para*-H_2 molecules, the ideal work to reach saturated LH_2 is between 2 and 3 kWh/kgLH_2 plus 0.625 kWh/kgLH_2 for the ortho- to *para*-H_2-conversion [195]. This improvement potential also emphasizes why the optimization of the pressure on the GH_2 balance is of interest which feeds into the LFP. The ideal work characteristics are shown in Fig. A2.5 using the regression in Eq. A10:

$$w_{LFP,ideal}(288.15\,K, p_{GH2bus}) = 4.0596 \cdot p_{GH2bus}^{-0.117}\ [kWh/kg_{H2}] \tag{A10}$$

A second aspect influencing the LFP's SEC is the process design of the LFP. In this study, a very efficient Claude Cycle process with a mixed refrigerant pre-cooling cycle is selected for larger plants based on [102,196,197]. The SEC of this cycle $e_{LFP,cycle}$ is calculated based on its coefficient of performance *COP* (0.46) and the ideal liquefaction work [102].

$$e_{LFP,cycle}(p_{GH2bus}) = \frac{w_{LFP,ideal}(p_{GH2bus})}{COP} \cdot \left(COP + 0.25 \cdot f_{LFP,HEX}(p_{GH2bus}) + 0.29\right) \tag{A11}$$

The equation describes that the exergy losses for the liquefaction process are proportional to the change of ideal work, but not for the factor of exergy losses in the heat exchangers $f_{LFP,HEX}$. It decreases by 1% for a feed pressure increase from 25 to 75 bar due to smaller heat exchanger volumes – an effect that requires the use of turbo expanders and which is limited to maximum feed pressures of 80 bar [102,198].

$$f_{LFP,HEX}(p_{GH2bus}) = 1.005 - 0.0002 \cdot p_{GH2bus} \tag{A12}$$

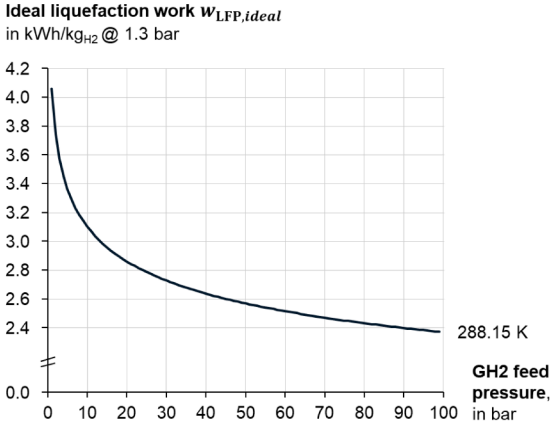

Fig. A2.5. Ideal work for H_2 liquefaction depending on the pressure of the GH_2 feed, data from [190,199].

The SEC also depends on the size of the plant x_{LFP}. Values for $e_{LFP,size}(x_{LFP})$ are derived from a literature overview where all process exergy calculations were adjusted to a GH_2 feed pressure of 30 bar, see Fig. A2.6. A regression for smaller plants of 100 tpd capacity and below is shown in Eq. A13, above this threshold a fixed optimized SEC is considered.

$$e_{LFP,size}(x_{LFP}) = \begin{cases} -1.85 \cdot \ln(x_{LFP}) + 15 - 0.41 kWh/kg_{H2}, for x_{LFP} \le 100 tpd \\ 6.1 kWh/kg_{H2}, for x_{LFP} > 100 tpd \end{cases} \tag{A13}$$

The final rated specific energy consumption at full load operation is calculated with the results from Eq. A11 and Eq. A13:

$$e_{\mathrm{LFP,rated}}\left(p_{\mathrm{GH2bus}},x_{\mathrm{LFP}}\right)=\frac{e_{\mathrm{LFP,cycle}}\left(p_{\mathrm{GH2bus}}\right)}{e_{\mathrm{LFP,cycle}}\left(p_{\mathrm{GH2bus,ref}}=30\mathrm{bar}\right)}\cdot e_{\mathrm{LFP,size}}\left(x_{\mathrm{LFP}}\right) \tag{A14}$$

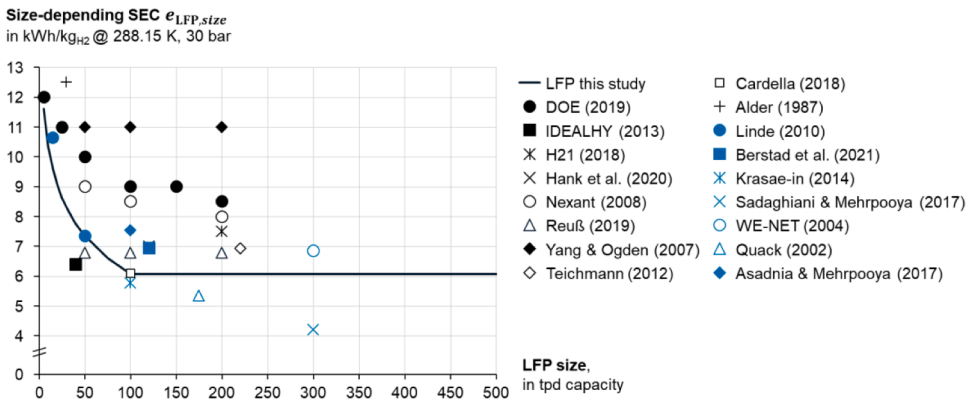

Fig. A2.6. Size-depending SEC of LFP based on [73,93,97–103,194,200–206].

The last aspect, which is considered for the calculation of the LFP's performance is the change of efficiency when operated in part-load. Even though data on the characteristic for part-load operation is only provided by the IDEALHY project [198] and a slightly different liquefaction process design, it is assumed to be relevant and applicable for the process chosen in this study, too. The increase of SEC for each mass flow setting is shown in Fig. A2.7 and described in Eq. A15:

$$e_{\mathrm{LFP,PL}}\left(\dot{m}_{\mathrm{LFP,in}}\right)=1+\left(\frac{2641}{\left(\frac{\dot{m}_{\mathrm{LFP,in}}}{\dot{m}_{\mathrm{LFP,in,max}}}\cdot 100\right)^{1.154}}-12.84\right)\cdot 0.01 \tag{A15}$$

Finally, the resulting SEC for the LFP and a given design pressure on the GH_2 balance, the design capacity of the LFP and the current operational point in terms of mass flow is determined:

$$e_{LFP}\left(p_{\mathrm{GH2bus}},x_{\mathrm{LFP}},\dot{m}_{\mathrm{LFP,in}}\right)=e_{\mathrm{LFP,rated}}\left(p_{\mathrm{GH2bus}},x_{\mathrm{LFP}}\right)\cdot e_{\mathrm{LFP,PL}}\left(\dot{m}_{\mathrm{LFP,in}}\right) \tag{A16}$$

In a next step, losses of the LFP are considered. H_2 losses occur mostly in compression and expansion steps. While literature values indicate a range of 0.5–1.65% losses per kgH_2 feed [46,97,102], these often include losses due to a compression of H_2 from 1 to 30 bar. Since this study excludes this compression step from the LFP (part of the ELY), H_2 losses are assumed to be 1% in the 2035 and 2050 base and 0.5% in the 2050 progressive scenarios. In addition to that, losses of the mixed-refrigerant (MR) occur: 0.5% of MR per kgH_2 feed going through the LFP [102]. Costs for the MR are taken from [102,207] with 0.50 USD/kgMR. Seal gas losses are very small and already part of the fixed OM costs.

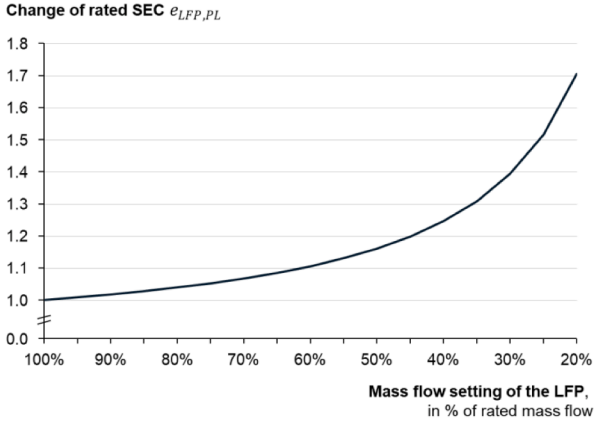

Fig. A2.7. Factor for SEC change in part-load operation depending on the LFP's mass flow setting from [198].

The specific total CAPEX $c_{\mathrm{CAPEX,total,LFP},t}$ of the LFP are shown in Fig. A2.8. In contrary to the CAPEX functions of other components, one additional effect has to be reflected for the LFP. The increase of the GH_2 feed pressure comes at a cost for more robust heat exchangers. In terms of the total CAPEX $C_{\mathrm{CAPEX,LFP},i}(x_{\mathrm{LFP}},p_{\mathrm{GH2bus}})$, this causes an increase of 1.5% for a heat exchanger in a LFP that is designed for 80 bar vs. a standard 30 bar feed pressure [102,208]. The total CAPEX for the LFP are calculated as follows with the additional cost factor for the heat exchanger pressure adoptions $f_{\mathrm{LFP,HEX}}$, which is valid for 30 bar $\leq p_{\mathrm{GH2bus}} \leq$ 80 bar:

$$C_{\mathrm{CAPEX,LFP},i}\left(x_{\mathrm{LFP}},p_{\mathrm{GH2bus}}\right)=r_{\mathrm{LFP},i}\cdot f_{\mathrm{LFP,HEX}}\left(p_{\mathrm{GH2bus}}\right)\cdot C_{\mathrm{CAPEX,total,LFP,2020}}\left(x_{\mathrm{LFP}}\right) \tag{A17}$$

with

$$f_{\mathrm{LFP,HEX}}(p_{\mathrm{GH2bus}}) = 0.0003 \cdot p_{\mathrm{GH2bus}} + 0.991 \tag{A18}$$

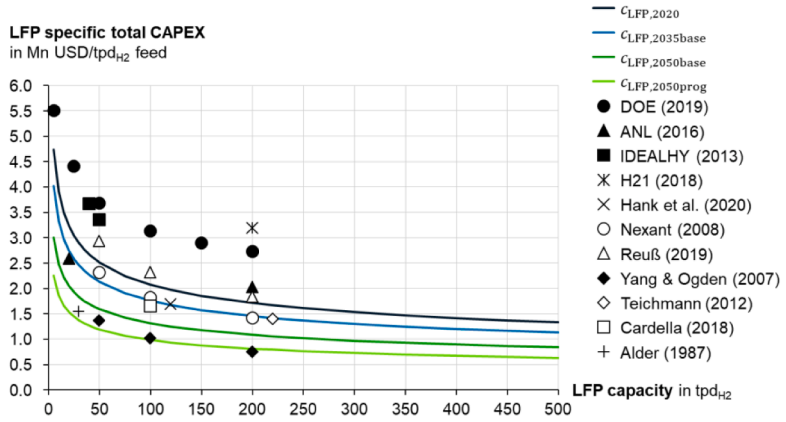

Fig. A2.8. Total CAPEX function for LFP depending on the design capacity, values based on DOE [200], ANL [89], IDEALHY project [97], H21 report [73], Hank et al. [98], Nexant report [99], Reuß [93], Yang & Ogden [100], Teichmann [101], Cardella [102], Alder [103].

Liquid hydrogen storage systems. There are different sizes and applications of LH_2 storages realized today. In this study, spherical shapes are considered. Such tanks come with a slightly higher ullage (not usable mass to ensure stable cryo-temperatures) of 10% compared to around 5% for cylindrical tanks (e.g., on LH_2 trucks) [209]. Even though the storages are double-wall vacuum insulated, boil-off occurs. The boil-off (BO), self-discharging factor $k_{\mathrm{BO,LH2Sto}}$ can be calculated using this regression in dependence of the storage size (Eq. A19) which is derived from literature values shown in Fig. A2.9:

$$k_{\mathrm{BO,LH2Sto}} = 0.014 x_{\mathrm{LH2Sto}}^{-0.255} \tag{A19}$$

The total stored mass m_{LH2Sto} in the LH_2 storages can be determined with the fill level of the storage F_{LH2Sto}, all LH_2 storage mass flows and the maximum capacity of the tank $m_{\mathrm{LH2Sto,max}}$:

$$\frac{d}{dt} m_{\mathrm{LH2Sto}} = \dot{m}_{\mathrm{LH2Sto,in}} - \dot{m}_{\mathrm{LH2Sto,out}} - k_{\mathrm{BO,LH2Sto}} \cdot F_{\mathrm{LH2Sto}} \cdot m_{\mathrm{LH2Sto,max}} \tag{A20}$$

The specific direct CAPEX functions for LH_2 storages are shown in Fig. A2.10.

For cryopumps, only limited information is available due to few realized products yet [34,37,93]. The pumps are designed based on maximum loading and unloading flow rates required for the LH_2 storages. They have a fixed electric energy consumption of 0.1 kWh/kgLH_2 flow rate and also a constant specific direct CAPEX factor of 256 USD per kg/h capacity in 2020 [47,93,99]. Due to learning effects this is assumed to decrease to 218 and 162 USD per kg/h in 2035 and both 2050 scenarios, respectively.

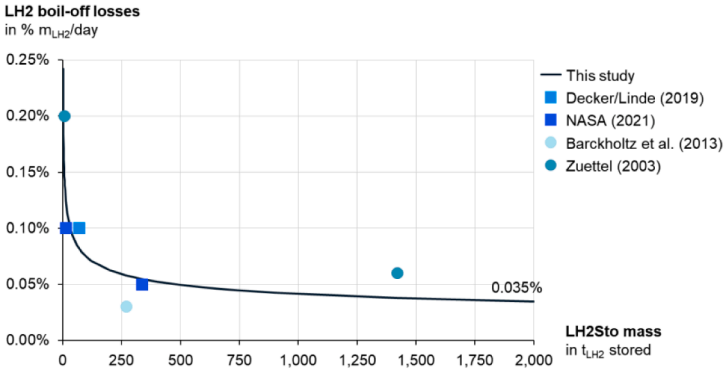

Fig. A2.9. Boil-off losses for LH_2 storages depending on storage size, values from Decker [209], NASA [159], Barckholtz et al. [210] and Zuettel [211].

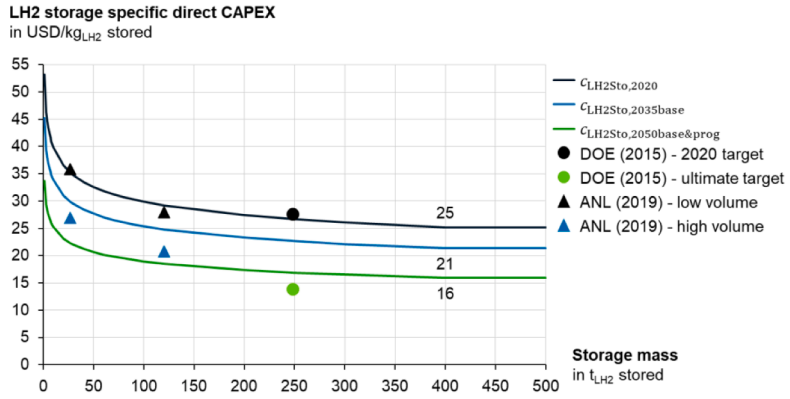

Fig. A2.10. Direct CAPEX function for LH_2 storages (excl. cryopumps) based on DOE [88] and ANL [106].

A.2.4. Hydrogen transport equipment

GH_2 pipelines and LH_2 vessels in combination with LH_2 trucks are the main H_2 transport modes in scope of this study. All relevant techno-economics are derived in this section.

GH_2 transport via pipelines

The GH_2 pipelines can be new built or retrofitted based on decommissioned natural gas pipelines. A pipeline system consists of many components – however, CAPEX are mainly caused by the pipes and the compressor stations. The number of compressor stations required for a given pipeline system is determined based on several design parameters like the mean flow speed through the pipeline $\dot{v}_{pipe,m}$.

The pipeline input pressure $p_{pipe,1}$ is set to 70 bar and the final output pressure $p_{pipe,2}$ to 30 bar, which is in line for the design of medium to larger transmission pipelines [57,80].

In a first step, the required diameter of the pipes has to be calculated with the cross-sectional area of the pipe A_{pipe}, the maximum flow rate $\dot{m}_{pipe,in,\,max}$, the mean density of H_2 in the pipes ρ_m and the mean flow speed (Eq. A21). The maximum flow rate is sized according to the maximum intake capacity of the LFP $\dot{m}_{LFP,in,\,max}$, while the mean flow speed must be at least 10 m/s and must not exceed 20 m/s. Further inputs for computation of the mean density is a regression from [190] in Eq. A22 and the mean pressure in the pipeline p_m (Eq. A23):

$$D_{pipe} = 2\cdot\sqrt{\frac{A_{pipe}}{\pi}} = 2\cdot\sqrt{\frac{\dot{m}_{pipe,in,\,max}}{\pi\cdot\rho_m\cdot\dot{v}_{pipe,m}}} \tag{A21}$$

With

$$\rho_m(p_m) = -5\cdot10^{-5}\cdot p_m^2 + 0.0841\cdot p_m + 0.0007 \tag{A22}$$

With

$$p_m = \frac{2}{3}\cdot\frac{p_{pipe,1}^3 - p_{pipe,2}^3}{p_{pipe,1}^2 - p_{pipe,2}^2} \tag{A23}$$

In a second step, the maximum length between two compressor stations $L_{GH2pipe,comp}$ is derived in Eq. A24 (Darcy–Weisbach-equation [212]) with the friction factor λ_{pipe} (Eq. A25 – Nikuradse-equation [213]), mean compressibility K_m (Eq. A26, [190]) and the norm volume flow rate $\dot{V}_n$ (Eq. A27):

$$L_{pipe,comp} = \left(p_{pipe,1}^2 - p_{pipe,2}^2\right)\cdot\left(\frac{D_{pipe}^5}{\lambda_{pipe}}\cdot\frac{\pi^2}{16}\cdot\frac{T_n}{T_m}\cdot\frac{1}{\rho_n\cdot p_n\cdot\dot{V}_n^2\cdot K_m}\right) \tag{A24}$$

with

$$\lambda_{pipe} = \left(2\cdot\log\left(\frac{D_{pipe}}{k_{pipe}}\right) + 1.138\right)^{-2} \tag{A25}$$

with

$$K_m = \frac{1}{Z_{H2,n}}\,\frac{p_m}{\rho_m(p_m)\cdot R_s\cdot T_m} \tag{A26}$$

with

$$\dot{V}_n = \frac{\dot{m}_{pipe,in,max}}{\rho_n} \text{ (A27)V}$$

Parameters are the pipe roughness coefficient $k_{pipe} = 0.0002$ m, the norm compressibility factor $Z_{H2,n}$(1.0005), norm and mean temperatures of GH_2 T_n (273.15 K), T_m (288.15 K), norm density and pressure of GH_2 ρ_n (0.0889 kg/m^3), p_n (101,325 Pa), and the specific gas constant R_s (4,124.2 J/kgK).

In a last step, the number of required compressors $n_{\text{pipe,comp}}$ (Eq. A28) is determined based on the total length of the pipes $L_{\text{pipe,total}}$ and the above calculated length between compressor stations:

$$n_{\text{pipe,comp}} = \frac{L_{\text{pipe,total}}}{L_{\text{pipe,comp}}} - 1 \tag{A28}$$

Then, the GH_2 mass losses $\dot{m}_{\text{pipe,losses}}$ via these compressor stations are derived (Eq. A29):

$$\dot{m}_{\text{pipe,losses}} = \dot{m}_{\text{pipe,in}} - \dot{m}_{\text{pipe,in}} \cdot 0.995^{n_{\text{pipe,comp}}} \tag{A29}$$

The specific total CAPEX functions for installing new pipelines (excl. compressors – see A2.2) or retrofitting existing pipelines depend on the diameter size of the pipes and are shown in Fig. A2.11.

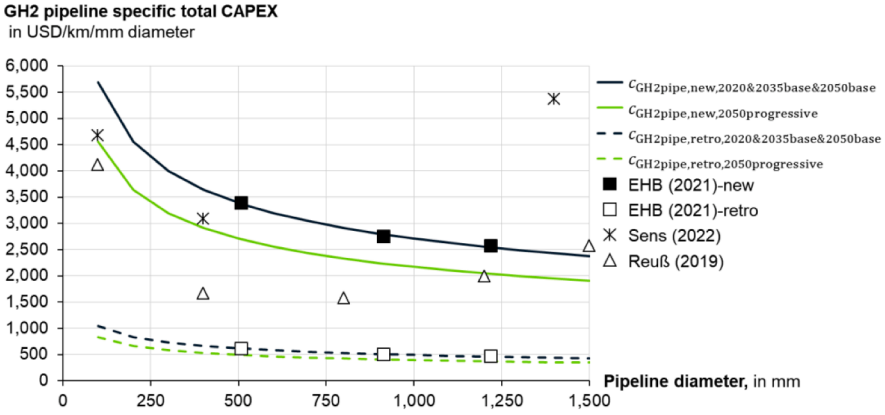

Fig. A2.11. Total CAPEX function for GH_2 pipelines (excl. compressors), new-built and retrofitted based on the EHB report [80], Sens [53] and Reuß [93].

LH_2 transport via vessels

The main techno-economics of LH_2 vessel transport depend on the number of vessels n_{vessel} required to operate the transport network (Eq. A30), the capacity of the vessels m_{vessel} (Eq. A31) and the trip characteristics.

In general, the amount of needed vessels is calculated with the number of possible annual departures $n_{\text{vessel,departures}}$ and the number of annual trips $n_{\text{vessel,trips}}$ that can be operated with one vessel (Eq. A32) given its trip performance (Eq. A33). The number of annual vessel departures is an optimization variable and characterizes the transport network design. As a constraint, a minimum of weekly departures is taken to ensure a supply reliability at the importing location. Thus, a maximum departure amount caps this optimization variable on the upper end – only sequential loading of vessels is assumed at the export terminal. With a loading and unloading time at the terminal $t_{\text{vessel,terminal}}$ of 48 h, only 3.5 vessels can be handled per week as a maximum.

$$n_{\text{vessel}} = \frac{n_{\text{vessel,departures}}}{n_{\text{vessel,trips}}} \tag{A30}$$

$$m_{\text{vessel}} = \frac{m_{\text{LH2demand}} \cdot f_{\text{LH2demand,peak}}}{n_{\text{vessel,departures}}} \tag{A31}$$

The trip characteristics are determined with the availability of the vessel $f_{\text{avail,vessel}}$ (0.91) (8,000 h per year [53,214]), the trip distance $L_{\text{vessel,trip}}$ and the speed of the vessel $v_{\text{vessel}} = 33.33$ km/h [53,123,214,215].

$$n_{\text{vessel, trips}} = \frac{8760\text{h}}{t_{\text{vessel,roundtrip}}} \cdot f_{\text{avail,vessel}} \tag{A32}$$

with

$$t_{\text{vessel,roundtrip}} = 2 \cdot \left(\frac{L_{\text{vessel,trip}}}{v_{\text{vessel}}} + t_{\text{vessel,terminal}} \right) \tag{A33}$$

While loading the vessel, H_2 flash losses might occur. In the 2035 and 2050 base cases, this is assumed to be 1% of the total mass being filled into the vessel. In the 2050 progressive scenario, solutions are available to eliminate such losses. On trips, BO occurs in the storages – the GH_2 is used for propulsion. Due to the mobile use of the LH_2 tanks on the vessel, a BO rate with a factor 2.5 is assumed compared to the BO characteristics of the stationary storages (Eq. A19, Fig. A2.9). This is in accordance with values from [53,75,120,123,214].

The specific total CAPEX per vessel are shown in Fig. A2.12 and depend on the LH_2 transport capacity.

As part of the OPEX, costs are accounted for the fuel consumption (if BO mass is not sufficient), fixed OM for the vessel and other annual OPEX for crew, port or navigation fees. The fuel consumption of 0.0189 kWh/tonscapacity/km [216] and the other OPEX of 11.3 Mn USD [80,124] are for a vessel with 11,000 tLH_2 capacity and are computed proportionally to the changing vessel sizes.

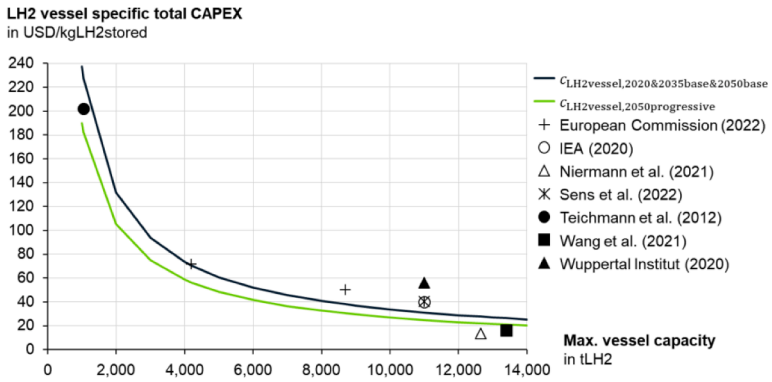

Fig. A2.12. Total CAPEX function defined for LH_2 vessels with 1,000–14,000 tLH_2 max. capacity, data from European Commission [120], IEA [75], Niermann et al. [121], Sens et al. [53], Teichmann et al. [101], EHB report/Wang et al. [80] and the Wuppertal Institut [122].

The design and costs of the import terminals are as large as the capacity of the vessels. Techno-economics are calculated as previously described in A.2.3 for LH_2 storages and cryopumps.

LH_2 transport via trucks

The truck carries a 4.5 tLH_2 trailer storage and an availability of 3,500 h per year [101]. The number of trips with one LH_2 truck system are calculated as for the vessel in Eq. A32 and A33. The mean truck speed is assumed to be 50 km/h [47,53]. The loading and unloading takes 45 min each [34,37].

As for the LH_2 vessel loading, same size of flash losses is assumed when loading the LH_2 truck storages. For the BO rate of the cylindrical tank 0.1% is taken [37]. Thus, a 0.07 kgH_2/km fuel consumption is chosen for the truck system [47].

Appendix B. Supplementary data

Supplementary data to this article can be found online at https://doi.org/10.1016/j.ecmx.2023.100442.

References

[1] Clean Sky 2 JU, FCH 2 JU, Hydrogen-powered aviation: A fact-based study of hydrogen technology, economics, and climate impact by 2050, 2020. https://doi.org/10.2843/766989.

[2] NLR - Royal Netherlands Aerospace Centre, SEO Amsterdam Economics, Destination 2050-A route to net zero European aviation, 2021.

[3] Grewe V, Rao AG, Grönstedt T, Xisto C, Linke F, Melkert J, et al. Evaluating the climate impact of aviation emission scenarios towards the Paris agreement including COVID-19 effects. Nat Commun 2021;12:1–10. https://doi.org/10.1038/s41467-021-24091-y.

[4] International Transport Forum, Decarbonising Air Transport: Acting Now for the Future, 2021.

[5] Mission Possible Partnership, Making Net-Zero Aviation Possible - An industry-backed, 1.5°C-aligned transition strategy, 2022.

[6] Bergero C, Gosnell G, Gielen D, Kang S, Bazilian M, Davis SJ. Pathways to net-zero emissions from aviation. Nat Sustain 2023;6(4):404–14.

[7] Dray L, Schäfer AW, Grobler C, Falter C, Allroggen F, Stettler MEJ, et al. Cost and emissions pathways towards net-zero climate impacts in aviation. Nat Clim Chang 2022;12:956–62. https://doi.org/10.1038/s41558-022-01485-4.

[8] Owen B, Lee DS, Lim L. Flying into the future : aviation emissions scenarios to 2050. Environ Sci Technol 2010. https://www.researchgate.net/profile/David_Lee81/publication/41941361_Flying_into_the_Future_Aviation_Emissions_Scenarios_to_2050/links/0046352b0deee58d53000000.pdf (accessed April 24, 2017.

[9] Lee DS, Fahey DW, Skowron A, Allen MR, Burkhardt U, Chen Q, et al. The contribution of global aviation to anthropogenic climate forcing for 2000 to 2018. Atmos Environ 2000;244(2021):1–29. https://doi.org/10.1016/j.atmosenv.2020.117834.

[10] V. Grewe, Addressing non-CO2 effects of aviation, presented at ICSA Aviation Decarbonization Forum, February, 2019.

[11] Brazzola N, Patt A, Wohland J. Definitions and implications of climate-neutral aviation. Nat Clim Chang 2022;12:761–7. https://doi.org/10.1038/s41558-022-01404-7.

[12] Becken S, Mackey B, Lee DS. Implications of preferential access to land and clean energy for Sustainable Aviation Fuels. Sci Total Environ 2023;886:163883. https://doi.org/10.1016/j.scitotenv.2023.163883.

[13] Mukhopadhaya J, Rutherford D. Performance Analysis of Evolutionary Hydrogen-Powered Aircraft, Washington DC, 2022.

[14] Scholz AE, Michelmann J, Hornung M. Fuel cell hybrid-electric aircraft: design, operational, and environmental impact. J Aircr 2023;60(3):606–22.

[15] P. Ansell, K. Haran, P. Laskaridis, Hydrogen-Electric Aircraft Technologies, 2022.

[16] Prewitz M, Bardenhagen A, Beck R. Hydrogen as the fuel of the future in aircrafts – challenges and opportunities. Int J Hydrogen Energy 2020;45:25378–85. https://doi.org/10.1016/j.ijhydene.2020.06.238.

[17] Ponater M, Marquart S, Ström L, Gierens K, R. Sausen, G. Hüttig, On the potential of the cryoplane technology to reduce aircraft climate impact, Proc. AAC-Conference, Friedrichshafen. (2003) 316–321.

[18] Khandelwal B, Karakurt A, Sekaran PR, Sethi V, Singh R. Hydrogen powered aircraft: the future of air transport. Prog Aerosp Sci 2013;60:45–59. https://doi.org/10.1016/j.paerosci.2012.12.002.

[19] Haglind F, Hasselrot A, Singh R. Potential of reducing the environmental impact of aviation by using hydrogen Part III: Optimum cruising altitude and airport implications. Aeronaut J 2006;110:553–65. https://doi.org/10.1017/s0001924000013853.

[20] Adler EJ, Martins JRRA. Hydrogen-powered aircraft: fundamental concepts, key technologies, and environmental impacts. Prog. Aerosp Sci 2023.

[21] Svensson F. Potential of reducing the environmental impact of civil subsonic aviation by using liquid hydrogen. Cranfield University; 2005.

[22] Airbus Deutschland GmbH, Cryoplane: Liquid Hydrogen Fuelled Aircraft - Final Technical Report, 2003.

[23] Kossarev K, Scholz AE, Hornung M. Comparative environmental life cycle assessment and operating cost analysis of long-range hydrogen and biofuel fueled transport aircraft. CEAS Aeronaut J 2023;14(1):3–28.

[24] Troeltsch F, Engelmann M, Peter F, J. Kaiser, M. Hornung, A.E. Scholz, Hydrogen Powered Long Haul Aircraft with Minimized Climate Impact, Aiaa Aviat. 2020 Forum. (2020) 14. https://doi.org/10.2514/6.2020-2660.

[25] Silberhorn D, Atanasov G, Walther J-N, Zill T. Assessment of Hydrogen Fuel Tank Integration At Aircraft Level, Proc. Dtsch. Luft- Und Raumfahrtkongress. (2019) 1–14.

[26] Verstraete D. The Potential of Liquid Hydrogen for long range aircraft propulsion. Cranfield University; 2009.

[27] Rompokos P, Rolt A, Nalianda D, Isikveren AT, Senné C, Gronstedt T, et al. Synergistic technology combinations for future commercial aircraft using liquid hydrogen. J Eng Gas Turbines Power 2021;143. https://doi.org/10.1115/1.4049694.

[28] Onorato G, Proesmans P, Hoogreef MFM. Assessment of hydrogen transport aircraft: Effects of fuel tank integration. CEAS Aeronaut J 2022;13:813–45. https://doi.org/10.1007/s13272-022-00601-6.

[29] Bloomberg, Airbus Warns Lack of Infrastructure May Delay Hydrogen Plane, (2022). https://www.bloomberg.com/news/articles/2022-11-30/airbus-warns-lack-of-infrastructure-may-delay-hydrogen-aircraft (accessed December 1, 2022).

[30] Janić M. Greening commercial air transportation by using liquid hydrogen (LH2) as a fuel. Int J Hydrogen Energy 2014;39:16426–41. https://doi.org/10.1016/j.ijhydene.2014.08.011.

[31] Pinheiro Melo S, Barke A, Cerdas F, Thies C, Mennenga M, Spengler TS, et al. Sustainability assessment and engineering of emerging aircraft technologies-challenges, methods and tools. Sustainability 2020;12(14):5663.
[32] Hydrogen Council, Hydrogen decarbonization pathways - A life-cycle assessment, 2021.
[33] Hoelzen J, Silberhorn D, Zill T, Bensmann B, Hanke-Rauschenbach R. Hydrogen-powered aviation and its reliance on green hydrogen infrastructure - review and research gaps. Int J Hydrogen Energy 2022;47:3108–30. https://doi.org/10.1016/j.ijhydene.2021.10.239.
[34] Mangold J, Silberhorn D, Moebs N, Dzikus N, Hoelzen J, Zill T, et al. Refueling of LH2 aircraft—assessment of turnaround procedures and aircraft design implication. Energies 2022;15:2475. https://doi.org/10.3390/en15072475.
[35] Amy C, Kunycky A. Hydrogen as a renewable energy carrier for commercial aircraft, ArXiv Prepr. ArXiv1910.05632. (2019) 1–41.
[36] Fusaro R, Vercella V, Ferretto D, Viola N, Steelant J. Economic and environmental sustainability of liquid hydrogen fuel for hypersonic transportation systems. CEAS Sp J 2020;12:441–62. https://doi.org/10.1007/s12567-020-00311-x.
[37] Hoelzen J, Flohr M, Silberhorn D, Mangold J, Bensmann A, Hanke-Rauschenbach R. H2-powered aviation at airports – design and economics of LH2 refueling systems. Energy Convers Manag X 2022;14:100206. https://doi.org/10.1016/j.ecmx.2022.100206.
[38] Cooper N, Horend C, Röben F, Bardow A, Shay N. A framework for the design & operation of a large-scale wind-powered hydrogen electrolyzer hub. Int J Hydrogen Energy 2022;47:8671–86. https://doi.org/10.1016/j.ijhydene.2021.12.225.
[39] Raab M, Körner R, Dietrich RU. Techno-economic assessment of renewable hydrogen production and the influence of grid participation. Int J Hydrogen Energy 2022;47:26798–811. https://doi.org/10.1016/j.ijhydene.2022.06.038.
[40] Heuser PM, Ryberg DS, Grube T, Robinius M, Stolten D. Techno-economic analysis of a potential energy trading link between Patagonia and Japan based on CO2 free hydrogen. Int J Hydrogen Energy 2019;44:12733–47. https://doi.org/10.1016/j.ijhydene.2018.12.156.
[41] Oliva SH, Garcia MG. Investigating the impact of variable energy prices and renewable generation on the annualized cost of hydrogen. Int J Hydrogen Energy 2023;48(37):13756–66.
[42] Hofrichter A, Rank D, Heberl M, Sterner M. Determination of the optimal power ratio between electrolysis and renewable energy to investigate the effects on the hydrogen production costs. Int J Hydrogen Energy 2023;48:1651–63. https://doi.org/10.1016/j.ijhydene.2022.09.263.
[43] Maurer W, Rechberger P, Justl M, Keuschnigg R. Parameter study for dimensioning of a PV optimized hydrogen supply plant. Int J Hydrogen Energy 2022;47:40815–25. https://doi.org/10.1016/j.ijhydene.2022.09.183.
[44] Heuser PM, Grube T, Heinrichs H, Robinius M, Stolten D. Worldwide Hydrogen Provision Scheme Based on Renewable Energy, (2020) 1–27.
[45] Robinius M, Markewitz P, Lopion P, Kullmann F, P.-M. Heuser, K. Syranidis, S. Cerniauskas, T. Schöb, M. Reuß, S. Ryberg, L. Kotzur, D. Caglayan, L. Welder, J. Linßen, T. Grube, H. Heinrichs, P. Stenzel, D. Stolten, Wege für die Energiewende - Kosteneffiziente und klimagerechte Tranformationsstrategie für das deutsche Energiesystem bis zum Jahr 2050, Forschungszentrum Jülich GmbH, 2020.
[46] Reuß M, Grube T, Robinius M, Stolten D. A hydrogen supply chain with spatial resolution: Comparative analysis of infrastructure technologies in Germany. Appl Energy 2019;247:438–53. https://doi.org/10.1016/j.apenergy.2019.04.064.
[47] Reuß M, Grube T, Robinius M, Preuster P, Wasserscheid P, Stolten D. Seasonal storage and alternative carriers: A flexible hydrogen supply chain model. Appl Energy 2017;200:290–302. https://doi.org/10.1016/j.apenergy.2017.05.050.
[48] Robles JO, Almaraz SDL, Azzaro-Pantel C. Optimization of a hydrogen supply chain network design by multi-objective genetic algorithms. Elsevier Masson SAS; 2016. 10.1016/B978-0-444-63428-3.50139-9.
[49] De-León Almaraz S, Azzaro-Pantel C, Montastruc L, Boix M. Deployment of a hydrogen supply chain by multi-objective/multi-period optimisation at regional and national scales. Chem Eng Res Des 2015;104:11–31. https://doi.org/10.1016/j.cherd.2015.07.005.
[50] De-León Almaraz S, Azzaro-Pantel C, Montastruc L, Domenech S. Hydrogen supply chain optimization for deployment scenarios in the Midi-Pyrénées region, France. Int J Hydrogen Energy 2014;39:11831–45. https://doi.org/10.1016/j.ijhydene.2014.05.165.
[51] Robles JO, Almaraz SDL, Azzaro-Pantel C. Hydrogen supply chain design: Key technological components and sustainable assessment, 2018. https://doi.org/10.1016/B978-0-12-811197-0.00002-6.
[52] Kotzur L, Nolting L, Hoffmann M, Groß T, Smolenko A, Priesmann J, et al. A modeler's guide to handle complexity in energy system optimization. Renew. Sustain Energy Rev. 2020.
[53] Sens L, Piguel Y, Neuling U, Timmerberg S, Wilbrand K, Kaltschmitt M. Cost minimized hydrogen from solar and wind – Production and supply in the European catchment area. Energy Convers Manag 2022;265:115742. https://doi.org/10.1016/j.enconman.2022.115742.
[54] Gronau S, Hoelzen J, Mueller T, Hanke-Rauschenbach R. Hydrogen-powered aviation in Germany: A macroeconomic perspective and methodological approach of fuel supply chain integration into an economy-wide dataset. Int J Hydrogen Energy 2023;48:5347–76. https://doi.org/10.1016/j.ijhydene.2022.10.168.
[55] Mueller T, Gronau S. Fostering macroeconomic research on hydrogen-powered aviation: a systematic literature review on general equilibrium models, Energies. 16 (2023) 109–134. https://doi.org/10.3390/en16031439.
[56] Janic M. Modelling the full costs of an intermodal and road freight transport network. Transp Res Part D: Transp Environ 2007;12:33–44. https://doi.org/10.1016/j.trd.2006.10.004.
[57] Wang A, Van der Leun K, Peters D, Buseman M. European Hydrogen Backbone, 2020.
[58] Krieg D.Konzept und Kosten eines Pipelinesystems zur Versorgung des deutschen Straßenverkehrs mit Wasserstoff, 2012.
[59] Pieton N, Abdel-Khalek H, Graf M, B. Drechsler, V. Lenivova, C. Nolden, E. Bergup, M. Fuhad Anwar Sinha, J. Fragoso, K. Franke, C. Kleinschmitt, V.P. Müller, M. Wietschel, M. Holst, F. Weise, C. Voglstätter, Export Potentials of Green Hydrogen – Methodology for a Techno-Economic Assessment, 2023.
[60] Chemical Engineering, The Chemical Engineering Plant Cost Index, (2022). https://www.chemengonline.com/pci-home (accessed August 8, 2022).
[61] IRENA, Renewable Power Generation Costs in 2021, Abu Dhabi, 2022.
[62] Kost C, Shammugam S, Fluri V, D. Peper, A.D. Memar, T. Schlegl, Stromgestehungskosten Erneuerbare Energien, 2021.
[63] N.R.E.L. (NREL), 2022 Annual Technology Baseline (ATB) Cost and Performance Data for Electricity Generation Technologies, 2022. https://doi.org/10.25984/1871952.
[64] FCHEA, Roadmap to a US Hydrogen Economy, 2021.
[65] European Technology & Innovation Platform PV, Fact sheets about photovoltaics: PV the cheapest electricity source almost everywhere, 2020.
[66] Sens L, Neuling U, Kaltschmitt M. Capital expenditure and levelized cost of electricity of photovoltaic plants and wind turbines – development by 2050. Renew Energy 2022;185:525–37. https://doi.org/10.1016/j.renene.2021.12.042.
[67] Wiser R, Rand J, Seel J, Beiter P, Baker E, Lantz E, et al. Expert elicitation survey predicts 37% to 49% declines in wind energy costs by 2050. Nat Energy 2021;6:555–65. https://doi.org/10.1038/s41560-021-00810-z.
[68] IRENA, Renewable Power Generation Costs in 2019, International Renewable Energy Agency, Abu Dhabi, 2020.
[69] M. Ram, D. Bogdanov, A. Aghahosseini, A. Gulagi, S.A. Oyewo, M. Child, U. Caldera, K. Sadovskaia, J. Farfan, L.S.N.S. Barbosa, M. Fasihi, S. Khalili, C. Breyer, Global Energy System based on 100% Renewable Energy – Power, Heat, Transport and Desalination Sectors. Study by Lappeenranta University of Technology and Energy Watch Group, Lappeenranta, Berlin, 2019.
[70] W. Cole, A.W. Frazier, C. Augustine, Cost Projections for Utility-Scale Battery Storage: 2021 Update, 2021.
[71] van Leeuwen C, Zauner A. Innovative large-scale energy storage technologies and Power-to-Gas concepts after optimisation - D8.3, 2018.
[72] IRENA, Green Hydrogen Cost Reduction: Scaling up Electrolysers to meet the 1.5°C Climate Goal, Abu Dhabi, 2020.
[73] Sadler D, Anderson HS, Sperrink M, A. Cargill, M. Sjovoll, K.I. Asen, J.E. Finnesand, T. Melien, R. Thorsen, L. Hagesaether, P. Ringrose, B. Nazarian, H.H. Kvadsheim, H21 North Of England, 2018.
[74] Hydrogen Council, McKinsey & Company, Hydrogen Insights - A perspective on hydrogen investment, market development and cost competitiveness, 2021.
[75] IEA, IEA G20 Hydrogen report: Assumptions annex, 2020.
[76] Energy Transitions Commission, Making the Hydrogen Economy Possible, 2021.
[77] Deutsch M, Andreaola S, C. Menos-Aikateriniadis, A. Paxton, H. Preißler, H. Miehling, M. Rehn, R. Sarsfield-Hall, B. Unger, G. Flis, No-regret hydrogen. Charting early steps for H_2 infrastructure in Europe, 2021.
[78] Bruce S, Temminghoff M, Hayward J, E. Schmidt, C. Munnings, D. Palfreyman, P. Hartley, National Hydrogen Roadmap, 2018.
[79] Stolzenburg K, Hamelmann R, Wietschel M, F. Genoese, J. Michaelis, J. Lehmann, A. Miege, S. Krause, C. Sponholz, S. Donadei, F. Crotogino, A. Acht, P.-L. Horvath, Integration von Wind-Wasserstoff-Systemen in das Energiesystem - Abschlussbericht, 2014.
[80] Wang A, Jens J, Mavins D, M. Moultak, M. Schimmel, K. Van der Leun, D. Peters, M. Buseman, European Hydrogen Backbone - Analysing future demand, supply, and transport of hydrogen, 2021.
[81] Smolinka T, Wiebe N, P. Sterchele, A. Palzer, F. Lehner, M. Jansen, S. Kiemel, R. Miehe, S. Wahren, F. Zimmermann, Studie IndWEDe, Bundesministerium für Verkehr und digitale Infrastruktur (BMVI), 2018.
[82] International Energy Agency, Global Hydrogen Review 2021, 2021. https://doi.org/10.1787/39351842-en.
[83] James B, Colella W, Moton J, Saur G, T. Ramsden, PEM Electrolysis H2A Production Case Study Documentation, 2013.
[84] DNV, Hydrogen Forecast to 2050 - Energy Transition Outlook 2022, 2022.
[85] Buttler A, Spliethoff H. Current status of water electrolysis for energy storage, grid balancing and sector coupling via power-to-gas and power-to-liquids: a review. Renew Sustain Energy Rev 2018;82:2440–54. https://doi.org/10.1016/j.rser.2017.09.003.
[86] International Energy Agency, Hydrogen in North-Western Europe.: A vision towards 2030, 2021.
[87] Ali Khan MH, Daiyan R, Han Z, Hablutzel M, Haque N, Amal R, et al. Designing optimal integrated electricity supply configurations for renewable hydrogen generation in Australia. IScience 2021;24(6):102539.
[88] Hydrogen and Fuel Cell Technologies Office, 3.2 Hydrogen Delivery, 2015.
[89] Reddi K, Elgowainy A, D.R. Brown, Hydrogen Delivery Infrastructure Analysis, 2016. https://doi.org/10.13140/RG.2.1.5159.8964.
[90] W. Krewitt, S. Schmid, CASCADE Mints - D1.1 Fuel cell technologies and H2 production/distribution options, 2005.
[91] Léon A. Hydrogen Technology - Mobile and Portable Applications. Berlin Heidelberg GmbH: Springer-Verlag; 2008.

[92] Yang C, Ogden JM.Analyzing Natural Gas Based Hydrogen Infrastructure - Optimizing Transitions from Distributed to Centralized H2 Production, 2005.
[93] Reuß ME. Techno-ökonomische Analyse alternativer Wasserstoffinfrastruktur. Schriften: Forschungszentrum Jülich GmbH Zentralbibliothek, Verlag; 2019.
[94] Broerman EL, Shade N, Brun K, Bennett J, N. Poerner, D. Strickland, J. Helffrich, S. Coogan, A. Rimpel, P. Bueno, Hydrogen Compression Application of the Linear Motor Reciprocating Compressor (LMRC), 2015.
[95] Ulleberg Ø, Nakken T, Eté A. The wind/hydrogen demonstration system at Utsira in Norway: evaluation of system performance using operational data and updated hydrogen energy system modeling tools. Int J Hydrogen Energy 2010;35:1841–52. https://doi.org/10.1016/j.ijhydene.2009.10.077.
[96] Song S, Lin H, Sherman P, Yang X, Nielsen CP, Chen X, et al. Production of hydrogen from offshore wind in China and cost-competitive supply to Japan. Nat Commun 2021;12:10–7. https://doi.org/10.1038/s41467-021-27214-7.
[97] Stolzenburg K, Berstad D, Decker L, A. Elliott, C. Haberstroh, C. Hatto, M. Klaus, N.D. Mortimer, R. Mubbala, O. Mwabonje, P. Nekså, H. Quack, J.H.R. Rix, I. Seemann, H.T. Walnum, Efficient Liquefaction of Hydrogen: Results of the IDEALHY Project, Proc. Energ. – Symp. Stralsund/Germany, Novemb. (2013) p.1-8.
[98] Hank C, Sternberg A, Köppel N, Holst M, Smolinka T, Schaadt A, et al. Energy efficiency and economic assessment of imported energy carriers based on renewable electricity. Sustain Energy Fuels 2020;4:2256–73. https://doi.org/10.1039/d0se00067a.
[99] Nexant, Air Liquide, Argonne National Laboratory, Chevron Technology Venture, Gas Technology Institute, The National Renewable Energy Laboratory, Pacific Northwest National Laboratory, TIAX LLC, H2A Hydrogen Delivery Infrastructure Analysis Models and Conventional Pathway Options Analysis Results, 2008.
[100] Yang C, Ogden J. Determining the lowest-cost hydrogen delivery mode. Int J Hydrogen Energy 2007;32:268–86. https://doi.org/10.1016/j.ijhydene.2006.05.009.
[101] Teichmann D, Arlt W, Wasserscheid P. Liquid Organic Hydrogen Carriers as an efficient vector for the transport and storage of renewable energy. Int J Hydrogen Energy 2012;37:18118–32. https://doi.org/10.1016/j.ijhydene.2012.08.066.
[102] Cardella UF. Large-scale hydrogen liquefaction under the aspect of economic viability. Technische Universität München; 2018.
[103] Alder HP. Hydrogen in air transportation - feasibility study for zurich-airport, Switzerland. Int J Hydrogen Energy 1987;12:571–85. https://doi.org/10.1016/0360-3199(87)90016-4.
[104] Stolzenburg K, Mubbala R. Integrated design for demonstration of efficient liquefaction of hydrogen (IDEALHY). Fuel Cells Hydrogen Joint Undertak 2013.
[105] d'Amore-Domenech R, Leo TJ, Pollet BG. Bulk power transmission at sea: Life cycle cost comparison of electricity and hydrogen as energy vectors. Appl Energy 2021;288:116625. https://doi.org/10.1016/j.apenergy.2021.116625.
[106] Ahluwalia RK, Papadias DD, Peng J-K, H.S. Roh, System Level Analysis of Hydrogen Storage Options, 2019.
[107] Stevenson R, Leadbetter A, Day L, Project HySecure Phase 1 Summary Sept 2019, 2019.
[108] Bünger U, Michalski J, Crotogino F, Kruck O. Large-scale underground storage of hydrogen for the grid integration of renewable energy and other applications. Elsevier Ltd 2016. https://doi.org/10.1016/b978-1-78242-364-5.00007-5.
[109] Michalski J, Bünger U, Crotogino F, Donadei S, Schneider GS, Pregger T, et al. Hydrogen generation by electrolysis and storage in salt caverns: potentials, economics and systems aspects with regard to the German energy transition. Int J Hydrogen Energy 2017;42:13427–43. https://doi.org/10.1016/j.ijhydene.2017.02.102.
[110] Kruck O, Crotogino F, Prelicz R, T. Rudolph, Overview on all Known Underground Storage Technologies for Hydrogen, 2013.
[111] Lord AS, Kobos PH, Borns DJ. Geologic storage of hydrogen: Scaling up to meet city transportation demands. Int J Hydrogen Energy 2014;39:15570–82. https://doi.org/10.1016/j.ijhydene.2014.07.121.
[112] Deutsches Zentrum für Luft- und Raumfahrt, Ludwig Bölkow Systemtechnik, Fraunhofer ISE, KBB Underground Technologies, Studie über die Planung einer Demonstrationsanlage zur Wasserstoff-Kraftstoffgewinnung durch Elektrolyse mit Zwischenspeicherung in Salzkavernen unter Druck, 2014.
[113] Le Duigou A, Bader A-G, Lanoix J-C, Nadau L. Relevance and costs of large scale underground hydrogen storage in France. Int J Hydrogen Energy 2017;42:22987–3003. https://doi.org/10.1016/j.ijhydene.2017.06.239.
[114] Karellas S, Tzouganatos N. Comparison of the performance of compressed-air and hydrogen energy storage systems: Karpathos island case study. Renew Sustain Energy Rev 2014;29:865–82. https://doi.org/10.1016/j.rser.2013.07.019.
[115] Carr S, Premier GC, Guwy AJ, Dinsdale RM, Maddy J. Hydrogen storage and demand to increase wind power onto electricity distribution networks. Int J Hydrogen Energy 2014;39:10195–207. https://doi.org/10.1016/j.ijhydene.2014.04.145.
[116] Parks G, Boyd R, J. Cornish, R. Remick, Hydrogen Station Compression, Storage, and Dispensing - Technical Status and Costs, 2014.
[117] van Gerwen R, Eijgelaar M, Bosma T. Hydrogen in the electricity value chain, 2019.
[118] Zoulias EI, Glockner R, Lymberopoulos N, Tsoutsos T, Vosseler I, Gavalda O, et al. Integration of hydrogen energy technologies in stand-alone power systems analysis of the current potential for applications. Renew Sustain Energy Rev 2006;10:432–62. https://doi.org/10.1016/j.rser.2004.10.001.
[119] NCE Maritime Cleantech, Norwegian future value chains for liquid hydrogen, 2019.
[120] Ortiz Cebolla R, Dolci F, Weidner E.Assessment of Hydrogen Delivery Options: Feasibility of Transport of Green Hydrogen within Europe, 2022. https://doi.org/10.2760/869085.
[121] Niermann M, Timmerberg S, Drünert S, Kaltschmitt M. Liquid Organic Hydrogen Carriers and alternatives for international transport of renewable hydrogen. Renew Sustain Energy Rev 2021;135:110171. https://doi.org/10.1016/j.rser.2020.110171.
[122] Merten F, Scholz A, Krüger C, Heck S, Y. Girard, M. Mecke, M. George, Bewertung der Vor- und Nachteile von Wasserstoffimporten im Vergleich zur heimischen Erzeugung, Wuppertal, 2020.
[123] Brändle G, Schönfisch M, Schulte S. Estimating long-term global supply costs for low-carbon hydrogen. Appl Energy 2021;302:117481. https://doi.org/10.1016/j.apenergy.2021.117481.
[124] Al-breiki M, Bicer Y. Comparative cost assessment of sustainable energy carriers produced from natural gas accounting for boil-off gas and social cost of carbon. Energy Rep 2020;6:1897–909. https://doi.org/10.1016/j.egyr.2020.07.013.
[125] Schenke F, Hoelzen J, Minke C, Bensmann A, Hanke-Rauschenbach R. Resource requirements for the implementation of a global H2-powered aviation. Energy Convers Manag X 2023;20:100435. https://doi.org/10.1016/j.ecmx.2023.100435.
[126] Caldera U, Breyer C. Assessing the potential for renewable energy powered desalination for the global irrigation sector. Sci Total Environ 2019;694:133598. https://doi.org/10.1016/j.scitotenv.2019.133598.
[127] IRENA. Renewable power generation costs in 2020. Abu Dhabi; 2021.
[128] Danish Energy Agency, Deutsche Energie-Agentur, China National Renewable Energy Centre, Distributed Wind and PV in Denmark and Germany, 2019.
[129] Shepherd A, Roberts S, Sünnenberg G, Lovett A, Hastings AFS. Scotland's onshore wind energy generation, impact on natural capital & satisfying no-nuclear energy policy. Energy Rep 2021;7:7106–17. https://doi.org/10.1016/j.egyr.2021.10.063.
[130] European Environment Agency, Europe's onshore and offshore wind energy potential, 2009.
[131] 4C Offshore, Global Offshore Renewable Map, (2022). https://map.4coffshore.com/offshorewind/ (accessed December 21, 2022).
[132] Taoufik M, Fekri A. GIS-based multi-criteria analysis of offshore wind farm development in Morocco. Energy Convers Manag X 2021;11:100103. https://doi.org/10.1016/j.ecmx.2021.100103.
[133] Staffell I, Pfenninger S. Using bias-corrected reanalysis to simulate current and future wind power output. Energy 2016;114:1224–39. https://doi.org/10.1016/j.energy.2016.08.068.
[134] Pfenninger S, Staffell I. Long-term patterns of European PV output using 30 years of validated hourly reanalysis and satellite data. Energy 2016;114:1251–65. https://doi.org/10.1016/j.energy.2016.08.060.
[135] Gaertner E, Rinker J, Sethuraman L, B. Anderson, F. Zahle, G. Barter, N. Abbas, F. Meng, P. Bortolotti, W. Skrzypinkski, G. Scott, R. Feil, H. Bredmose, K. Dykes, M. Shields, C. Allen, A. Viselli, Definition of the IEA 15-Megawatt Offshore Reference Wind Turbine, 2020.
[136] National Renewable Energy Laboratory, Onshore Wind Turbine Documentation: 2020ATB_NREL_Reference_7MW_200, (2020). https://nrel.github.io/turbine-models/2020ATB_NREL_Reference_7MW_200.html#references (accessed November 12, 2022).
[137] Wiser R, Bolinger M, Hoen B.Land-based wind market report: 2022 edition, 2022.
[138] European Commission, Commission delegated regulation (EU) of 10.2.2023, Brussels, 2023.
[139] Flightradar24, Live Flight Tracker, (2023). https://www.flightradar24.com/ (accessed February 2, 2023).
[140] German Airports Association (ADV), ADV Monthly Traffic Report, Berlin, 2020.
[141] Hamburg Airport, Starts 2019 - Linien- und Touristikverkehr, 2021.
[142] Lohr C, Peterssen F, Schlemminger M, Bensmann A, Niepelt R, Brendel R, et al. Multi-criteria energy system analysis of onshore wind power distribution in climate-neutral Germany. SSRN 2023. https://doi.org/10.2139/ssrn.4367164.
[143] Bolinger M, Bolinger G. Land requirements for utility-scale PV : an empirical update on power and energy density. IEEE J Photovoltaics 2022;12:589–94. https://doi.org/10.1109/JPHOTOV.2021.3136805.
[144] Caglayan DG, Weber N, Heinrichs HU, Linßen J, Robinius M, Kukla PA, et al. Technical potential of salt caverns for hydrogen storage in Europe. Int J Hydrogen Energy 2020;45:6793–805. https://doi.org/10.1016/j.ijhydene.2019.12.161.
[145] IRENA, Global hydrogen trade to meet the 1.5 °C climate goal: Part I – Trade outlook for 2050 and way forward, Abu Dhabi, 2022.
[146] Ammonia Energy Association, Yara and Nel collaborate to reduce electrolyzer costs; announce green ammonia pilot in Norway by 2022, (2019). https://www.ammoniaenergy.org/articles/yara-and-nel-collaborate-to-reduce-electrolyzer-costs-announce-green-ammonia-pilot-in-norway-by-2022/ (accessed June 5, 2021).
[147] Kamiya S. World's first ocean going liquid hydrogen carrier, 2021.
[148] BloombergNEF, Hydrogen Economy Outlook - Key messages, 2020.
[149] IRENA, Global hydrogen trade to meet the 1.5 °C climate goal: Part II – Technology review of hydrogen carriers, Abu Dhabi, 2022.
[150] Cardella U, Decker L, Klein H. Roadmap to economically viable hydrogen liquefaction. Int J Hydrogen Energy 2017;42:13329–38. https://doi.org/10.1016/j.ijhydene.2017.01.068.
[151] Berstad D, Gardarsdottir S, Roussanaly S, Voldsund M, Ishimoto Y, Nekså P. Liquid hydrogen as prospective energy carrier: a brief review and discussion of underlying assumptions applied in value chain analysis. Renew Sustain Energy Rev 2022;154:111772. https://doi.org/10.1016/j.rser.2021.111772.

[152] HyNEAT Project, Hydrogen Supply Networks' Evolution for Air Transport - Development of hydrogen supply networks for H2-powered aviation and its integration into renewable energy systems, (2023). https://www.hyneat.de/en/ (accessed March 28, 2023).
[153] T. Bollerhey, M. Exenberger, F. Geyer, K. Westphal, H2GLOBAL – Idea, Instrument and Intentions, Hamburg, 2023.
[154] Wilson C. Up-scaling, formative phases, and learning in the historical diffusion of energy technologies. Energy Policy 2012;50:81–94. https://doi.org/10.1016/j.enpol.2012.04.077.
[155] Hayward JA, Graham PW. A global and local endogenous experience curve model for projecting future uptake and cost of electricity generation technologies. Energy Econ 2013;40:537–48. https://doi.org/10.1016/j.eneco.2013.08.010.
[156] Rubin ES, Azevedo IML, Jaramillo P, Yeh S. A review of learning rates for electricity supply technologies. Energy Policy 2015;86:198–218. https://doi.org/10.1016/j.enpol.2015.06.011.
[157] Pieper F, Das Konzept von Lernkurven im Energiesektor — Beschreibung , Modellierung und Aggregation Diplomarbeit, (2003).
[158] IEA, Experience Curves for Energy Technology Policy, 2000.
[159] J.E. Fesmire, A. Swanger, DOE / NASA Advances in Liquid Hydrogen Storage Workshop, 2021.
[160] Hydrogen Council and McKinsey & Company, Hydrogen for Net-Zero: A critical cost-competitive energy vector, 2021.
[161] Hydrogen Council, Path to hydrogen competitiveness - A cost perspective, 2020.
[162] P. Graham, J. Hayward, J. Foster, L. Havas, GenCost 2021-22: Final report, 2022.
[163] Mayyas A, Ruth M, B. Pivovar, G. Bender, K. Wipke, Manufacturing Cost Analysis for Proton Exchange Membrane Water Electrolyzers, 2019.
[164] Fette M, Brandstaett C, Kimmer L, C. Rickert, I. Roller, H.C. Gils, H. Gardian, T. Pregger, F. Cebulla, E. Meyer, J. Schaffert, E. Tali, N. Bruecken, M. Koeppke, N. Duenne, S. von Berg, Multi-Sektor-Kopplung - Modellbasierte Analyse der Integration Erneuerbarer Stromerzeugung durch die Kopplung der Stromversorgung mit dem Wärme, Gas- und Verkehrssektor, 2020.
[165] Rinne E, Holttinen H, Kiviluoma J, Rissanen S. Effects of turbine technology and land use on wind power resource potential. Nat Energy 2018;3:494–500. https://doi.org/10.1038/s41560-018-0137-9.
[166] Barthelmie RJ, Jensen LE. Evaluation of wind farm efficiency and wind turbine wakes at the Nysted offshore wind farm. Wind Energy 2010;13:573–86. https://doi.org/10.1002/we.408.
[167] Yang H, Xie K, Tai HM, Chai Y. Wind farm layout optimization and its application to power system reliability analysis. IEEE Trans Power Syst 2016;31:2135–43. https://doi.org/10.1109/TPWRS.2015.2452920.
[168] Gebraad P, Thomas JJ, Ning A, Fleming P, Dykes K. Maximization of the annual energy production of wind power plants by optimization of layout and yaw-based wake control. Wind Energy 2017;20:97–107. https://doi.org/10.1002/we.1993.
[169] Krohn S, Morthorst P-E, S. Awerbuch, The Economics of Wind Energy, 2009. https://doi.org/10.1111/j.1745-6622.2009.00231.x.
[170] Wagner M, Neumann F, U.O. Reilly, Optimizing the Layout of 1000 Wind Turbines Massachusetts Institute of Technology, Eur. Wind Energy Assoc. Annu. Event. (2011) 10. https://domino.mpi-sb.mpg.de/intranet/ag1/ag1publ.nsf/0/08f2e8f1d20ab7fec125785d00343a1b?OpenDocument.
[171] Sørensen T, Nielsen P, M.L. Thøgersen, Recalibrating wind turbine wake model parameters - Validating the wake model performance for Large offshore Wind Farms, Eur. Wind Energy Conf. Exhib. 2006, EWEC 2006. 2 (2006) 1660–1665.
[172] Wu YK, Su YS, Wu TY, Lee ZJ. Estimation of wake losses in an offshore wind farm by WAsP - a real project case study in Taiwan. IET Semin Dig 2015;2015. https://doi.org/10.1049/ic.2015.0264.
[173] Penä A, Schaldemose Hansen K, Ott S, Paul Van Der Laan M. On wake modeling, wind-farm gradients, and AEP predictions at the Anholt wind farm. Wind Energy Sci 2018;3:191–202. https://doi.org/10.5194/wes-3-191-2018.
[174] Rehman S, Mohammed AB, Alhems L. A heuristic approach to siting and design optimization of an onshore wind farm layout. Energies 2020;13(22):5946.
[175] Odoi-Yorke F, Adu TF, Ampimah BC, Atepor L. Techno-economic assessment of a utility-scale wind power plant in Ghana. Energy Convers Manag X 2023;18:100375. https://doi.org/10.1016/j.ecmx.2023.100375.
[176] Härtel P, Vrana TK, Hennig T, von Bonin M, Wiggelinkhuizen EJ, Nieuwenhout FDJ. Review of investment model cost parameters for VSC HVDC transmission infrastructure. Electr Pow Syst Res 2017;151:419–31. https://doi.org/10.1016/j.epsr.2017.06.008.
[177] Gorman W, Mills A, Wiser R. Improving estimates of transmission capital costs for utility-scale wind and solar projects to inform renewable energy policy. Energy Policy 2019;135:110994.
[178] Godron P, Neubarth J, Soyah M, V. Asceri, G. Callegari, B. Cova, F. Banez, L. Olmos, A. Ramos, M. Rivier, Desert Power: Getting connected, 2014.
[179] Mills A, Wiser R, Porter K. The cost of transmission for wind energy in the United States: A review of transmission planning studies. Renew Sustain Energy Rev 2012;16:1–19. https://doi.org/10.1016/j.rser.2011.07.131.
[180] Miao B, Giordano L, Chan SH. Long-distance renewable hydrogen transmission via cables and pipelines. Int J Hydrogen Energy 2021;46:18699–718. https://doi.org/10.1016/j.ijhydene.2021.03.067.
[181] Fasihi M, Breyer C. Baseload electricity and hydrogen supply based on hybrid PV-wind power plants. J Clean Prod 2020;243:118466. https://doi.org/10.1016/j.jclepro.2019.118466.
[182] Schaber K, Steinke F, Mühlich P, Hamacher T. Parametric study of variable renewable energy integration in Europe: advantages and costs of transmission grid extensions. Energy Policy 2012;42:498–508. https://doi.org/10.1016/j.enpol.2011.12.016.
[183] Lauria S, Schembari M, Palone F, Maccioni M. Very long distance connection of gigawattsize offshore wind farms: extra high-voltage AC versus high-voltage DC cost comparison. IET Renew Power Gener 2016;10:713–20. https://doi.org/10.1049/iet-rpg.2015.0348.
[184] Schönberger D, P2G durch Elektrolyse – eine flexible Speicherlösung, 2016.
[185] Bertuccioli L, Chan A, Hart D, F. Lehner, B. Madden, E. Standen, Development of Water Electrolysis in the European Union, 2014.
[186] Holst M, Aschbrenner S, T. Smolinka, C. Voglstätter, G. Grimm, Cost Forecast for Low Temperature Electrolysis - Technology Driven Bottom-up Prognosis for PEM and Alkaline Water Electrolysis Systems, 2021.
[187] Saravia F, Graf F, Schwarz S, F. Gröschl, Genügend Wasser für die Elektrolyse - Wieviel Wasser wird für die Erzeugung von grünem Wasserstoff benötigt und gibt es ausreichende Ressourcen?, n.d.
[188] Saba SM, Mu M, Robinius M, Stolten D. The investment costs of electrolysis – a comparison of cost studies from the past 30 years. Int J Hydrogen Energy 2018;43:1209–23. https://doi.org/10.1016/j.ijhydene.2017.11.115.
[189] Proost J. State-of-the art CAPEX data for water electrolysers, and their impact on renewable hydrogen price settings. Int J Hydrogen Energy 2018;44:4406–13. https://doi.org/10.1016/j.ijhydene.2018.07.164.
[190] Leachman JW, Jacobsen RT, S.G. Penoncello, E.W. Lemmon, Fundamental equations of state for parahydrogen, normal hydrogen, and orthohydrogen, J. Phys. Chem. Ref. Data. 38 (2009) 721–748. https://doi.org/10.1063/1.3160306.
[191] Concepts NREC, Development Of A Centrifugal Hydrogen Pipeline Gas Compressor - Final Report, 2015.
[192] Groenenberg R, Juez-Larré J, Goncalvez C, Wasch L, H. Dijkstra, B. Wassing, B. Orlic, K. Van Der Valk, T.H. Van Der Meulen, K. Kranenburg-Bruinsma, Techno-Economic Modelling of Large-Scale Energy Storage Systems, Utrecht, 2020.
[193] Quack H, Essler J, Haberstroh C, P. Nekså, D. Berstad, M. Drescher, J. Stang, H.T. Walnum, L. Decker, P. Treite, Boundary Conditions and assumptions Influencing the Power Needed to Liquefy Hydrogen, 2012.
[194] Berstad D, Skaugen G, Wilhelmsen Ø. Dissecting the exergy balance of a hydrogen liquefier: analysis of a scaled-up claude hydrogen liquefier with mixed refrigerant pre-cooling. Int J Hydrogen Energy 2021;46:8014–29. https://doi.org/10.1016/j.ijhydene.2020.09.188.
[195] Gardiner MR. Energy requirements for hydrogen gas compression and liquefaction as related to vehicle storage needs, 2009.
[196] Cardella U, Decker L, Sundberg J, Klein H. Process optimization for large-scale hydrogen liquefaction. Int J Hydrogen Energy 2017;42:12339–54. https://doi.org/10.1016/j.ijhydene.2017.03.167.
[197] Cardella U, Decker L, Klein H. Economically viable large-scale hydrogen liquefaction. IOP Conf Ser Mater Sci Eng 2017;171:012013.
[198] J. Essler, C. Haberstroh, H.T. Walnum, D. Berstad, P. Nekså, J. Stang, S.A. Energi, L. Decker, P. Treite, L.A. Kryotechnik, Report on Technology Overview and Barriers to Energy- and Cost-Efficient Large Scale Hydrogen Liquefaction, 2012.
[199] Bell IH, Wronski J, Quoilin S, Lemort V. Pure and pseudo-pure fluid thermophysical property evaluation and the open-source thermophysical property library coolprop. Ind Eng Chem Res 2014;53:2498–508. https://doi.org/10.1021/ie4033999.
[200] Connelly E, Penev M, Elgowainy A, Hunter C. DOE hydrogen and fuel cells program record 19001. United States of America: Department of Energy; 2019.
[201] Ohlig K, Decker L. The latest developments and outlook for hydrogen liquefaction technology. AIP Conf Proc 2014;1573:1311–7. https://doi.org/10.1063/1.4860858.
[202] Krasae-in S. Optimal operation of a large-scale liquid hydrogen plant utilizing mixed fluid refrigeration system. Int J Hydrogen Energy 2014;39:7015–29. https://doi.org/10.1016/j.ijhydene.2014.02.046.
[203] Sadaghiani MS, Mehrpooya M. Introducing and energy analysis of a novel cryogenic hydrogen liquefaction process configuration. Int J Hydrogen Energy 2017;42:6033–50. https://doi.org/10.1016/j.ijhydene.2017.01.136.
[204] Asadnia M, Mehrpooya M. A novel hydrogen liquefaction process configuration with combined mixed refrigerant systems. Int J Hydrogen Energy 2017;42:15564–85. https://doi.org/10.1016/j.ijhydene.2017.04.260.
[205] Ohira K. A Summary of liquid hydrogen and cryogenic technologies in Japan's WE-NET project. AIP Conf Proc 2004;710. https://doi.org/10.1063/1.1774663.
[206] Quack H. Conceptual design of a high efficiency large capacity hydrogen liquefier. AIP Conf Proc 2002;613. https://doi.org/10.1063/1.1472029.
[207] U.S. Energy Information Administration, Hydrocarbon gas liquids explained - prices for hydrocarbon gas liquids, (2022). https://www.eia.gov/energyexplained/hydrocarbon-gas-liquids/prices-for-hydrocarbon-gas-liquids.php (accessed January 2, 2023).
[208] Syed MT, Sherif SA, Veziroglu TN, Sheffield JW. An economic analysis of three hydrogen liquefaction systems. Int J Hydrogen Energy 1998;23:565–76.
[209] Decker L. Liquid Hydrogen Distribution Technology - HYPER closing seminar, 2019.
[210] Barckholtz T, Burgunder A, Casey D, S. Dillich, A. Elgowainy, J. Merritt, G. Parks, S. Pawel, J. Simnick, H. Soto, E. Sutherland, Hydrogen Delivery Technical Team Roadmap, Washington DC, 2013. https://doi.org/https://doi.org/10.2172/1220133.
[211] Züttel A. Materials for hydrogen storage. Mater Today 2003;6:24–33. https://doi.org/10.1016/S1369-7021(03)00922-2.
[212] Mischner J, Fasold H-G, J. Heymer, Systemplanerische Grundlagen der Gasversorgung, 2015.
[213] Mischner J. Fluiddynamische Berechnung von Hochdruckgasleitungen. In: Horlacher H–B, Helbig U, editors. Rohrleitungen 2 Einsatz. Heidelberg: Verlegung, Berechnung, Rehabil., Springer Vieweg; 2018. p. 587–622. https://doi.org/10.1007/978-3-662-50355-3_103.

[214] Ishimoto Y, Voldsund M, Neksa P, Roussanaly S, Berstad D, Gardarsdottir SO. Large-scale production and transport of hydrogen from Norway to Europe and Japan: Value chain analysis and comparison of liquid hydrogen and ammonia as energy carriers. Int J Hydrogen Energy 2020;45:32865–83. https://doi.org/10.1016/j.ijhydene.2020.09.017.

[215] Alkhaledi AN, Sampath S, Pilidis P. A hydrogen fuelled LH2 tanker ship design. Ships Offshore Struct 2021;17:1555–64. https://doi.org/10.1080/17445302.2021.1935626.

[216] Schmied M, Knörr W. Carbon Footprint - Teilgutachten “Monitoring für den CO2-Ausstoß in der Logistikkette, 2012.